Shielding Effectiveness of Reverberant Enclosures Containing Printed Circuit Boards

Sarah Louise Parker

PhD

University of York

Electronic Engineering

December 2018

Abstract

Shielded enclosures are a convenient and widely used method of protecting electronic equipment from an undesirable electromagnetic environment. The amount of protection the enclosure provides is known as Shielding Effectiveness (SE). Generally, the SE is given for an empty enclosure. However, the contents of an enclosure, such as Printed Circuit Boards (PCBs), will change the SE.

In this thesis, the absorption and transmission of a set of PCBs has been investigated and this information used to predict the SE of populated enclosures. Power balance modelling was used to predict the SE of a number of configurations of a single cavity and two cavity enclosure with and without contents. These results were compared to measurements made in a reverberation chamber (RC). Measurements and analysis were made of the absorption of individual PCBs and the absorption was shown to change when PCBs were stacked together or positioned close to the RC wall. The transmission through a set of PCBs was measured and found to be low enough to ignore in the models.

The results presented in this thesis have shown how the absorption of a PCB can change in different situations and how this information can be used in power balance modelling to estimate the SE of an enclosure. Further investigation into the absorption and transmission of PCBs will refine the models for more accurate results.

It is important to know the SE of an enclosure and its contents as a whole system as under or over estimating the amount of SE could lead to equipment malfunctions. If the SE is underestimated additional, unnecessary, shielding may be used which will add weight, cost and space to the equipment. Too little shielding and equipment may not be fully protected.

Contents

List of Tables

List of Figures

Acknowledgements

Thanks to my supervisors Dr. John Dawson and Prof. Andy Marvin for all their help and patience. Thanks to the other members of the Applied Electromagnetics Group at the University of York including Dr. Ian Flintoft and Dr. Simon Bale. I would also like to thank Huawei for the use of their enclosures and PCBs.

This PhD was funded by Eurofins York (previously known as York EMC Services).

Declaration

I declare that this thesis is a presentation of original work and I am the sole author. This work has not previously been presented for an award at this, or any other, university. All sources are acknowledged as references.

This thesis contains research presented in the following publications:

- S. L. Parker, I.D. Flintoft, A.C. Marvin, J. F. Dawson, S.J. Bale, M. P. Robinson, M. Ye, C. Wan and M. Zhang , "Absorption Cross Section measurement of stacked PCBs in a reverberation chamber," *2016 Asia-Pacific International Symposium on Electromagnetic Compatibility (APEMC)*, Shenzhen, 2016, pp. 991-993
- S. L. Parker, I.D. Flintoft, A.C. Marvin, J. F. Dawson, S.J. Bale, M. P. Robinson, M. Ye, C. Wan and M. Zhang , "Predicting shielding effectiveness of populated enclosures using absorption cross section of PCBs," *2016 International Symposium on Electromagnetic Compatibility - EMC EUROPE*, Wroclaw, 2016, pp. 324-328[1]
- S. L. Parker, A. C. Marvin, J. F. Dawson and M. Ye, "Measurement of transmission through printed circuit boards: Application to enclosure shielding," *2017 International Symposium on Electromagnetic Compatibility - EMC EUROPE*, Angers, 2017, pp. 1-6
- S. L. Parker, I.D. Flintoft, A.C. Marvin, J. F. Dawson, S.J. Bale, M. P. Robinson, M. Ye, C. Wan and M. Zhang , "Changes in a printed circuit board's absorption cross section due to proximity to walls in a reverberant environment," *2016 IEEE International Symposium on Electromagnetic Compatibility (EMC)*, Ottawa, ON, 2016, pp. 818-823
- I.D. Flintoft, S. L. Parker, S. J. Bale, A. C. Marvin, J. F. Dawson and M. P. Robinson, "Measured Average Absorption Cross-Sections of Printed

[1] This paper won the Best Student Paper Award at EMC Europe 2016 in Wroclaw, Poland

Circuit Boards from 2 to 20 GHz," in *IEEE Transactions on Electromagnetic Compatibility*, vol. 58, no. 2, pp. 553-560, April 2016.

The author of this thesis has also contributed to the following publications:

- I. D. Flintoft, S. J. Bale, A. C. Marvin, M. Ye, J. F. Dawson, C. Wan, M. Zhang, S. L. Parker and M. P. Robinson, "Representative Contents Design for Shielding Enclosure Qualification From 2 to 20 GHz," in *IEEE Transactions on Electromagnetic Compatibility*, vol. 60, no. 1, pp. 173-181, Feb. 2018
- I. D. Flintoft, S. J. Bale, S. L. Parker, A. C. Marvin, J. F. Dawson and M. P. Robinson, "On the Measurable Range of Absorption Cross Section in a Reverberation Chamber," in *IEEE Transactions on Electromagnetic Compatibility*, vol. 58, no. 1, pp. 22-29, Feb. 2016

Chapter 1

Introduction

1.1. Electromagnetic Compatibility and Shielded Enclosures

Electronic systems and components produce intentional and unintentional electromagnetic (EM) fields when operating. Good electromagnetic compatibility (EMC) practice is used to reduce any unwanted emissions from equipment and to protect equipment from any threats produced by external sources. EMC considers both radiated and conducted threats and emissions. As electronic equipment becomes more and more prevalent in modern society sources of unwanted EM fields have the potential to become more troublesome and the design of equipment to deal with these EM threats becomes more important.

One method of reducing the effect of radiated EM fields on sensitive equipment is to use shielded enclosures. When sensitive or noisy equipment is placed within a suitable enclosure the EM field is reduced. The contents of an enclosure are protected from external EM sources or external equipment is protected from radiated fields produced from the equipment inside the enclosure.

Shielding effectiveness (SE) is the value used to define how well a shielded enclosure reduces the EM field incident upon it. SE can be defined as the ratio of the EM field without the enclosure in place and the EM field with the enclosure in place. This ratio is generally given in decibels (dB). A perfectly shielded enclosure would stop all penetration of EM fields. However, perfect enclosures do not exist as real equipment enclosures differ from the ideal as materials are not perfect and enclosures have apertures for cables, holes for cooling and other slots and gaps required for lids and access.

There are a number of different standards, for example [1] and [2], that describe methods that can be used to measure the shielding effectiveness of an equipment enclosure; one of the most widely used being IEEE Standard 299.1 [3]. The methods described in these standards are intended for the SE measurement of empty enclosures. However, in reality, the enclosure will be used with contents inside and the SE of the enclosure will be affected by this. Introducing contents, such as printed circuit boards (PCBs), into an enclosure reduces the EM field inside the enclosure as the contents will absorb energy. Decreasing the internal EM field will increase the

observed SE of the enclosure. Therefore, the amount of EM energy absorbed by the enclosure contents is significant when considering the enclosure shielding.

It is important to have an accurate value for the SE of an enclosure as if the shielding given by an enclosure is underestimated excessive shielding will lead to greater costs, weight and a larger than necessary size. Alternatively, if the shielding is overestimated the enclosure may not give enough protection leading to potential failure of the equipment.

The absorption cross section (ACS) of a lossy object is the cross sectional area of a perfectly absorbing object which would absorb the same amount of energy as the object being considered [4]. In this thesis, ACS is used to quantity the amount of EM energy absorbed by enclosure contents, specifically PCBs. In addition to ACS, the transmission cross section (TCS) of a PCB is also of interest. The TCS is the ratio between the transmitted power through an aperture or, more generally, a point of entry to the mean incident power on the aperture. In the case of the PCB, it is used to show how much power is able to pass through the PCB. The ACS and TCS of PCBs can be used to give a more accurate value for the SE of a populated shielded enclosure by using analytical models [5][6].

1.2. Research Scope

The work presented in this thesis describes a number of investigations into ACS and how the ACS can be used to predict the SE of shielded enclosures populated with PCBs. This is carried out by using an analytical technique called power balance modelling (PWB) [5], ACS results from reverberation chamber measurements and explained using relevant theory. This main aim can be separated into several smaller goals:

- Obtain the ACS of a set of PCBs measured individually and in stacks
- Investigate how the ACS of the PCBs vary depending on the position inside the enclosure and in relation to other PCBs and consider whether these factors are a significant influence on the SE of an enclosure

- Use the information about ACS to predict the SE of a shielded enclosure containing different configurations of PCBs. The modelled results of the SE of populated enclosure models should be compared to measured results of equivalent enclosures.

These points can be summarised in the following hypothesis:

The shielding effectiveness of a simple enclosure populated by PCBs can be predicted using the transmission cross section of any apertures in the enclosure and the absorption and transmission cross section of the PCBs.

1.3. Outline of thesis

Chapter 2 of this thesis examines the theory behind reverberant environments and how this relates to SE measurements of enclosures. Current research, practices and methods of measuring the SE of enclosures are explored and it is shown why it is necessary to include the contents of enclosures when considering the enclosure SE. The theory of ACS and how this may be used to predict SE of an enclosure with contents is explained and the measurements and analytical methods which will be used throughout this thesis discussed.

Chapter 3 describes the method used to measure the ACS of PCBs using a reverberation chamber. The ACS results of a set of PCBs measured individually and stacked together are presented and analysed.

Chapter 4 expands on these initial results to explore the changes in ACS due to the position of PCBs in an enclosure and the changes due to the proximity to the enclosure walls.

Chapter 5 looks at developing a method of finding the ACS of one side of a PCB using reverberation chamber measurements. The ACS of the individual sides of the PCB is required when considering enclosures as multiple cavities formed by dividing PCBs. The results from these measurements and analysis are presented.

The transmission of EM fields through a PCB is considered in Chapter 6. The transmission is used to calculate the TCS of the PCB which can be used in the PWB.

Chapter 7 shows how PWB and the ACS results detailed in the previous parts of the thesis can be used to predict the SE of an enclosure with these contents in. This prediction is compared with SE measurements of an enclosure with PCBs.

Finally, in Chapter 8 conclusions are drawn from the work presented in the thesis. This includes the main results from each chapter and how these results could be improved. Additional research that could be carried out to further explore shielded enclosures with contents in is also discussed.

Chapter 2

Reverberant Environments and Shielded Enclosures

2.1. Overview

This chapter provides background information on the subject of reverberant environments and shielded enclosures. The chapter introduces the theories and concepts that will be used throughout this thesis.

The concepts of reverberant environments, shielded enclosures and shielding effectiveness (SE) are introduced and how these topics relate to each other is discussed. The reasons why contents affect the SE of enclosures are explained and an example measurement of the SE of an enclosure with and without contents is presented. Information is also provided on how to use power balance modelling (PWB) to calculate the SE of a shielded enclosure.

2.2. Reverberant Environments

2.2.1. Reverberation Chambers

A reverberation chamber (RC), also known as a mode stirred chamber, is an enclosed metallic chamber used for EM field measurement and testing. The RC is required to be electrically large. The EM fields excited in the chamber form standing wave patterns. The energy in the chamber is then stirred to change the boundary conditions. This, in turn, causes the field pattern to change [7]. If an RC is well stirred it provides a uniform field throughout the chamber which has the same energy in all field components with equal energy from all directions [7]. A great deal has been written previously on the subject of field statistics in reverberation chambers. For full information [7] should be consulted.

The metallic enclosure of an RC has a shielded door or access panel. A metallic stirrer is connected to a motor and used to stir the energy in the chamber. Bulkhead connections are made through the wall of the chamber in order to connect to external test equipment.

The equipment under test (EUT) should be positioned in the working volume of the chamber. The working volume is defined as an area within the RC where there is a statistically uniform field. A quarter of a wavelength from the chamber walls is an accepted approximation of where the working volume starts [8][10]. At distances closer than a quarter of a wavelength, boundary effects cause poor field uniformity close to the chamber walls [9]. A photo of the large reverberation chamber belonging to the Applied Electromagnetics Group (AEG) at the University of York (UoY) is shown in Figure 2.1.

One of the main standards which describe using reverberation chambers for EMC measurements is IEC 61000-4-21 [10]. This standard details both the measurement methodology that should be used for testing and also the calibration requirements and tests that need to be undertaken before using the chamber. A number of other standards are starting to incorporate reverberation chambers as a possible test

environment for EMC. These include military standards [11], [12] and airborne equipment standards [13].

The next part of this chapter reviews important performance parameters of RCs including resonances, lowest usable frequency, stirring, independent sampling, K factor and Q factor. Full, detailed information on RCs can be found in [7][8] and [10].

Figure 2.1: Photograph of the Applied Electromagnetics Group reverberation chamber at the University of York. The mechanical stirrer is at the back of the chamber and a polystyrene block is used to place equipment under test in the working volume of the chamber.

2.2.2. Resonances

Resonant frequencies of a rectangular cavity are calculated using (2.1).

$$f_{ijk} = \frac{c_0}{2}\sqrt{\frac{i}{a}^2 + \frac{j}{b}^2 + \frac{k}{c}^2}\ Hz \quad \textbf{(2.1)}$$

In this equation i,j,k are integers (only one of which can be zero), c_0 is the velocity of waves in free space ($3x10^8$ m/s) and a, b and c are the dimensions of the enclosure. Weyl's Law [7] gives an approximate solution to the number of resonant modes in a cavity below a given frequency and a more accurate version is available for a rectangular cavity such as a reverberation chamber [7] as:

$$N_{modes} = \frac{8\pi f^3 abc}{3c_0^2} - \frac{(a+b+c)f}{c_0} + \frac{1}{2} \quad \textbf{(2.2)}$$

where f is frequency, a, b and c are the dimensions of the rectangular reverberation chamber and c_0 is the velocity of waves in free space.

2.2.3. Lowest Usable Frequency

Equation (2.1) can be used to find the frequency at which the first resonance occurs in a chamber. With only one or a low number of resonant modes active, not enough modes can be excited in the RC to provide a statistically uniform environment.

It necessary to know the lowest useable frequency (LUF) of a reverberation chamber to ensure measurements are made within the operating range of the chamber. There are several rules of thumb that can be used to decide the LUF of a chamber. One method to calculate the LUF, in Hz, is to use (2.3) where c_0 is the velocity of waves in free space and V is the volume of the chamber [7].

$$f_{min} = c_0\left(\frac{90}{4\pi V}\right)^{\frac{1}{3}} \quad \textbf{(2.3)}$$

More common methods of calculating the LUF is to use a frequency between 3 and 6 times the first chamber resonance frequency [16] or use the frequency below which 60 modes exist [15]. Alternatively, the modal density or Q factor can be used [16] or the LUF can be found experimentally.

2.2.4. Stirring

From the above it can be seen that the dimensions and volume of the chamber are important parameters when considering how well the chamber will perform. In addition to this the method of stirring the field in the chamber is important to get good field uniformity.

2.2.4.1. Mechanical Stirring

The majority of RCs use a mechanical paddle to stir the field. The mechanical paddle inside the large RC chamber used for the work in this thesis can be seen at the back of the chamber in Figure 2.1. There are two methods of using a mechanical paddle to stir the field in an RC. For mode tuned operation, measurements are made with the stirrer stationary at a number of different positions. The measurements are then averaged over the stirrer positions at each frequency [8]. During stirred mode testing the stirrer is moved continuously while a number of measurements are taken [15][16]. The measurements are then averaged over the stirrer positions at each frequency [8]. Although this method can be less time consuming obtaining repeatable results is more difficult. Mode tuned stirring is used throughout the work presented in this thesis unless otherwise stated.

2.2.4.2. Frequency Stirring

Frequency stirring (also known as electronic stirring) is another method used to improve the field uniformity in an RC and is applied by averaging the measurement over a certain frequency bandwidth (BW) [17]. This technique is more useful at high frequencies as the BW is related to mode density. At high frequencies a small BW is required but at lower frequencies a large BW is needed. Both mechanical and frequency stirring can be applied to one measurement in order to improve uncertainty in results [18]. If frequency stirring is used, additional mechanical stirring may still be needed in order to obtain good field uniformity [17].

The minimum BW used for frequency stirring must be much greater than the right hand side (RHS) of the following equation, as suggested by the IEEE standard 299.1 [22].

$$BW \gg \frac{c_0^3}{8\pi V f^2} \tag{2.4}$$

In equation (2.4) c_0 is the velocity of light, V is the volume of the enclosure being tested and f is the centre frequency.

2.2.4.3. Other Methods of Stirring

In addition to the methods described above the field within the chamber can be stirred in other ways. When source stirring [23], the transmitting antenna in the RC is moved to different positions in order change the boundary conditions. Similarly, the receiving antenna can also be moved to different positions and then an average taken at each frequency.

2.2.5. Independent Samples

In order to get a statistically average field in an RC it is important to have enough independent samples [10]. This means that the samples at each stirrer position must be uncorrelated i.e. the boundary conditions have changed sufficiently. The number of independent samples can be found by autocorrelating the measured S_{21} (the scattering parameters between two antennas, as measured by a VNA) with stirrer position [10]. When the autocorrelation drops below 1/e (approximately 0.37) the difference in stirrer positions is enough for samples to be independent. This can be defined mathematically for a mechanical stirrer using (2.5).

$$N_{mech} = \frac{2\pi}{\theta_c} \tag{2.5}$$

N_{mech} is the number of independent samples and Θ_c is the stirrer movement angle required for the autocorrelation to drop below 1/e.

Figure 2.2 shows the autocorrelation against stirrer position for the small RC discussed in Section 2.2.8.2. For this measurement 100 stirrer positions were used (4800 were possible). The graph shows that at 1GHz the chamber is not well stirred as it requires several stirrer position changes for the autocorrelation function (ACF) to reduce below 1/e. However, at higher frequencies the chamber is working well as each stirrer position is producing an independent sample.

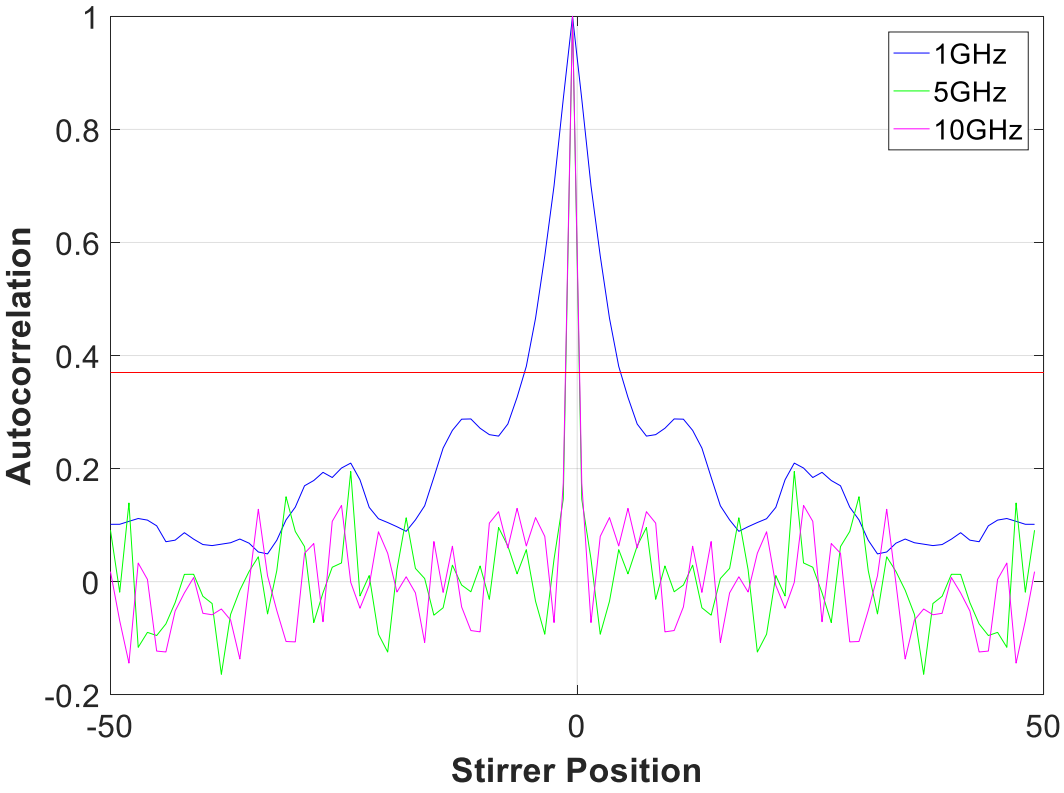

Figure 2.2: Autocorrelation in a small reverberation chamber over stirrer position

For frequency stirring, the positions of mechanical stirrer are replaced by the number of samples the data is being averaged over.

$$N_{freq} = \frac{\Delta f}{B_c} \qquad \textbf{(2.6)}$$

Here, Δf is the frequency size of the average window applied to the data and B_c is the frequency window required for 1/e drop in the autocorrelation. If both mechanical

and frequency stirring are applied to one measurement the total number of independent samples, N, is given by (2.7).

$$N = N_{mech} \times N_{freq} \quad \textbf{(2.7)}$$

2.2.6. Rician K-Factor

The Rician K-factor is the ratio of unstirred to stirred energy in a chamber [18]. Energy is unstirred when there is a direct path from antenna to antenna in a chamber and energy is stirred when there is an indirect path from antenna to antenna. In order to get good field statistics the unstirred energy in an RC should be reduced as much as possible [21].

The Rician K-factor can be calculated using (2.8). This is one of the measures of quantifying how well an RC is working; a low Rician K-factor indicates a well stirred chamber. The numerator of the equation gives the unstirred component of S_{21}. This is the magnitude of S_{21}squared, where $S_{21}$is measured between two antennas in a RC averaged over a number of stirrer positions. The denominator gives the stirred component of S_{21} by subtracting the unstirred component of S_{21} from the overall S_{21}. The brackets indicate averaging over stirrer positions.

$$K = \frac{|\langle S_{21} \rangle|^2}{\langle |S_{21} - \langle S_{21} \rangle|^2 \rangle} \quad \textbf{(2.8)}$$

2.2.7. Q Factor

The Q factor of an RC is the ratio of stored energy to lost energy in the chamber. It is defined as follows:

$$Q = \frac{maximum\ stored\ energy}{average\ power\ loss} = \frac{\omega \langle U_s \rangle}{\langle P_d \rangle} \quad \textbf{(2.9)}$$

Where ω is angular frequency (2πf), U_s is stored energy and P_d is average power dissipated. The brackets indicate averaging over stirrer positions. The following simple equation can be used to calculate the Q factor of an empty, ideal RC [8]:

$$Q = \frac{3V}{2S\delta} \tag{2.10}$$

In this equation, V is the volume of enclosure, S is the surface area and δ is the skin depth of the material. The skin depth of a material is the distance a wave has to travel through a material to be reduced by a value of 1/e and can be calculated as follows:

$$\delta = \sqrt{\frac{1}{\pi f \sigma \mu}} \tag{2.11}$$

Here, f is frequency, σ is the conductivity of the RC wall material and μ is the permeability of the RC wall material. The actual skin depth value will be different as the equation assumes that chamber is completely empty and has no apertures. This method also assumes that the reverberation chamber has highly conducting walls. The actual Q factor has several different contributions [5]. This is discussed in Section 2.5 where power balance modelling is introduced.

2.2.8. University of York Applied Electromagnetics Group Reverberation Chambers

There are two RCs used for the work described in this thesis.

2.2.8.1. Large Reverberation Chamber

The large RC has dimensions of 4.7m x 3m x 2.37m and a large paddle stirrer. A photograph of the large RC is shown in Figure 2.1. There are two bulkhead connection panels which are used to connect the internal test equipment to the equipment outside the chamber. The LUF of this chamber is approximately 180 MHz and the size of this chamber means that it was only used for the shielding effectiveness measurement of enclosures.

Measurements in the large RC were taken using a blade antenna. The blade antenna, shown in Figure 2.3, has a frequency range of 200MHz to 26GHz [24]. The blade antenna ground plane is mounted on the RC wall by several magnets and is positioned facing a corner of the RC in order to minimise direct paths to other antennas in the chamber.

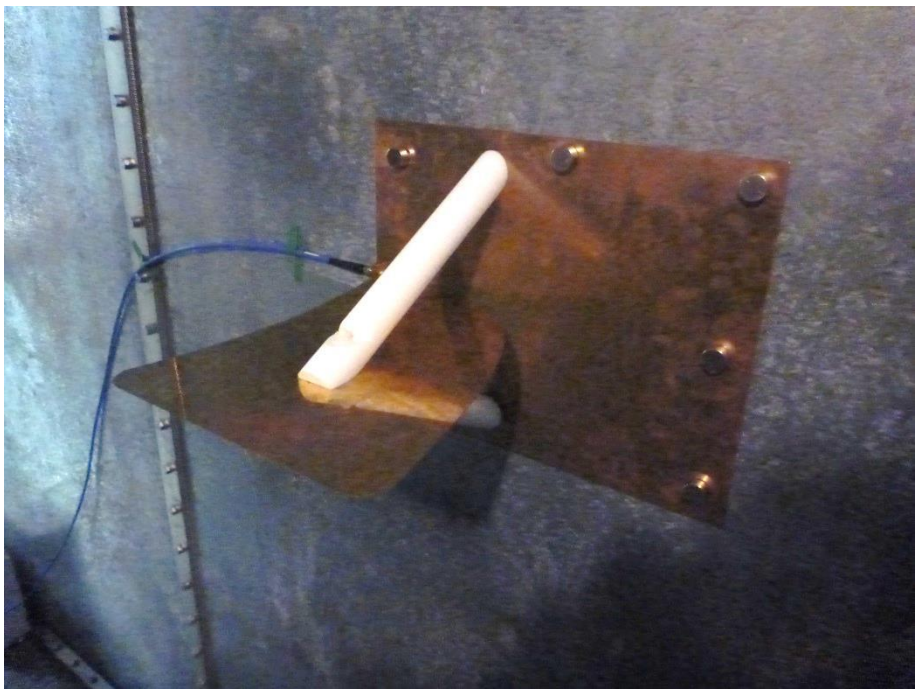

Figure 2.3: Photo of blade antenna inside the large RC

2.2.8.2. Small Reverberation Chamber

The small RC is constructed from brass and has dimensions of 0.8m x 0.7m x 0.6m and is located inside the large chamber. A photograph of the inside of the chamber is shown in Figure 2.4. A small paddle stirrer can be placed in the bottom of the chamber. It is accessed by top hatch and bulkhead connections are used to connect to equipment outside of the chamber. The LUF of this chamber is approximately 900 MHz.

The antennas used with this chamber were small 'snake' broadband monopoles which are shown in Figure 2.5 and mounted on sub miniature version A (SMA) bulkhead jacks. The overall length of each antenna is 80mm and the width is 10mm. The antennas have been folded in order to reduce their size and when folded have dimensions of 60mm x 10mm x 6mm. The antennas are placed in different corners of the RC and are cross polarised in order to reduce the unstirred component of the scattering parameter between the antennas, S_{21}, in the chamber.

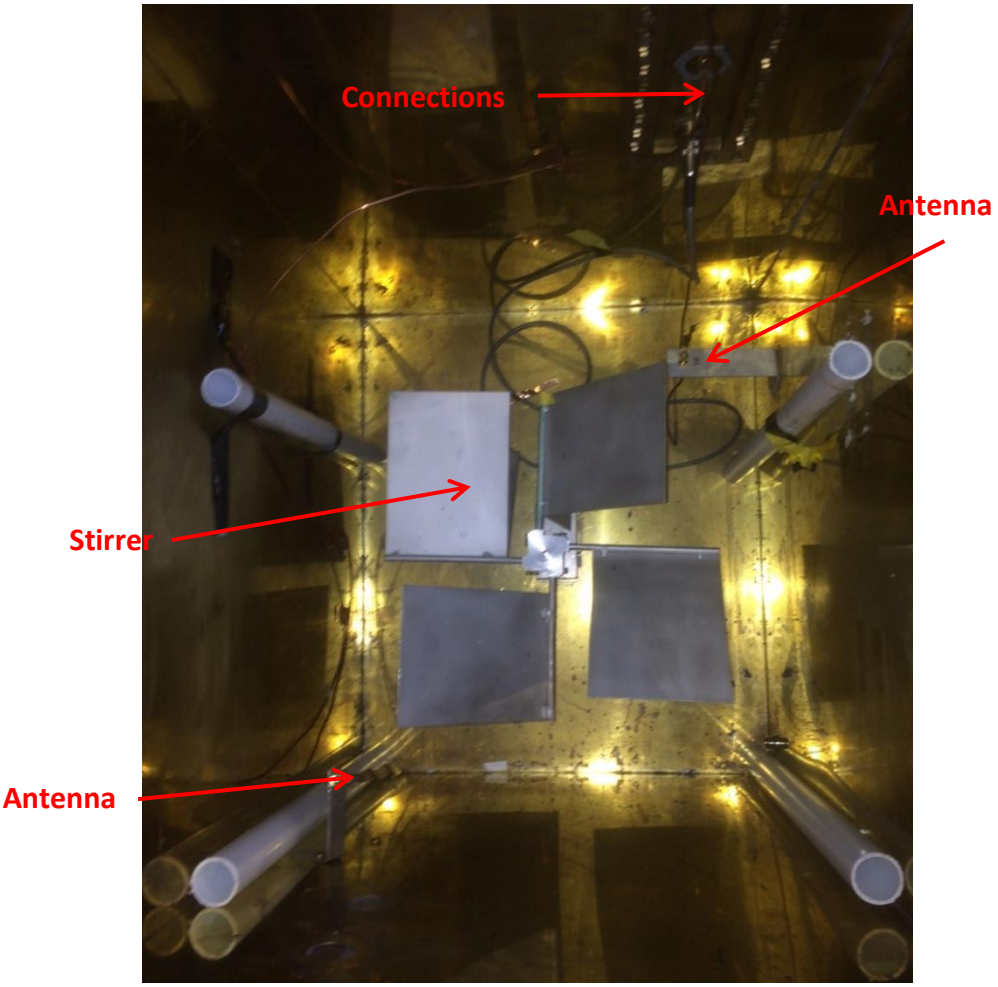

Figure 2.4: A photograph looking down into the small reverberation chamber. The stirrer can be seen in the centre of the chamber, antennas nearer the walls and the connector panel in the chamber wall. The four white struts are used to support a sheet of polystyrene which the EUT is placed on.

Figure 2.5: A photograph of the monopole antennas used in the small reverberation chamber

2.3. Shielded Enclosures

The first part of this chapter discussed reverberant environments such as reverberation chambers. The theory of reverberant environments is also applicable to shielded enclosures as at high enough frequencies the EM environment inside the enclosure will become reverberant. RCs and shielded enclosures can be similar in construction and it is important to know the amount of EM energy the chamber or enclosure is capable of attenuating. This attenuation is known as shielding effectiveness (SE). Unlike RCs, shielded enclosures tend to have significantly more areas where radiation can escape, such as apertures, cable connections and cooling measures which reduces the SE. The second part of this chapter reviews the theory of shielded enclosures and shielding effectiveness.

2.3.1. Shielding Effectiveness

Shielding effectiveness is the measure of how well an enclosure (or material) protects equipment from EM fields. The most common and simplest equations used to calculate SE are equations (2.12) and (2.13).

$$SE = 20 * log_{10}\left(\frac{E_0}{E_S}\right) dB \quad \textbf{(2.12)}$$

$$SE = 20 * log_{10}\left(\frac{H_0}{H_S}\right) dB \quad \textbf{(2.13)}$$

In these equations E_0 and H_0 are the electric field and magnetic field without the enclosure in place and E_S and H_S are the electric field and magnetic field with the shielding in place. SE is almost always stated in decibels, dB.

The equations above are simple to calculate but they have several disadvantages. The field may vary significantly throughout the enclosure due to it acting like a reverberation chamber at high frequencies. As discussed previously (Section 2.2), standing wave patterns can be produced in enclosures which mean the field strength changes throughout the enclosure. In this case, the field at several positions inside the enclosure needs to be measured and then averaged to get a more accurate SE

value at each frequency. Another factor that may affect the SE is the polarisation of any antennas inside the enclosure.

Generally, the SE of an empty enclosure is calculated. As contents inside an enclosure may absorb some of the energy this could change the SE of that enclosure. It is important to have an accurate value for the SE of an enclosure as if SE is either under or overestimated then too little or too much shielding could be used. If too little shielding is used then the equipment may not work in its required EM environment. If too much shielding is used this will add unnecessary cost, space and weight to the equipment.

2.3.2. Shielding of Materials and Enclosure Theory

Schelkunoff [25] developed a wave impedance theory which can be used to calculate the SE of an infinite sheet. In this model, the reflections from the material surface due to impedance mismatch and the absorption by the material due to the skin effect are used to calculate the total transmitted wave.

Although the Schelkunoff model is useful for enclosures which are very large compared to the wavelength, λ, a model for an enclosure rather than a sheet of material is of more practical use. Kaden [26] developed a model for the calculation of a finite enclosure which shows the effect the size and shape of an enclosure has on SE. This work assumed an ideal enclosure, however, practically it is necessary to take into account apertures and joints when calculating SE.

At DC, the SE of a metallic enclosure is infinite for electric (E) fields and zero for magnetic (H) fields. At low frequencies, an external E field will cause charges on the enclosure to appear. These charges create an E field which then cancels out the external E field. As the frequency increases, the charges find it more difficult to cancel out the external field and the SE of the enclosure decreases. The SE of an enclosure can be increased by using a thicker material to construct it from; a thicker material will attenuate more of the field. The higher the conductivity of the material the higher the SE will be.

For an enclosure to have magnetic SE at low frequencies it must be made from ferromagnetic materials. An external H field causes eddy currents to flow on the enclosure. These currents create a H field which cancels out the external H field. As the frequency of the field increases the SE of the enclosure also increases. Like E field SE, at lower frequencies, the SE against H fields can be increased by increasing the thickness of the enclosure material. The higher the permeability of the material the greater the SE the enclosure will provide.

At high frequencies, the dimensions of the enclosure, and its apertures, start to become comparable to the wavelength of the field. At these frequencies, the losses through the apertures in an enclosure are much greater than those in the enclosure material. The different loss mechanisms are explained in Section 2.5; Figure 2.12 shows the aperture losses for an enclosure are greater than the wall losses in the frequency range 1GHz to 20GHz. At high frequencies, the skin effect (see section 2.2.7) is the mechanism by which the external E field is attenuated.

At high frequencies, shielded enclosures are reverberant environments, as described in the above sections. The field at different positions in the enclosure will be different; therefore the SE of the enclosure will be different depending on the position in the enclosure.

2.3.3. Shielding Effectiveness Measurements

In this section, an SE measurement of a shielded enclosure is made in an RC. Alternative methods of SE measurements are also presented, both using RCs and other test facilities.

2.3.3.1. Shielding Effectiveness Standards

There are a number of current standards for the measurement of shielding effectiveness. IEEE 299 is the IEEE Standard Method for Measuring the Effectiveness of Electromagnetic Shielding Enclosures [1]. This is the standard used for large enclosures when the sides of the enclosure are greater than 2m in length. IEEE 299.1 is the IEEE Standard Method for Measuring the Shielding Effectiveness of Enclosures and Boxes Having all Dimensions between 0.1m and 2m [22]. The original IEEE 299

standard focuses on large enclosures such as RCs. As smaller enclosures have become more prevalent IEEE 299.1 was developed so that accurate measurements could be made of these smaller enclosures. As IEEE 299 looks at large shielded enclosures, such as reverberation chambers, the effect of contents in these enclosures was not considered as they took up such a small part of the overall chamber volume. This has been carried on in IEEE 299.1 where the main part of the standard only accounts for empty enclosures; there is, however, an annex on the effect of contents on SE.

2.3.3.2. Reverberation Chamber Measurements

This section describes a SE measurement carried out in an RC. A photograph of the enclosure under test is shown in Figure 2.6. The enclosure has dimensions of 0.3m x 0.29m x 0.12m and is constructed from brass. One side of the enclosure was fitted with a plate with an aperture of dimensions 200mm x 200mm. The enclosure and its lid are fitted with fingerstock to ensure a good EM seal around the lid of the enclosure. A monopole antenna can be positioned in seven places on the lid of the enclosure, Figure 2.6 shows the antenna in position 2.

Figure 2.6: Photograph of the enclosure under test inside the large reverberation chamber

Figure 2.7 shows the RC setup for measuring the SE of an enclosure. The measurement was carried out in the UoY AEG large RC. The mechanical stirrer, controlled by a PC external to the chamber, was rotated and stopped at 100 equally stepped positions over one full rotation. No mechanical stirrer was used inside the enclosure under test. A Vector Network Analyser (VNA) was used to collect a full set of S-parameters between the blade and monopole antenna. The measurement was carried out over the frequency range 1GHz – 20GHz at 10,001 measurement points. The sweep time was 2.5s. A moving average filter with a BW of 100MHz was applied to the data after it had been collected to provide frequency stirring.

Stirring inside a shielded enclosure can be used in addition to, or instead of, the main mechanical stirrer in the chamber [18]. Frequency stirring has a useful advantage over other stirring methods as it does not require a physical stirrer within the enclosure under test. A mechanical stirrer takes up space in the enclosure which may be a problem if the enclosure has contents.

Two measurements are required to calculate SE. One with the enclosure in place and the monopole antenna positioned inside and a second, reference measurement with the enclosure removed from the set up. The SE can be calculated using these two sets of measurements using equation (2.14).

$$\boldsymbol{SE = 20\log_{10}\frac{\langle|S_{21\,ref}|^2\rangle}{\langle|S_{21\,enc}|^2\rangle}} \qquad \textbf{(2.14)}$$

The results of the measurement are shown in Figure 2.8. At frequencies below 3GHz, the results should be ignored. The LUF (see section 2.2.3) of the enclosure is 3GHz and so as the enclosure is not properly reverberant the results are not credible. Above 3GHz, the SE varies between 0dB and 8dB. The SE of this enclosure is low as the enclosure is empty and has a large aperture. Section 2.4 of this chapter discusses what happens to the SE of the enclosure when absorbing contents are included in the enclosure.

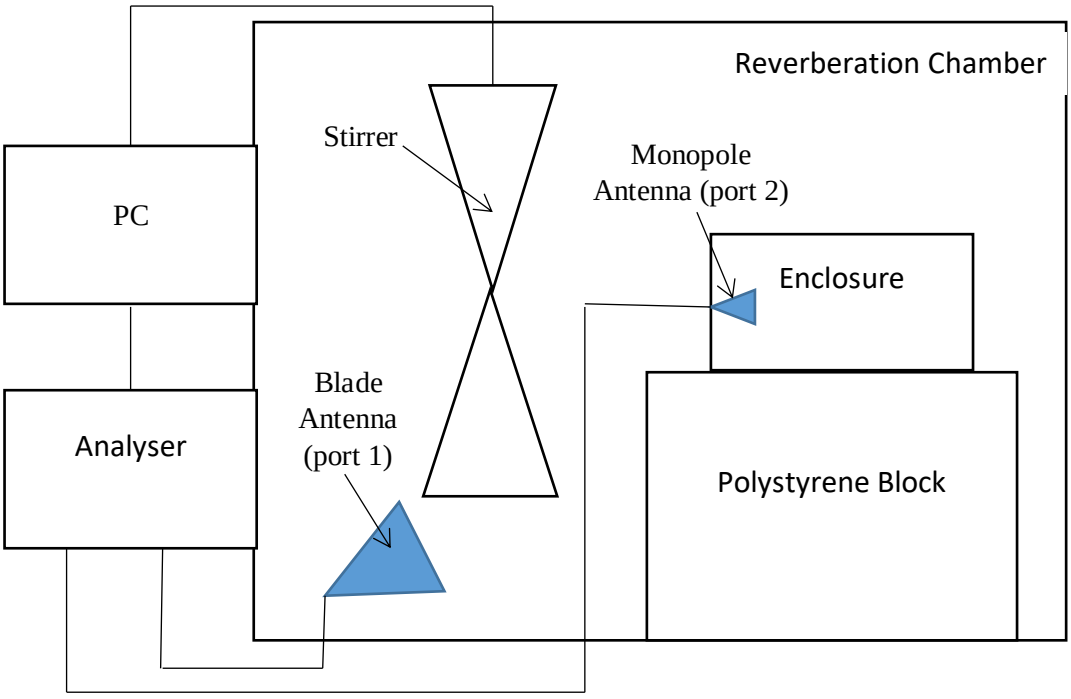

Figure 2.7: Diagram of the SE measurement setup of an enclosure in the large reverberation chamber

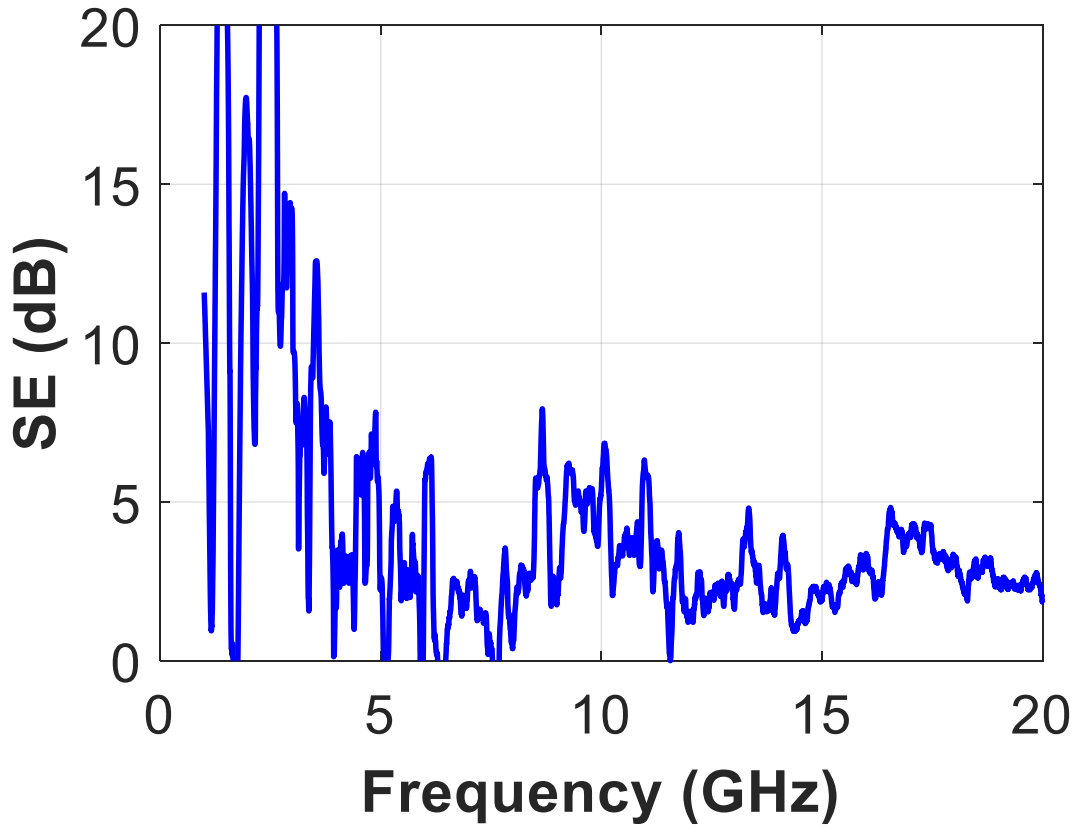

Figure 2.8: Graph of the measured shielding effectiveness of an empty enclosure with a single aperture

2.3.3.3. Anechoic Chamber Measurements

Anechoic chambers can also be used to measure the SE of enclosures. An anechoic chamber absorbs EM fields in the materials which line its walls. This is to simulate an open area as there are no reflections from the absorbing walls. Armstrong [27] discusses using an anechoic chamber to calculate the SE of an enclosure by measuring its Q factor. This method has the advantage of requiring only one set of measurements (rather than the two sets of measurements needed in other methods; with and without the enclosure) and the author states it is most useful for enclosures with dominant aperture loss. A comparison between RCs and anechoic chambers is presented in [28].

Anechoic chambers are sometimes preferred to RCs as the results are easier to repeat as small variations in RCs can cause large variations in the field. Disadvantages of anechoic chambers are that they can be much more time consuming as multiple test positions and polarisations are required as the waves only come from one direction at a time. RCs are also capable of much greater field strengths and so higher levels of shielding can be measured.

2.3.4. Analytical Calculations of Shielding Effectiveness

Performing measurements to obtain the SE of an enclosure can be time-consuming and requires specialist test equipment. Analytical methods, such as those created by Robinson in [29], are an alternative method of finding the SE of an enclosure. Robinson's method calculates the SE of an enclosure with a rectangular aperture using a circuit model. This method was developed further in [30] to include circular and multiple apertures and enclosure contents. Nie and Du [31] have produced a more accurate circuit model for when the aperture is positioned centrally in the enclosure.

Hill [5] was the first to describe the power balance model which can be used to calculate SE of enclosures at higher frequencies. This technique is discussed in Section 2.5. Solin [33] used Hill's method as a comparison against his analytical solution for the SE of an enclosure with an aperture. Solin has also published other formulas which can be used to calculate SE [34][35].

The methods described above have generally been used for empty enclosures with no contents, such as PCBs, inside. The next section looks at how the contents can affect the SE of an enclosure.

2.4. Shielding Effectiveness of Populated Enclosures

The previous section discussed the measurement of shielding effectiveness for empty enclosures. This section looks at how contents can affect the SE of enclosures and the methods available that take this into account. This is an area of research which is not as well understood and not as widely researched as the SE of empty enclosures. Due to this when designing and buying enclosures for equipment, the contents of the enclosure are not often taken into account.

Introducing contents, such as PCBs, into an enclosure reduces the EM field inside the enclosure as they absorb energy. Decreasing the internal field increases the SE of the enclosure. This could lead to over shielding the contents as the SE of the populated enclosure has been underestimated. A measurement of SE is first described to show the effect contents can have on the SE.

2.4.1. Measurements in Reverberation Chambers

The same set up, test equipment parameters and method described in Section 2.3.3.2 were used to make a measurement of the same enclosure with a reco inside. The reco is a set of representative contents designed to have the same absorption as a PCB. Recos are discussed in Section 2.4.2 below and the recos used in the work described in this thesis are described fully in Chapter 5. The reco used for this measurement is a single sided reco with eight pieces of absorber on one side.

When making the measurement of an enclosure the reco was placed on a block of polystyrene in the centre of the enclosure. A photograph of this set up is shown in Figure 2.9.

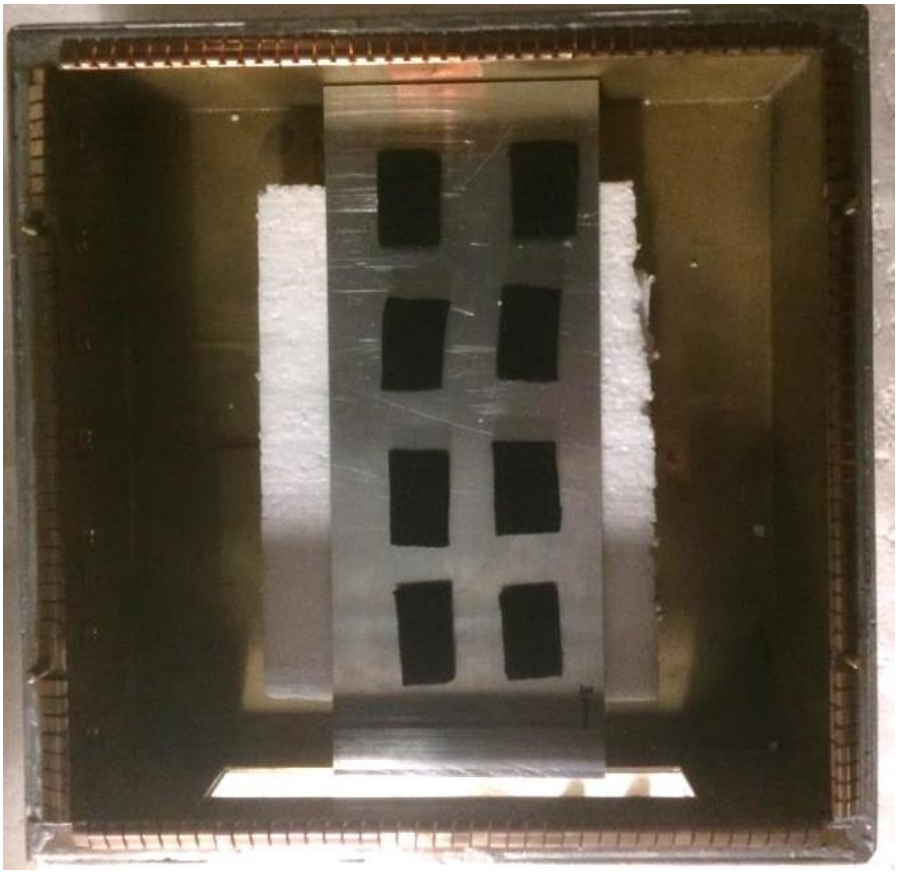

Figure 2.9: Photograph of the reco inside the enclosure

Once the measurement had been carried out Equation 2.7 was used to calculate the SE. The results of this measurement are shown in Figure 2.10 with the empty enclosure SE result for comparison.

The SE of the enclosure with the reco inside varies between approximately 10dB and 18dB above 3GHz. The SE is between 12dB and 14dB for the majority of this frequency range. Including the reco in the enclosure has increased the SE by approximately 10dB compared to the empty enclosure. This is a very significant difference which shows that the contents of an enclosure need to be considered when designing equipment.

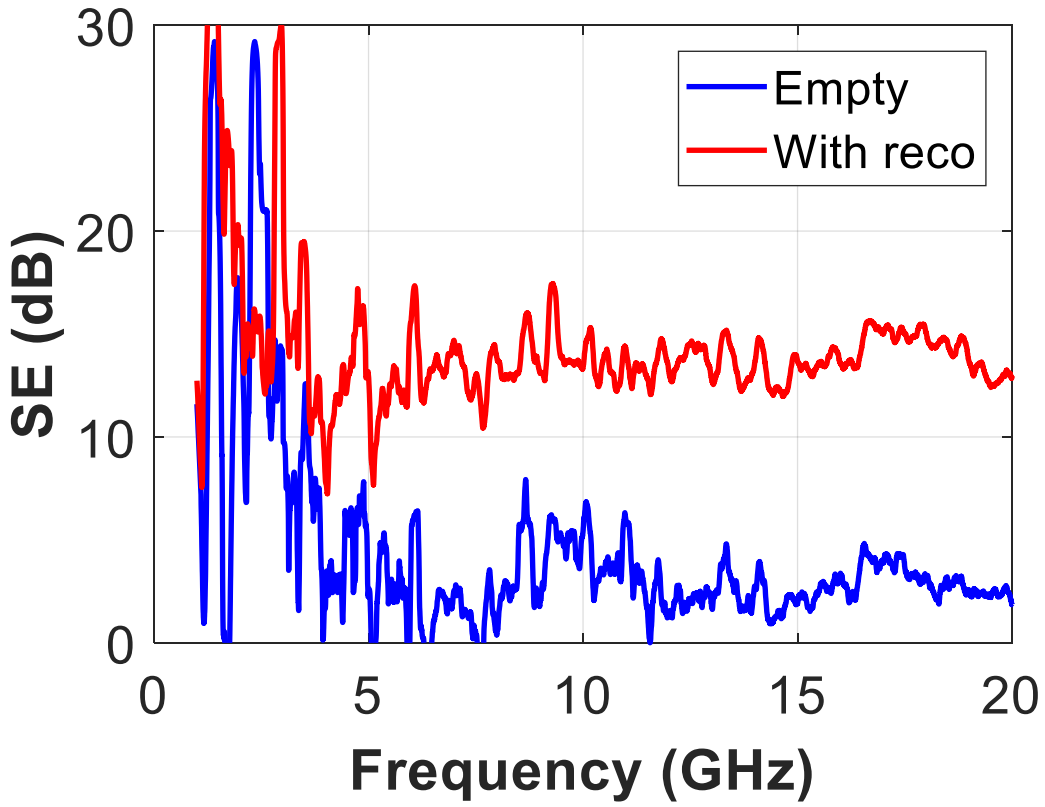

Figure 2.10: Shielding effectiveness of an enclosure with and without a reco inside

2.4.2. Representative Contents

When making SE measurements of enclosures a set of representative contents (recos) can be used as a test PCB or surrogate enclosure contents. They are designed to have properties, such as absorption, of a general PCB of the type that is of interest. Recos may also be useful for numerical and analytical techniques where simplified contents can be used for ease of calculation. An advantage of having a well-designed set of recos is that they can be used for a wide variety of testing rather than only for one specific EUT.

The Applied Electromagnetics Group (AEG) at the University of York (UoY) has considered the effect of enclosure contents on shielding in a number of different papers. The shielding power ratio was defined to provide a measurement to show the SE of an enclosure whilst also taking into account its contents [36]. A set of recos were used and this measurement technique could be carried out in both an anechoic

and reverberation chamber. The same authors also proposed the shielding aperture which is defined as the ratio of power absorbed by the enclosure contents to the power incident on them [37]. This means that the absorption of the enclosure contents (in this case a set of recos) is included in the results. This method takes longer to carry out than other methods and the paper presents results up to 1GHz only. The AEG have used a set of instrumented recos to carry out SE measurements of populated enclosures in both reverberation and anechoic chambers [28]. One set of instrumented recos consisted of a groundplane and carbon loaded foam which was instrumented with magnetic surface field probes. A second set of recos consisted of a ground plane with carbon loaded foam but used a comb generator as an emission source which could be moved around the board. In these papers they show that the position of the contents within the enclosure has an effect on SE.

Section 2.3.4 alluded to using Hill's power balance model (PWB) to calculate the SE of an enclosure. As well as including factors such as enclosure wall losses and apertures, the contents of an enclosure are also considered. The next section describes PWB in detail and includes an example SE calculation of an empty and populated enclosure.

2.5. Power Balance Modelling

Hill's power balance method states that the energy that enters an enclosure must equal the energy dissipated in the four loss mechanisms which are described below [5]. Using this power balance method allows the field strength in a cavity to be calculated. The SE can then be calculated using equation (2.15).

$$SE = 10\log_{10}\left(\frac{2\pi V}{\sigma_t \lambda Q}\right) dB \quad \textbf{(2.15)}$$

In this equation:

- V enclosure volume
- σ_t transmission cross section of apertures (see Section 2.5.2)
- λ wavelength
- Q Q factor

If there is a significant amount of absorption by the contents of the enclosure (or by the other loss mechanisms) there will be a low Q factor. This will result in a higher shielding effectiveness value which we have seen in the measurements carried out earlier in this chapter. Hill [5] models the total Q factor of an enclosure as a summation of the individual Q factors of each loss mechanism as shown in (2.16).

$$Q^{-1} = Q_{wall}^{-1} + Q_{object}^{-1} + Q_{aperture}^{-1} + Q_{antenna}^{-1} \quad \textbf{(2.16)}$$

Each of these individual Q factors relate to the following:

- Q_{wall} Q factor of the loss mechanism of the cavity walls
- Q_{object} Q factor of the power absorbed in lossy objects in the enclosure
- $Q_{aperture}$ Q factor of aperture leakage
- $Q_{antenna}$ Q factor of power dissipated in the loads of receiving antennas

Each of these Q factors can be calculated using equations provided in Hill's paper [5]. However, it may be considered easier to consider these loss mechanisms in terms of

absorptions rather than Q factors. In [46], Junqua provides equations for each of the loss mechanisms in an enclosure, these are discussed in the next sections.

2.5.1. Wall Losses in a Metallic Cavity

To calculate the wall losses in a metallic enclosure the following equation [46] is used:

$$\sigma_{walls}^{a} = \frac{4A}{3c}\sqrt{\frac{\pi f \mu_r}{\mu_0 \sigma_w}}\left[1 + \frac{3\lambda A}{32V}\right] \quad \textbf{(2.17)}$$

In this equation:

- σ_{walls}^{a} absorption loss in the enclosure walls
- A surface area of the enclosure walls
- c speed of light in a vacuum
- f frequency
- μ_r relative permittivity of the enclosure wall material
- μ_0 permittivity of free space
- σ_w^{cond} conductivity of the enclosure wall material
- λ wavelength
- V enclosure volume.

2.5.2. Transmission Cross Section of Apertures

The losses due to the transmission cross sections (TCS) of any apertures are a significant form of loss in the enclosure. An ONERA report [46] provides equations to calculate the cross section of apertures in an enclosure. The equations are used depending on whether the aperture is considered electrically large or small compared to the wavelength.

2.5.2.1. Low Frequency Transmission Cross Section of an Aperture

For electrically small apertures a low frequency transmission cross section is used. The ONERA report provides a number of different equations for different shapes of apertures. For this thesis, only rectangular apertures are considered. The equation for the transmission cross section of an aperture is given in(2.18).

$$\sigma_{aperture}^{t} = \frac{2}{9\pi}\left(\frac{2\pi}{\lambda}\right)^{4}\left(\alpha_{e}^{2} + \alpha_{mxx}^{2} + \alpha_{myy}^{2}\right) \quad \textbf{(2.18)}$$

For a rectangular aperture, the polarizability tensors in an infinite ground plane are given by α_e , α_{mxx} and α_{myy}.

$$\alpha_{e} = \frac{S^{\frac{3}{2}}}{3\sqrt{\pi}E(e)}\frac{b}{a} \quad \textbf{(2.19)}$$

$$\alpha_{mxx} = \frac{S^{\frac{3}{2}}e^{2}}{3\sqrt{\pi}\big(K(e) - E(e)\big)}\left(\frac{a}{b}\right)^{\frac{3}{2}} \quad \textbf{(2.20)}$$

$$\alpha_{myy} = \frac{S^{\frac{3}{2}}}{3\sqrt{\pi}}\frac{e^{2}\left(\frac{a}{b}\right)^{\frac{3}{2}}}{\left(\frac{a}{b}\right)^{2}E(e) - K(e)} \quad \textbf{(2.21)}$$

The equations for e, $E(e)$ and $K(e)$ are given in (2.22), (2.23)and (2.24).

$$e = \sqrt{1 - \left(\frac{b}{a}\right)^{2}} \quad \textbf{(2.22)}$$

$$K(e) = \int_{0}^{\frac{\pi}{2}} (1 - e^{2}\sin^{2}\theta)^{-\frac{1}{2}}.d\theta \quad \textbf{(2.23)}$$

$$E(e) = \int_{0}^{\frac{\pi}{2}} (1 - e^{2}\sin^{2}\theta)^{\frac{1}{2}}.d\theta \quad \textbf{(2.24)}$$

2.5.2.2. High Frequency Transmission Cross Section of an Aperture

The high frequency TCS of an aperture is calculated using equation (2.25). The enclosure aperture used in the work covered in this thesis is electrically large at the frequencies of interest. Therefore, this equation is used for all PWB calculations.

$$\sigma_{aperture}^{t} = \frac{A_{aperture}}{4} \quad \textbf{(2.25)}$$

In equation (2.25):

- $\sigma_{aperture}^{t}$ transmission cross section of the aperture
- $A_{aperture}$ area of the aperture

2.5.3. Antenna Losses

When carrying out a measurement an antenna will need to be located in the enclosure. Therefore, to be able to compare a measurement with a PWB the losses for a receiving antenna need to be included in the model.

Equation (2.26) is used to calculate the loss due to the antenna in the enclosure [46].

$$\sigma_{ant} = \frac{\lambda^2}{8\pi}(1 - |S_{11}|^2) \quad \textbf{(2.26)}$$

In this equation:

- σ_{ant} Coupling cross section of the antenna
- S_{11} reflection coefficient of the antenna
- $(1 - |S_{11}|^2)$ This term is the mismatch factor for the antenna

The reflection coefficient, S_{11}, used is the measured S_{11} collected when carrying out the SE measurements described in this thesis. The reflection coefficients have been interpolated using the interp1 Matlab function as the data points in the measured frequency range are different to those in the modelled frequency range.

2.5.4. Absorption Cross Section of Objects

The absorption cross section (ACS) of objects is left to the last section as this subject is the main focus of this thesis. Knowledge of the ACS allows the energy absorbed by an object to be quantified. The ACS of a lossy object is the surface area of a perfectly absorbing object which would absorb the same amount of energy as the object being

considered. As it is a measurement of surface area the unit of ACS is m^2. Alternatively, it can be defined as the power absorbed by the object under test divided by the power density in the incident field. The ACS of a lossy object can be measured using a RC [4]. As this thesis considers the contents of shielded enclosures the lossy objects that will be considered are PCBs.

Usually ACS is measured or calculated for one object at a time. In real enclosures it is probable that there will be several PCBs stacked together in different parts of the enclosure. In this case, it is possible that the absorption of objects in the enclosure may change due to the proximity of other objects and the walls of the enclosures itself. In [4], Carlberg showed that the ACS of lossy objects is different when measured individually and in groups. Melia also comments in his thesis [42] that he observed changes in human body ACS when measuring in different positions (stood up, sat down etc). He attributes this to a shadowing effect as surface area is reduced and to using chairs made from different materials.

2.5.4.1. Measured ACS in a Reverberation Chamber Calculation

As the PCBs are being measured in a reverberation environment the average ACS shall be used. When measured in an RC the average ACS of an object is defined as the ratio of the average power absorbed to the average power density of the incident field and is calculated using (2.27),

$$\langle \sigma_a \rangle = \frac{\lambda^2}{8\pi}\left(\frac{1}{G_{wo}} - \frac{1}{G_{no}}\right) \qquad \textbf{(2.27)}$$

Where:

- $\langle \sigma_a \rangle$ average ACS of the object
- λ wavelength,
- G_{wo} mean net transfer function with the PCB
- G_{no} mean net transfer function without PCB (the reference measurement).

G_{wo} and G_{no} are calculated using equation (2.28):

$$G = \frac{\langle |S_{21}|^2 \rangle}{(1 - |\langle S_{11} \rangle|^2)(1 - |\langle S_{22} \rangle|^2)} \quad \textbf{(2.28)}$$

S_{21} is the transmission coefficient measured between two antennas in the reverberation chamber and S_{11} and S_{22} are the reflection coefficients of the two antennas. Since here we are interested in relative ACS measurements the radiation efficiencies of the antennas are assumed to be unity.

The brackets <…> in these equations indicate that averaging using mechanical or frequency stirring (or both) has been used during the measurement. In this thesis, the details of the stirring used for each measurement will be included in the relevant measurement descriptions.

2.5.4.2. Accuracy of ACS Measurements in a Reverberation Chamber

It is important to consider the accuracy of an ACS measurement in a RC. Carlberg's original paper [4] assumes a small relative error between G_{wo} and G_{no} which are also independent. This gives a measurement accuracy of:

$$\frac{\delta\langle\sigma_a\rangle}{\langle\sigma_a\rangle} = \frac{\sqrt{2}G_r}{(G_r - 1)}\frac{\delta G}{G} \quad \textbf{(2.29)}$$

With $\delta G/G = k/\sqrt{N}$, where k equals the number of standard deviations in the error and N is the number of independent samples in the averaged measurement. G_r is G_{no}/G_{wo}. This equation shows that the smaller the amount of energy absorbed by the EUT the greater the error as the difference between G_{wo} and G_{no} is smaller.

Flintoft et al [43] developed this calculation by including the loading effect of the object in the RC and the effect of the Rician K-factor. The K-factor is a measure of the non-stochastic energy in the measurement i.e. the energy which has not been stirred; either by the mechanical stirrer in the chamber or electronically using frequency stirring.

The equation used to calculate the uncertainty of an ACS measurement including the RC being loaded by an object is given in (2.30)

$$\alpha = \frac{L}{L-1}\sqrt{L^2 + \frac{1}{L^2}}\sqrt{\frac{1}{N_{ind}^{unloaded}}} \tag{2.30}$$

L is the chamber loading factor and is given by

$$L = 1 + \frac{\langle \sigma_{wo}^{a} \rangle}{\langle \sigma_{no}^{a} \rangle} \tag{2.31}$$

N is the number of independent samples in the measurement without an object in the RC. This was discussed in Section 2.2.5 of this thesis.

The effect of unstirred energy in the RC is calculated using (2.32).

$$\alpha = \frac{L}{L-1}\sqrt{\frac{1}{N_{ind}^{wo}} + K_{loaded}^2 + \frac{1}{L^2}\left(\frac{1}{N_{ind}^{no}} + K_{loaded}^2\right)} \tag{2.32}$$

In this equation K is the Rician K factor discussed in Section 2.2.6. This can be calculated using equation (2.33).

$$K = \frac{|\langle S_{21} \rangle|^2}{\langle |S_{21} - \langle S_{21} \rangle|^2 \rangle} \tag{2.33}$$

2.5.5. Power Balance Model of an Enclosure

The previous sections explained how to consider individual parts of an enclosure. This section will use these parts together to model a simple, single cavity enclosure with and without contents.

2.5.5.1. Single Cavity Enclosure

The first model presented is a simple single cavity enclosure. Although unlikely to be encountered in real engineering problems it is an important starting point to show how including a single PCB in an enclosure can affect the SE.

Empty Enclosure Model

A diagram of an empty metallic enclosure with a single aperture in one wall of the enclosure is shown in Figure 2.11. For the models presented it is assumed that the walls of the enclosure are metallic and have a small amount of loss.

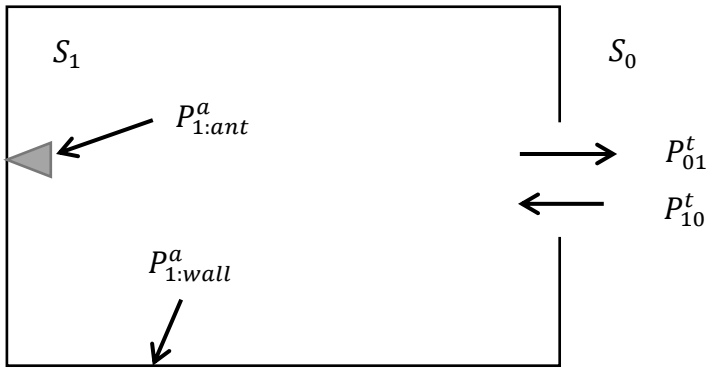

Figure 2.11: Empty metallic enclosure with a single aperture

In Figure 2.11, the symbols refer to the following:

- S_0 power density external to the enclosure
- S_1 power density internal to the enclosure
- $P^a_{1:wall}$ power absorbed by the inside of the enclosure wall
- P^t_{01} power transmitted from the inside to outside of the enclosure through the aperture
- P^t_{10} power transmitted from the outside to inside of the enclosure through the aperture

The power balance equation for cavity 1 is given in equation (2.34). This equation states that the power absorbed by the wall, $P^a_{1:wall}$, and the power that leaves the

enclosure through the aperture in the enclosure, P_{01}^{t}, is equal to the power that enters the enclosure through the aperture, P_{10}^{t}.

$$P_{1:wall}^{a} + P_{1:\text{ant}}^{a} + P_{01}^{t} = P_{10}^{t} \quad \textbf{(2.34)}$$

The power absorbed by the walls is given in equation (2.35). In this equation $\sigma_{1:wall}^{a}$ is the ACS of the enclosure walls.

$$P_{1:wall}^{a} = \sigma_{1:wall}^{a} S_1 \quad \textbf{(2.35)}$$

The power absorbed by the antenna inside the enclosure is given in equation (2.36). In this equation $\sigma_{1:ant}^{a}$ is the ACS of the antenna.

$$P_{1:\text{ant}}^{a} = \sigma_{1:\text{ant}}^{a} S_1 \quad \textbf{(2.36)}$$

Equations (2.37) and (2.38) define the power transmitted through the aperture in each direction. The transmission cross section (TCS) of the aperture, σ_{10}^{t}, is assumed to be the same in each direction.

$$P_{01}^{t} = \sigma_{10}^{t} S_1 \quad \textbf{(2.37)}$$

$$P_{10}^{t} = \sigma_{10}^{t} S_0 \quad \textbf{(2.38)}$$

Substituting the three equations for loss, (2.35), (2.36) and (2.37), into the power balance equation, (2.34), gives the equation in (2.39). As the SE of an enclosure can be defined as the ratio of the power density internal to the enclosure to the power density external to the enclosure the SE of the enclosure can then be calculated using equation (2.40).

$$\sigma_{1:wall}^{a} S_1 + \sigma_{1:\text{ant}}^{a} S_1 + \sigma_{10}^{t} S_1 = \sigma_{10}^{t} S_0 \quad \textbf{(2.39)}$$

$$SE = \frac{S_1}{S_0} = \frac{\sigma_{1:wall}^{a} + \sigma_{1:\text{ant}}^{a} + \sigma_{10}^{t}}{\sigma_{10}^{t}} \quad \textbf{(2.40)}$$

Equation (2.40) shows that as the absorption of the walls increases the SE of the enclosure increases.

Empty Enclosure Calculation

Equation (2.40) can be used to calculate the SE of an enclosure. The parameters of this enclosure have been chosen to match the enclosure described and measured in Section 2.3.3.2. The results of the two methods can then be compared.

To calculate the SE of the enclosure using equation (2.40) the TCS of the aperture and the ACS of the enclosure walls are calculated using equations (2.17) and (2.23).

To calculate the surface area of the walls for use in equation (2.17) the area of the aperture in the enclosure was subtracted from the total surface of the enclosure. The conductivity of brass is approximately 1.67×10^7S/m. However, a value of 1.67×10^6S/m was used in the calculation. Past experience of measurements made in metallic enclosures has shown that the wall conductivity can be reduced by a factor of 10. The conductivity is adjusted to fit the cavity wall loss result. The reason for this discrepancy has not been widely researched but it is suspected that surface effects, such as surface roughness, could be the cause in the differences in the conductivity. Benson [44] has previously shown that surface roughness can affect the attenuation seen in waveguides.

Figure 2.12 shows the calculated values for the individual losses due to the wall, the antenna and the aperture in the example enclosure. As the enclosure walls are metallic they have a much lower loss than the aperture. As the high frequency TCS approximation is used for the aperture the TCS remains constant throughout the frequency range at 1.25×10^{-4}m^2. The loss due to the antenna is small compared to the enclosure walls and antenna.

Figure 2.13 compares the SE calculated using the PWB equations above and the measured SE results presented in Section 2.3.3.2.

The SE of the modelled enclosure is between 2dB and 5dB. Over the frequency range the SE increases; this is due to the absorption of the walls increasing over the

frequency range, as shown in Figure 2.12. As the losses in the model are relatively small the SE is correspondingly small. Although the measured SE shows more variation the two methods of obtaining the SE show good agreement above 5GHz.

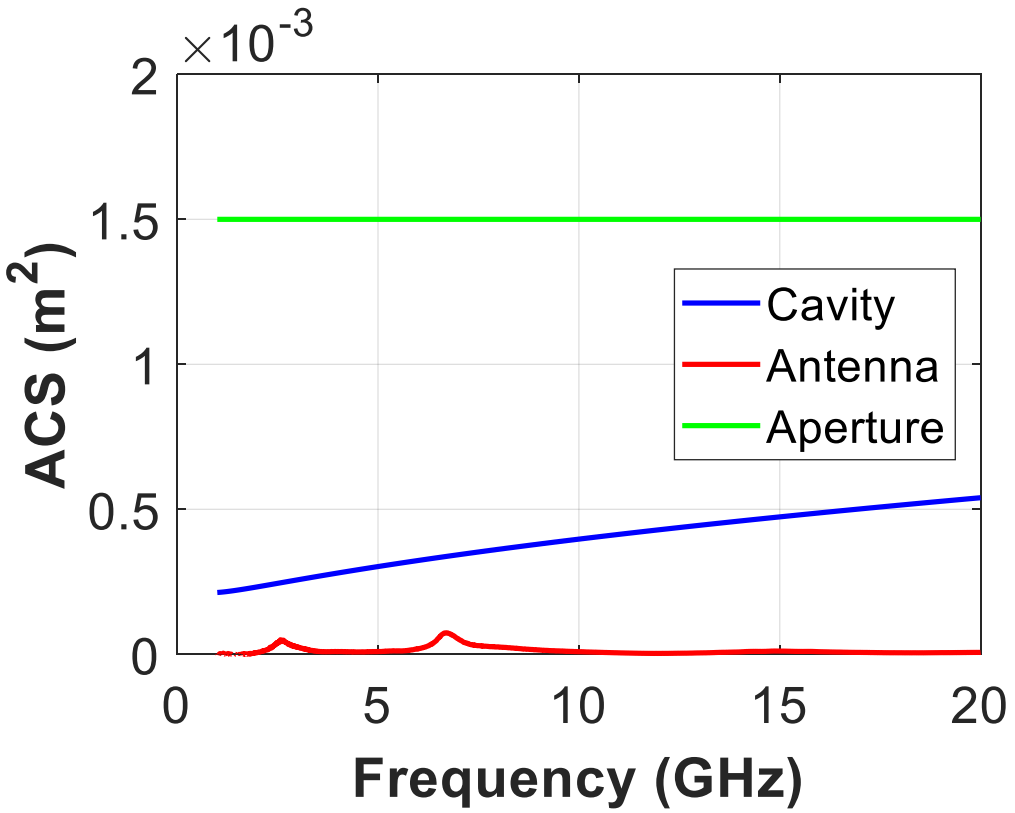

Figure 2.12: Wall, antenna and aperture losses in an empty brass enclosure with single aperture.

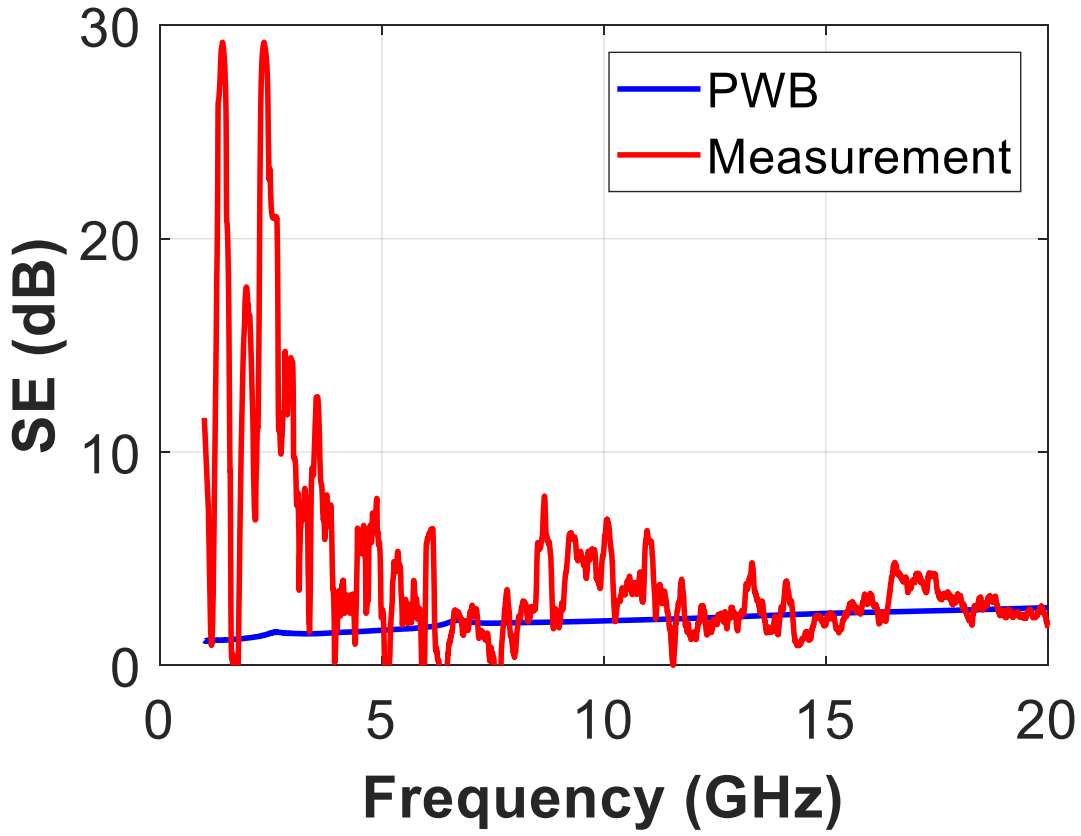

Figure 2.13: Comparison of PWB modelled and measured SE of a single cavity empty enclosure with an aperture.

Enclosure Containing a PCB

The next configuration builds on the previous empty model by including a single reco positioned centrally in the enclosure away from the enclosure walls. A diagram of the PWB is shown in Figure 2.14. In this model $P^a_{1:reco}$ is the power absorbed by the reco and $\sigma^a_{1:reco}$ is the ACS of the reco.

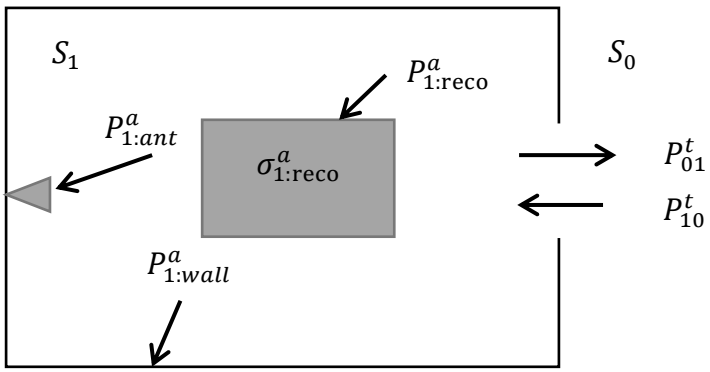

Figure 2.14: Power balance model of an enclosure with aperture and single, central reco positioned centrally

Using the same method of substituting the equations for the loss mechanisms in the enclosure into the power balance equations used in the previous section, the absorption cross section of the reco is summed into the numerator of the expression.

$$SE = \frac{S_1}{S_0} = \frac{\sigma^a_{1:wall} + \sigma^a_{1:\text{ant}} + \sigma^a_{1:\text{reco}} + \sigma^t_{10}}{\sigma^t_{10}} \qquad \textbf{(2.41)}$$

Equation (2.41) shows that adding a reco into the model increases the numerator giving a greater SE. As the ACS of the reco increases the SE of the enclosure will also increase. In order to calculate the SE using this equation, the ACS of the reco, PCB or object inside the enclosure needs to be found. The following chapters of this thesis, investigate the ACS of PCBs and recos and how the ACS is used to predict the SE of an enclosure with contents in using the PWB.

The two models presented in this chapter are very simple. Junqua et al. [46] use a power balance method to model multiple cavities. Their work shows that a network

formulation of the power balance method is a useful tool for high frequency analysis of enclosures with more than one cavity. Hill's original work considered single cavity problems. However, a more realistic enclosure may be separated into different cavities by enclosure contents, such as PCBs, or by partitions which form the internal structure of the enclosure itself. The multi-cavity power balance model can be used to calculate the SE of these more complex enclosures.

2.6. Summary

This chapter provided background information on the subject of reverberant environments and shielded enclosures. The chapter introduced the theories and concepts that will be used throughout this thesis.

The SE of an enclosure with and without contents was measured and the results presented. Including a reco in the enclosure increased the SE by 10dB. A PWB of this enclosure was also created. The SE of the empty enclosure calculated using the PWB showed good agreement with the measured SE. In order to calculate the SE of an enclosure with contents, further information on the ACS of objects is required.

In the measurement described in Section 2.4.1 the reco was positioned in the centre of the enclosure. In a 'real' equipment enclosure, PCBs and other contents may be positioned stacked together and close to the enclosure walls. The next chapter of this thesis investigate the measurement of ACS of PCBs and how the ACS changes in different situations, for example, when the PCB is positioned next to a wall. This information is then used in Chapter 7 to determine the SE of complex enclosures using the multi-cavity power balance model.

Chapter 3

Absorption Cross Section of Printed Circuit Boards

3.1. Overview

Chapter 2 discusses the SE of enclosures and shows why it is important to quantify the effect of contents on SE. Chapter 2 also explains how the ACS of contents, such as PCBs, is a method of doing this. This chapter discusses ACS and how it is measured in a reverberation chamber. ACS measurement results are presented for a set of PCBs which are measured individually and a subset measured in a number of stacked configurations.

3.2. Printed Circuit Boards under Test

Four information and communication technology (ICT) cabinet enclosures were provided to the AEG by Huawei for use in a research project [47]. Two of the enclosures have dimensions of 440mm x 305mm x 85mm (size 2U enclosures). One of the enclosures is fully populated with PCBs, shown in Figure 3.1, and the other is unpopulated and has blanking plates to cover the PCB slots. The other two enclosures have dimensions of 440mm x 235mm x 265mm (size 6U enclosures). Again, one is populated and one is unpopulated with blanking plates. PCBs from both sizes of enclosure were used throughout this work.

Figure 3.1: Photograph of the 6U enclosure populated with PCBs. The photograph has been blurred, at the request of Huawei, to preserve design confidentiality.

The 6U enclosure contains 12 PCBs and the 2U enclosure contains 11 PCBs. Table 3.1 lists the dimensions and type of each PCB. The PCBs are a variety of sizes and range from having a few components and little shielding to having a significant amount of components and shielding covering the PCB. The dimensions, component coverage and shielding coverage are used to classify the PCBs. The depth of the PCBs is measured as the depth of the front plate not the depth of the PCB substrate or its components. Figure 3.2 shows photos of each type of PCB.

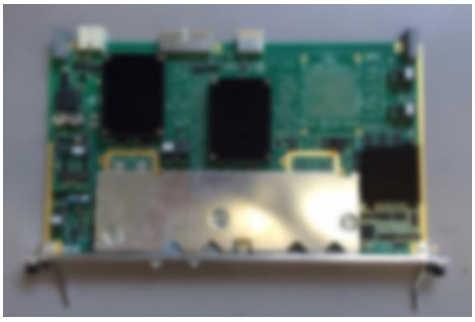

High component, low shielding coverage – 6U PCB1

Low component, low shielding coverage – 6U PCB11

High component, high shielding coverage – 2U PCB3

Low component, high shielding coverage, double sided PCB – 2U PCB9

Figure 3.2: Photographs of each classification of PCB. The photograph has been blurred, at the request of Huawei, to preserve design confidentiality

Table 3.1: Details of the PCBs used for ACS measurements in the RC

Name	Dimensions (mm)	Component Coverage	Shielding Coverage
6U_PCB1	365 x 210 x 20	High	Low
6U_PCB2	365 x 210 x 23	High	Low
6U_PCB3	365 x 210 x 20	High	Low
6U_PCB4	365 x 210 x 20	High	Low
6U_PCB5	365 x 210 x 20	High	Low
6U_PCB6	365 x 210 x 20	High	Low
6U_PCB7	365 x 210 x 10	High	Low
6U_PCB8	365 x 210 x 25	High	Low
6U_PCB9	210 x 170 x 25	High	Low
6U_PCB10	210 x 170 x 25	High	Low
6U_PCB11	210 x 170 x 25	Low	Low
6U_PCB12	210 x 85 x 25	Low	Low
6U_PCB13	210 x 150 x 25	High	Low
2U_PCB1	283 x 145 x 20	High	Low
2U_PCB2	283 x 145 x 20	High	Low
2U_PCB3	283 x 145 x 20	High	High
2U_PCB4	283 x 145 x 20	High	High
2U_PCB5	283 x 145 x 20	High	Low
2U_PCB6	283 x 145 x 20	High	Low
2U_PCB7	283 x 145 x 20	High	Low
2U_PCB8	283 x 145 x 20	High	Low
2U_PCB9*	283 x 75 x 40	Low	High
2U_PCB10*	283 x 75 x 40	Low	High
* These PCBs consist of two PCBs, separated 40mm apart with spacers.			

3.3. Measuring ACS in a Reverberation Chamber

The small AEG reverberation chamber described in Section 2.2.8.1 was used to carry out all ACS RC measurements described in this thesis. The ACS measurement setup is shown diagrammatically in Figure 3.3; a photograph from the open top of the chamber with no PCB is shown in Figure 3.4 and a photograph with the PCB inside in Figure 3.5. A stepped mechanical stirrer, controlled by a PC external to the reverberation chamber, was used to stir the chamber using 100 positions uniformly spaced over one rotation. A VNA was used to collect a full set of S-parameters between two monopole antennas. 10,001 points were taken over the frequency range of 1GHz to 20GHz with a sweep time of 4.5 seconds. Frequency stirring, using a bandwidth of 50MHz, was applied to the measurement data. A polystyrene sheet was used to support the PCBs in the working volume of the chamber above the stirrer.

Two sets of measurements are required to calculate the ACS; one with the object in the reverberation chamber and a second reference measurement with the reverberation chamber empty. One reference measurement was carried out on each day measurements were being made.

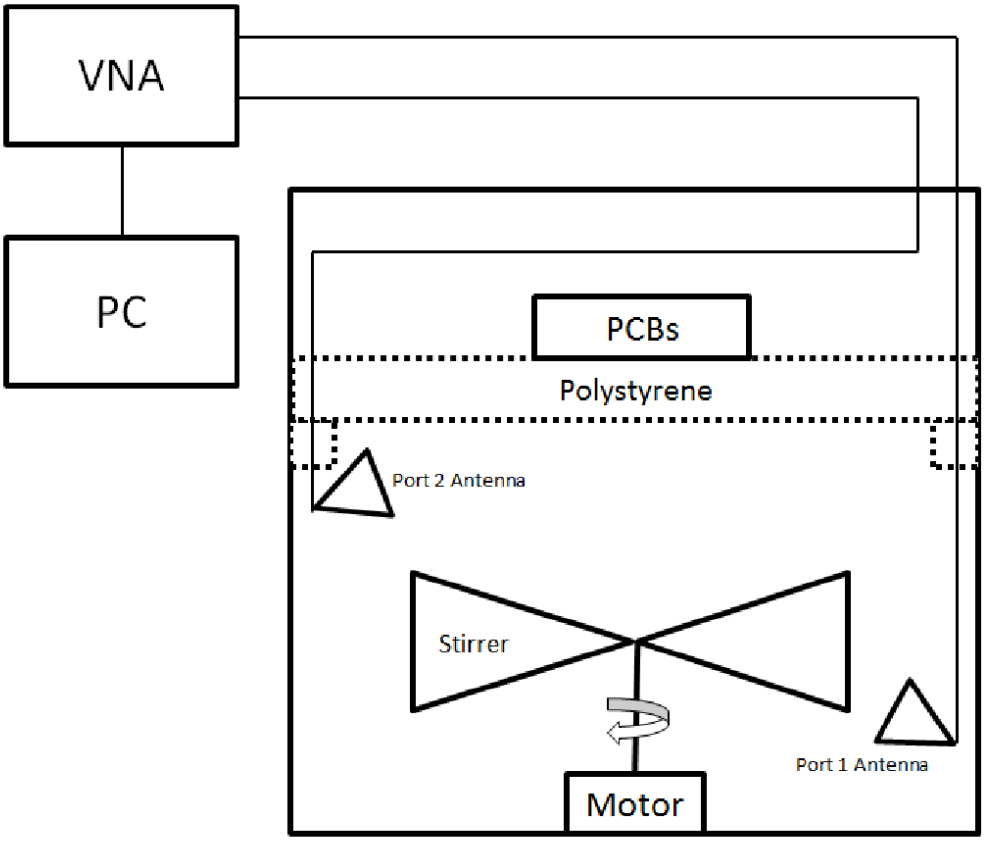

Figure 3.3: Side view of the ACS measurement set up in the small RC

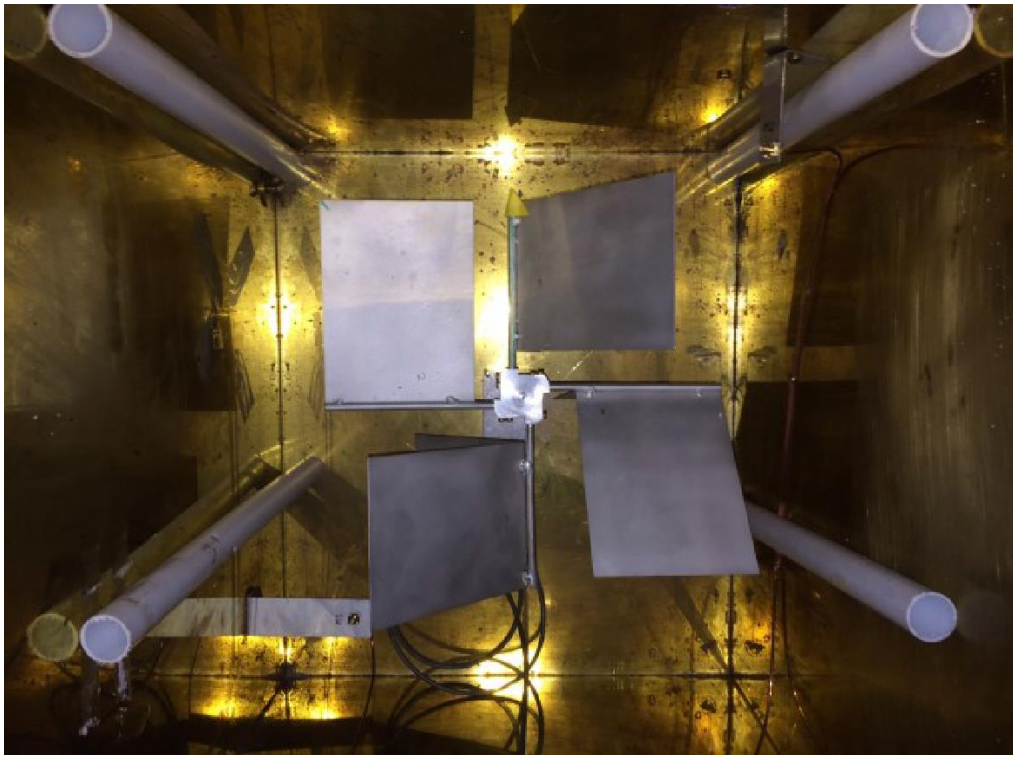

Figure 3.4: View from above the RC set up showing the stirrer in the centre, supports for the polystyrene and antennas in the bottom left and top right

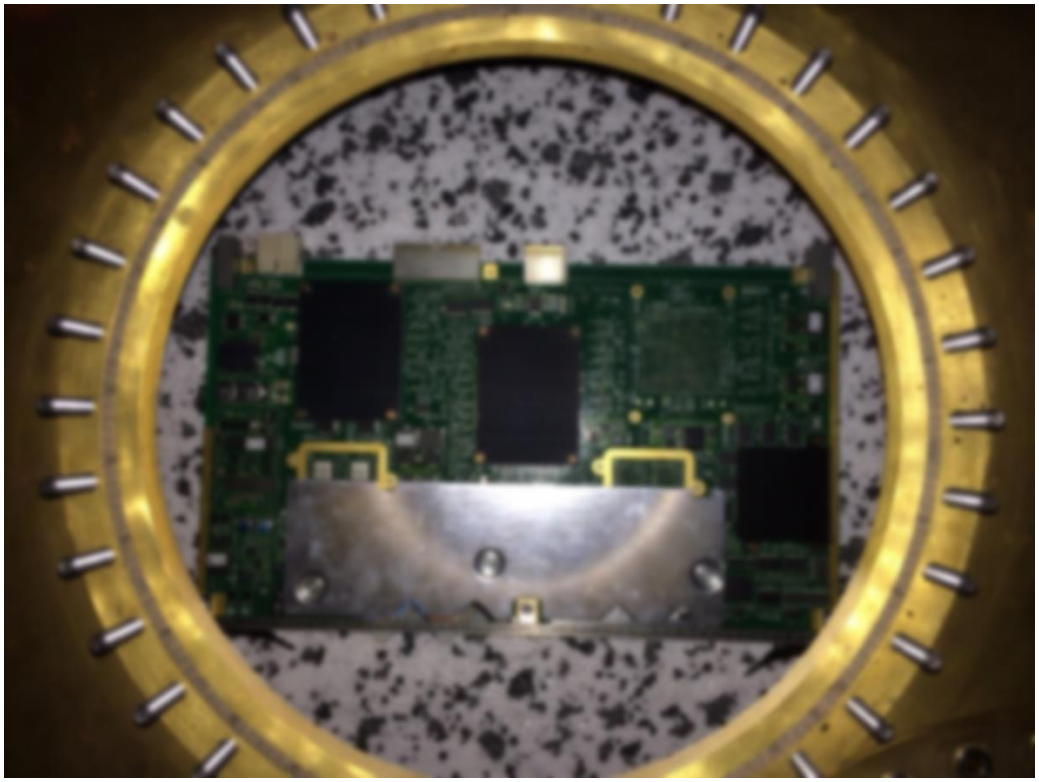

Figure 3.5: View from above the RC set up showing the PCB under test supported in the working volume of the chamber on a polystyrene sheet through the chamber access opening

3.4. ACS of Individual PCB Measurement Results

3.4.1. Validation of ACS Measurement

A validation of the ACS measurement was carried out using the object shown in Figure 3.6. It consists of a sheet of metal with a sheet of LS22 radio absorbing material (RAM) [47] placed on it. A number of waveguides were taped together in order to make ACS of the validation object frequency dependent. Each waveguide had dimensions of 22mm x 22mm x 76mm and are positioned vertically on the LS22 sheet. The maximum size of the wavelength that can propagate down the waveguide determines the cut-off frequency, f_c, of the waveguide (3.1) [49]. In this case, this frequency is 6.8GHz.

$$f_c = \frac{c}{2a} = 6.8GHz \tag{3.1}$$

Below this frequency the area of RAM covered by the waveguides does not absorb any energy as the wavelength becomes too large to travel through the waveguide. Above this frequency the majority of the RAM can absorb and the ACS will increase.

Figure 3.6: Photograph of the LS22 cube used for the ACS validation measurement

Figure 3.7 shows the result for this validation test. It can be seen that at approximately 7GHz the ACS increases. This is what is expected from the calculation in (3.1) which gives a cut-off frequency of 6.8GHzand so provides confidence in the measurement.

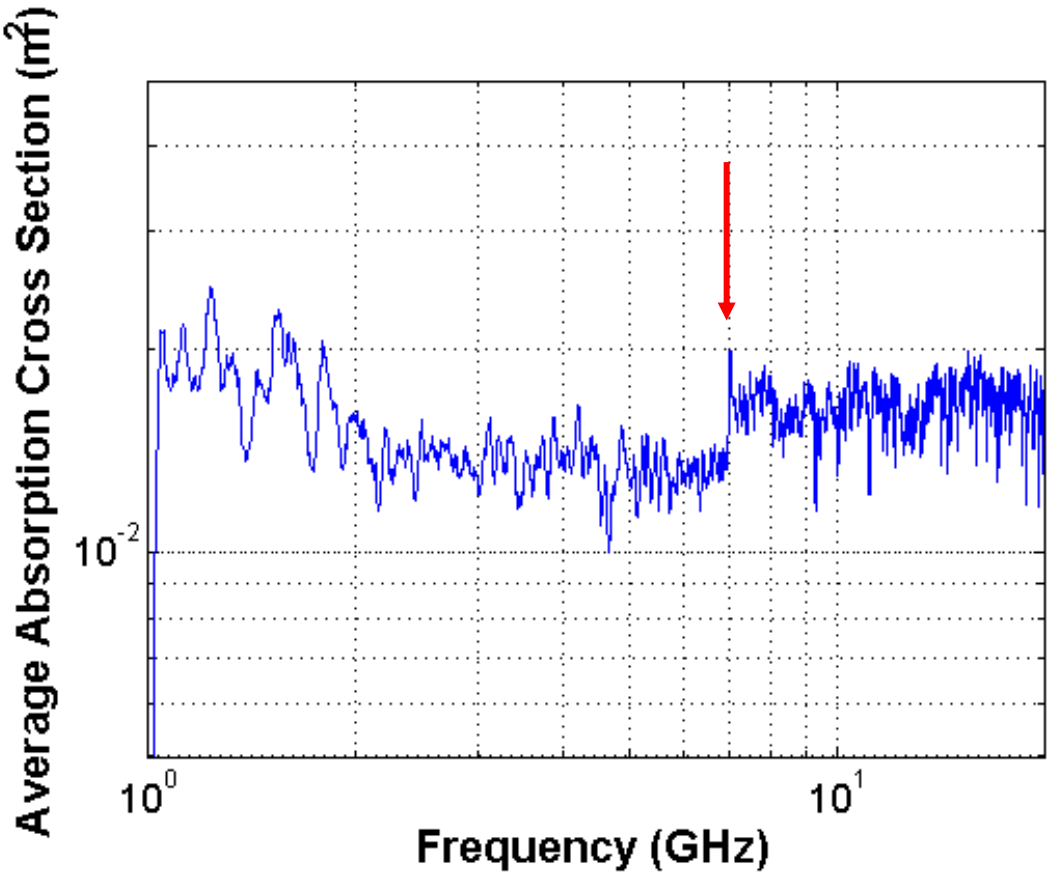

Figure 3.7: ACS of the LS22 cube as measured in the small RC

3.4.2. Absorption Cross Section of Individual PCBs

Each of the 23 PCBs described in Section 3.2 were measured individually in the small RC. This is to aid understanding of how ACS varies with frequency for a PCB and to see if there are any noticeable trends depending on the type of PCB.

During the measurements, each PCB is placed in the centre of the polystyrene support in the same orientation each time, as shown in Figure 3.5.

Figure 3.8 shows the measured ACS of a selection of individual PCBs. The ACSs of all the PCBs can be found in [48]. Table 3.2 lists the details of these PCBs. For the majority of the PCBs the ACS ranges from $2x10^{-3}$ m^2 to 8×10^{-3} m^2. The surface area of the PCBs with dimensions of 283mm by 145mm is approximately 0.082mm^2. Therefore, the ACS of these PCBs is between 3% and 10% of the physical area of the PCBs.

6U_PCB12 has smaller dimensions than the other PCBs and so has a smaller ACS of between 3×10^{-3} m^2 to 5×10^{-4} m^2. It also has a greater variation in ACS with frequency which could be due to its smaller size. The ACS of 6U_PCB12 is between 1% and 9% of its physical area. The PCBs that have little shielding and those with a high component density have the highest ACSs. 2U_PCB3 has more shielding on its surface and has a slightly lower ACS than the other PCBs of the same size. The results show that the type of PCB, its components and dimensions greatly affect the ACS.

Measuring the ACS of individual PCBs has shown that, as expected, the amount of energy absorbed by the PCBs is heavily dependent on the size of the PCB. The type of PCB (for example whether it has a high amount of component or metallic coverage) is also a good indicator of whether the PCB will have a higher or lower ACS. The results for a single PCB measured in the centre of a reverberation chamber have been shown. However, in more realistic situations, it is unlikely that a single PCB would be sitting alone in the centre of an enclosure. The next section looks at stacked PCBs and how this affects the amount of energy absorbed by the PCBs.

Table 3.2: Summary of PCB types shown in Figure 3.8

PCB	Dimensions, mm	Component Coverage	Shielding Coverage
2U_PCB2	283 x 145 x 20	High	High
2U_PCB3	283 x 145 x 20	High	High
2U_PCB5	283 x 145 x 20	High	Low
2U_PCB9	283 x 75 x 40	Low	High
6U_PCB12	210 x 85 x 25	Low	Low

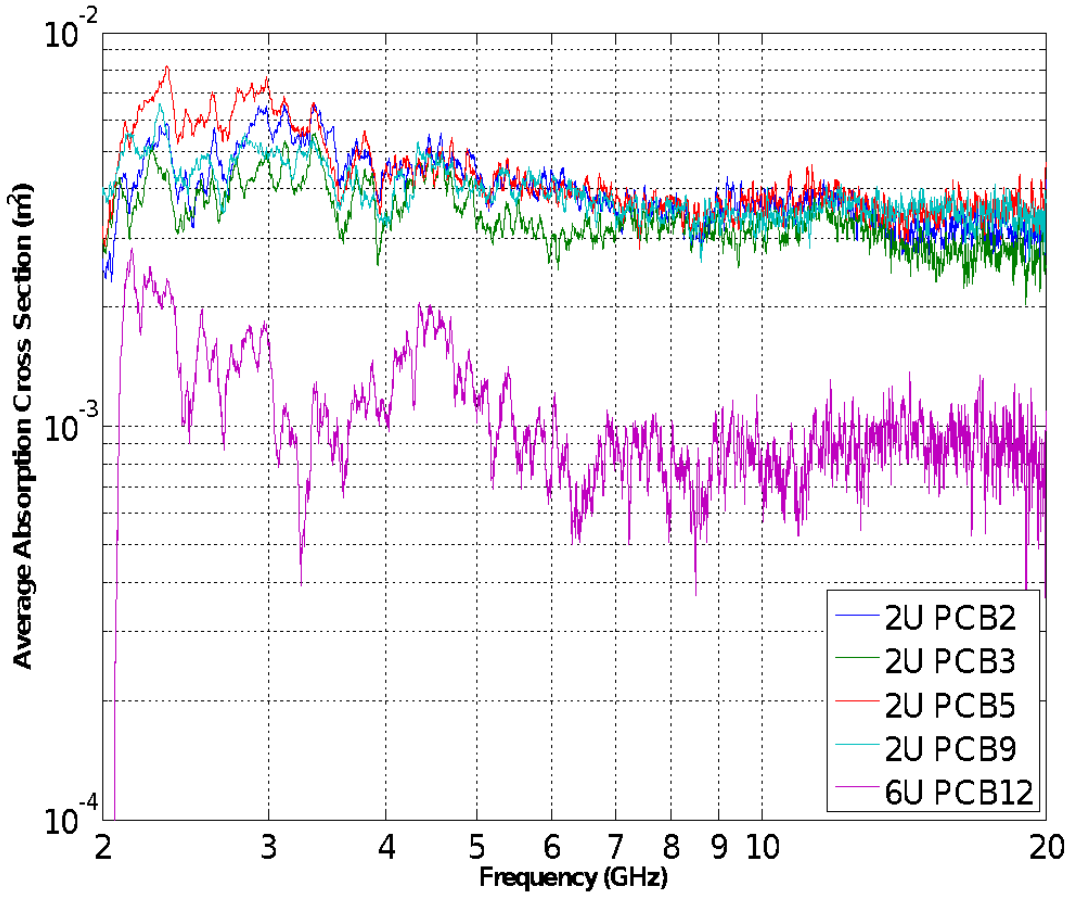

Figure 3.8: Measured ACS of a selection of the individual PCBs under test

3.5. ACS of Stacked PCB Measurement Results

3.5.1. PCB Configuration

The ACSs of four PCBs in different stacked configurations have been measured. The PCBs used in these measurements are 2U_PCB5 to 2U_PCB8 and have been described in Section 3.2. Each of these PCBs has dimensions of 283mm x 145mm and is classed depending on its shielding and component coverage. The ACS of each individual PCB has been measured and described in [48].

The ACS of the following stacks of PCBs was measured. The PCBs in each configuration were grouped together as they would be when installed in the ICT enclosure.

- All four PCBs
    - 2U_PCB5, 2U_PCB6, 2U_PCB7, 2U_PCB8
- Two sets of three PCBs
    - 2U_PCB5, 2U_PCB6, 2U_PCB7
    - 2U_PCB6, 2U_PCB7, 2U_PCB8
- Three sets of two PCBs
    - 2U_PCB5, 2U_PCB6
    - 2U_PCB6, 2U_PCB7
    - 2U_PCB7, 2U_PCB8

A plastic backplane was used to hold the stack of PCBs together. The spacing between the PCBs was 20mm; the same as when installed in their enclosure. The backplanes of the PCBs were not connected together during these measurements; however the front plates of the PCBs were in contact. Again, the stack of PCBs was placed in the centre of the RC and measured in the same position each time. All four PCBs are shown stacked together in Figure 3.9.

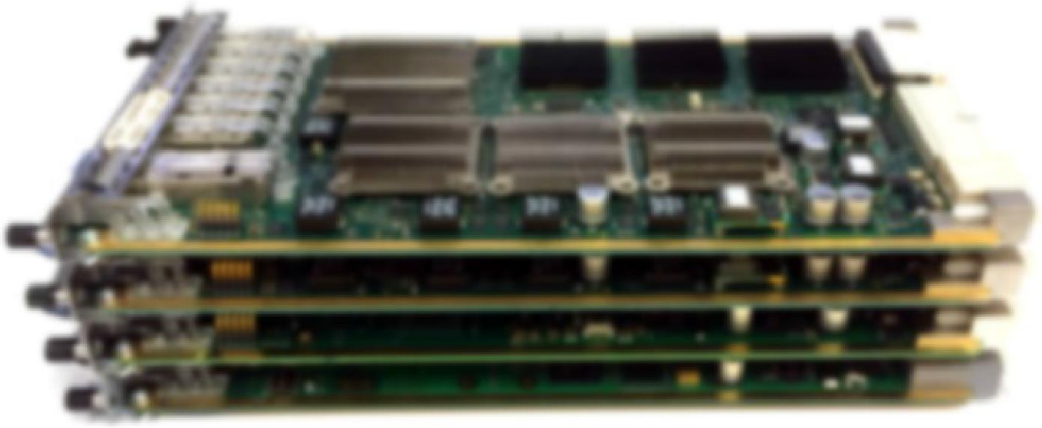

Figure 3.9: Photograph of all four PCBs stacked together with the plastic backplane. The photograph has been blurred, at the request of Huawei, to preserve design confidentiality

3.5.2. Measured ACS of Stacked PCBs

Figure 3.10, Figure 3.11 and Figure 3.12 each show three different sets of ACS measurements. Each graph shows:

- the ACS of each PCB measured individually
- the sum of the individual PCB ACSs
- the ACS of the PCBs when measured stacked together.

Figure 3.10 shows the results for two of PCBs, 2U_PCB5 and 2U_PCB6, stacked together. In the figure it can be seen that the ACS of the stacked PCBs is less than the summed ACSs of the individual PCBs. With a stack of two PCBs, below 10 GHz the ACS is reduced to approximately 75% of the sum of individual ACSs, a difference of 2.5×10^{-3} m^2. Between 10 GHz and 20 GHz the difference between the measured and summed ACS reduces to about 10^{-3} m^2, a reduction to 85% of the summed value.

Figure 3.11 and Figure 3.12 show a similar outcome for stacks of three and four PCBs. Figure 3.11 shows that for a stack of three PCBs there is a difference of approximately 5×10^{-3} m^2 between the summed and measured cases. This is a reduction to around 80% of the summed value. For the stack of four PCBs shown in Figure 3.12 the ACS is

reduced to approximately 75% of the summed ACS value with a difference of approximately 5×10^{-3} m^2, which reduces slightly as frequency increases.

The reduction in ACS shows that there is a 'shadowing' effect reducing the ACS when the PCBs are stacked together. The proportion it is reduced by increases as the number of PCBs in the stack increases. In the case of two PCBs, there are a total of 4 sides (each PCB has two sides). When the PCBs are stacked together two of the four sides are close together (are 'shadowed') which is 50% of the total PCB surface area. The two outer PCB sides have nothing shadowing them. When four PCBs are considered there are 8 sides in total and 75% of the surface area is shadowed. Therefore, the ACS is reduced more when there are more PCBs in a stack.

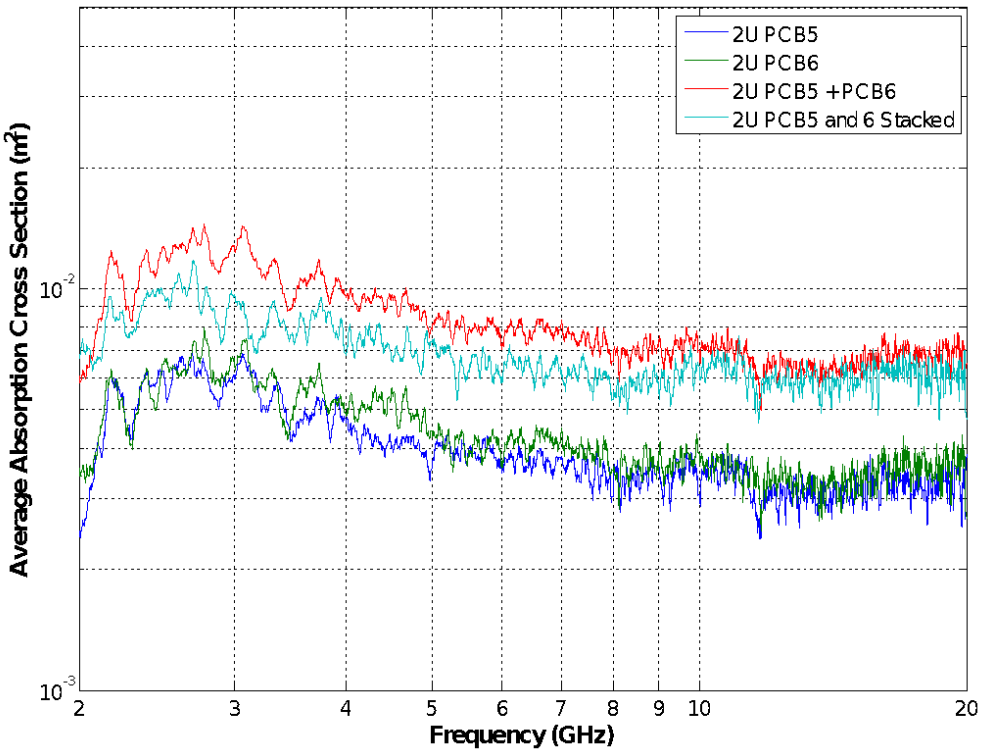

Figure 3.10: Measured ACS of two stacked PCBs showing ACS of each individual PCB, the summation of these and the measured ACS of both PCBs when stacked together

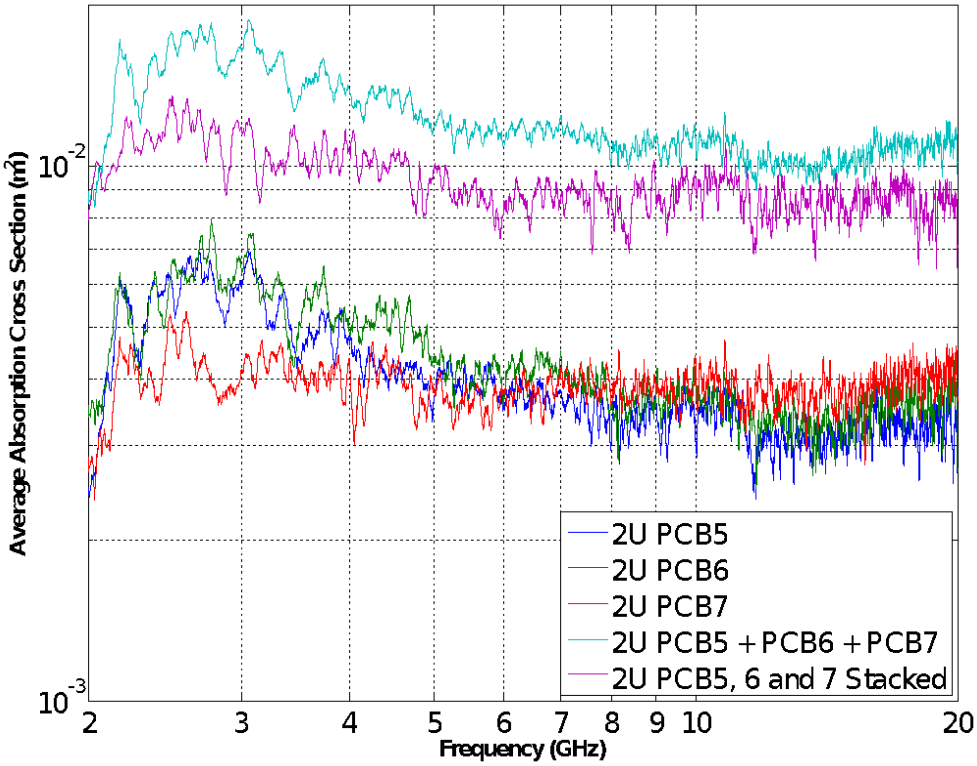

Figure 3.11: Measured ACS of three stacked PCBs showing ACS of each individual PCB, the summation of these and the ACS of the PCBs when stacked together

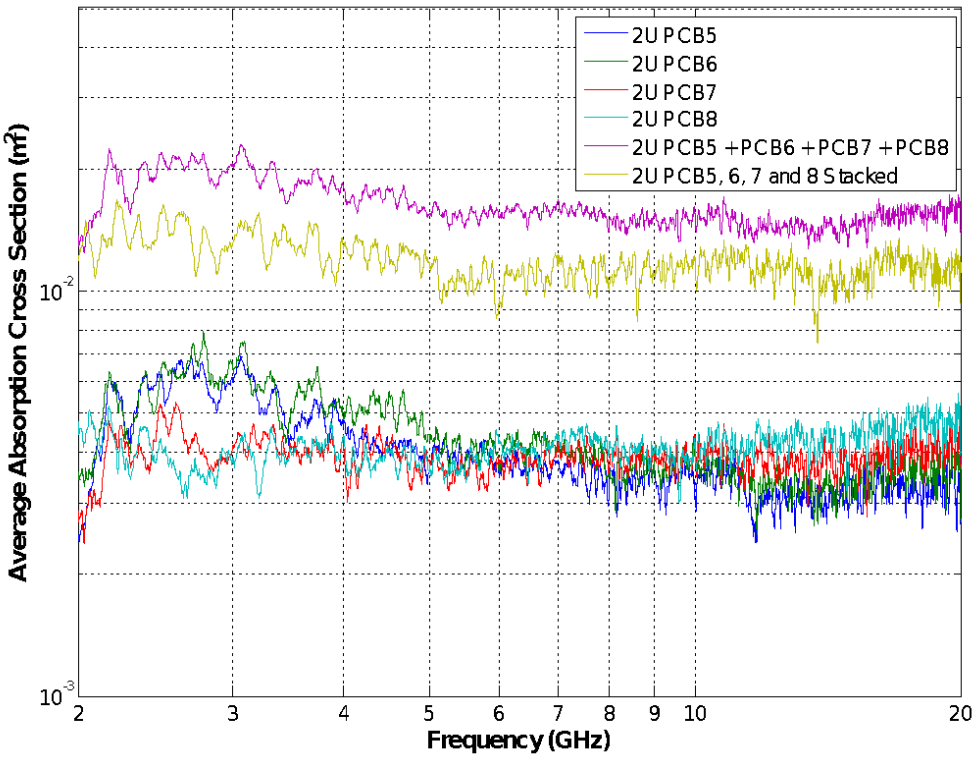

Figure 3.12: Measured ACS of four stacked PCBs showing ACS of each individual PCB, the summation of these and the ACS of all PCBs when stacked together

Figure 3.13 shows the measured ACS of all six configurations of stacked PCBs. The ACSs are grouped together depending on the number of PCBs stacked and it can be seen that as the number of PCBs in the stack increases the ACS also increases. This is to be expected as the greater the number of PCBs the greater the surface area there is to absorb energy. However, as observed in Figure 3.10 to Figure 3.12, as the number of PCBs in the stack increases the greater the reduction in ACS is.

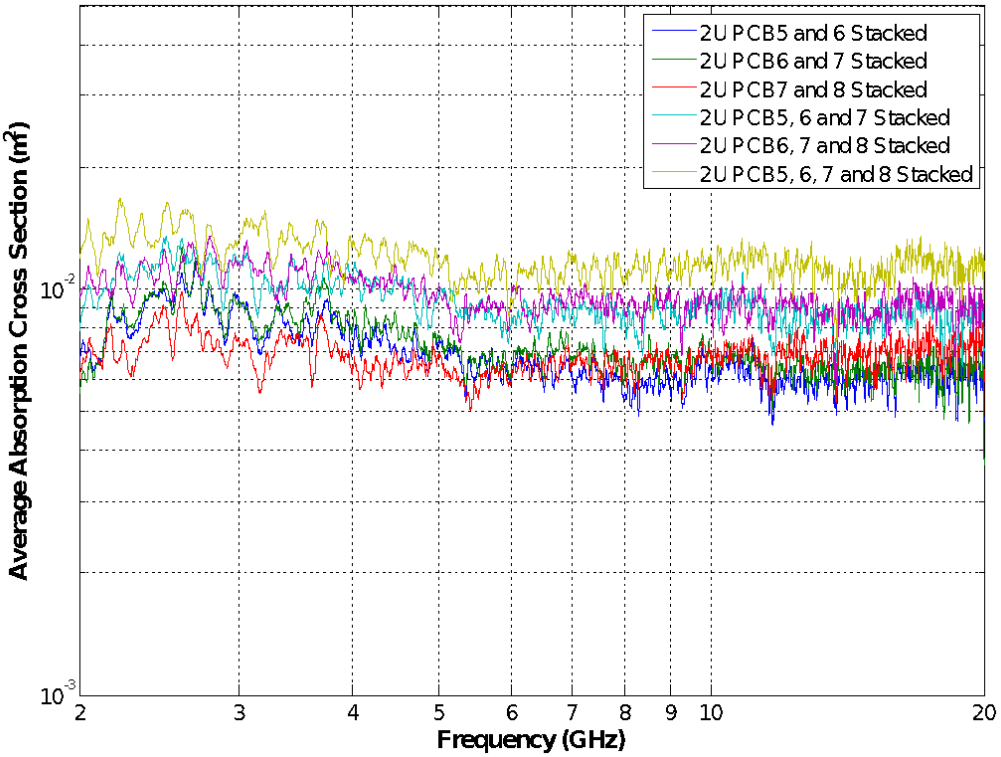

Figure 3.13: Measured ACS of all stacked configurations of the PCBs

The ACSs of four individual PCBs and six configurations of stacked PCBs have been measured in a RC over the frequency range of 2GHz to 20GHz. The results shown in this section show that stacking PCBs close together reduces the total ACS. This effect is increased with a greater number of PCBs. The results show a 'shadowing' effect occurs which reduces the ACS of stacked PCBs.

3.6. Absorption Efficiency of Individual and Stacked PCBs

Not all of the energy incident on the PCB or object inside the RC will be absorbed, even when the PCB is measured on its own. Unless it is a perfect absorber, some of the energy will be reflected from the surface of the PCBs or objects being measured. The average absorption efficiency, $<Q_a>$, is the proportion of the energy incident on the object which is absorbed [47]. The parameter is an averaged quantity as it is being calculated from a reverberation chamber measurement. Knowing how absorption efficiency changes with different PCBs allows us to see what type of PCBs absorb different amounts of energy as the dimensions of the PCBs have been normalised.

The average absorption efficiency can be calculated from the ACS using equation (3.2).

$$\langle Q_a \rangle = \frac{\langle \sigma_a \rangle}{A_s} \tag{3.2}$$

$\langle Q_a \rangle$ is the average absorption efficiency and A_s is the average silhouette area of the PCB calculated using equation (3.3).

$$A_s = \frac{S}{4} \tag{3.3}$$

In (3.3) S is the surface area of the object under test. For individual PCBs, the surface area is simply taken as 2 x (length x width). The depth of the PCB and its components are not taken into account in order to simplify the calculation. It would be significantly time consuming to calculate the surface area of the PCB and all its components.

Figure 3.14 shows the absorption efficiency of the set of PCBs whose results are shown in Section 3.4.2. The absorption efficiency has been calculated using equations (3.2) and (3.3) and the PCB dimensions stated in Table 3.2. For this set of PCBs the absorption efficiency ranges from approximately -12dB to -4dB.

PCBs 2U_PCB2, 3 and 5 have similar absorption efficiency which lies between -8dB and -6dB for the majority of the frequency range. As frequency increases the absorption efficiency is slowly decreasing. For these PCBs, the only difference is that 2U_PCB5 has low shielding coverage; all three of these PCBs have the same dimensions and a high coverage of components.

PCBs 2U_PCB9 and 6U_PCB12 have an absorption efficiency of approximately -4dB to -2dB, lower than the other three PCBs. 2U_PCB9 is smaller in width than the first three PCBs and is made up of two stacked PCBs. As absorption efficiency is being considered the smaller dimensions are not the cause of the lower absorption efficiency. The reduction in absorption efficiency indicates some shadowing between the two PCBs where the power is not able to be absorbed as efficiently as the individual PCBs. 6U_PCB12 is significantly smaller than the other PCBs. This could explain why it shows a greater variability in absorption efficiency; it could be almost too small to measure in the RC. It also has a very low amount of components compared to the other PCBs. The three PCBs with higher absorption efficiency all have high component coverage. This could show that a lot of the energy is being absorbed into the components which increase the PCB's absorption efficiency.

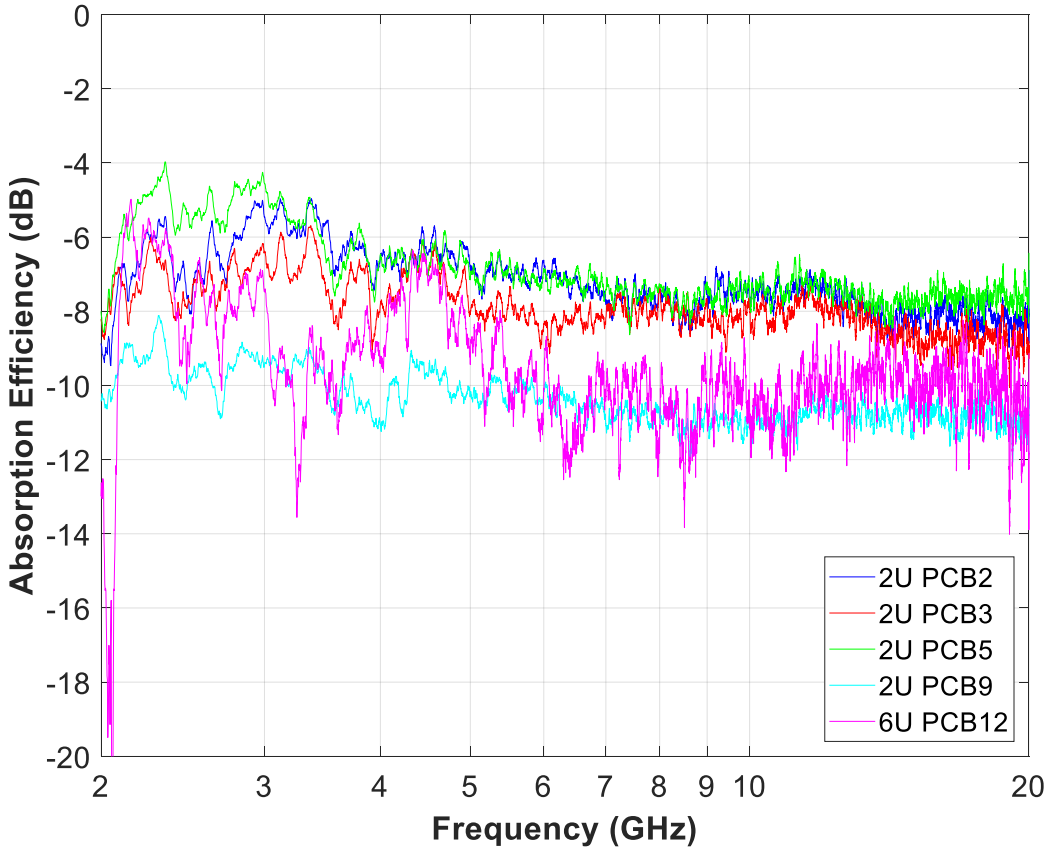

Figure 3.14: Measured absorption efficiency of the individual PCBs whose ACS results are shown in Section 3.4.2

Figure 3.15 shows the absorption efficiency of each set of stacked PCBs. The absorption efficiency of the stacked PCBs has a much smaller spread than the individual PCBs as the size of the PCB has been normalised. Figure 3.16 shows the absorption efficiency of the stacked PCBs in more detail. The stacks of PCBs have an absorption efficiency between -10dB and -5dB and have a similar structure to each other throughout the frequency range. In Figure 3.16 it is possible to see that the absorption efficiency decreases as the number of PCBs in the stack increases. The difference between the highest and lowest absorption efficiency is approximately 1.5dB which is a small but still noticeable difference. This indicates that that as a greater total surface area is being shadowed in the stacks of PCBs, less power than expected can be absorbed. This is similar to 2U_PCB9 having a smaller absorption efficiency in Figure 3.14. The next section explores the 'shadowing' effect in more detail.

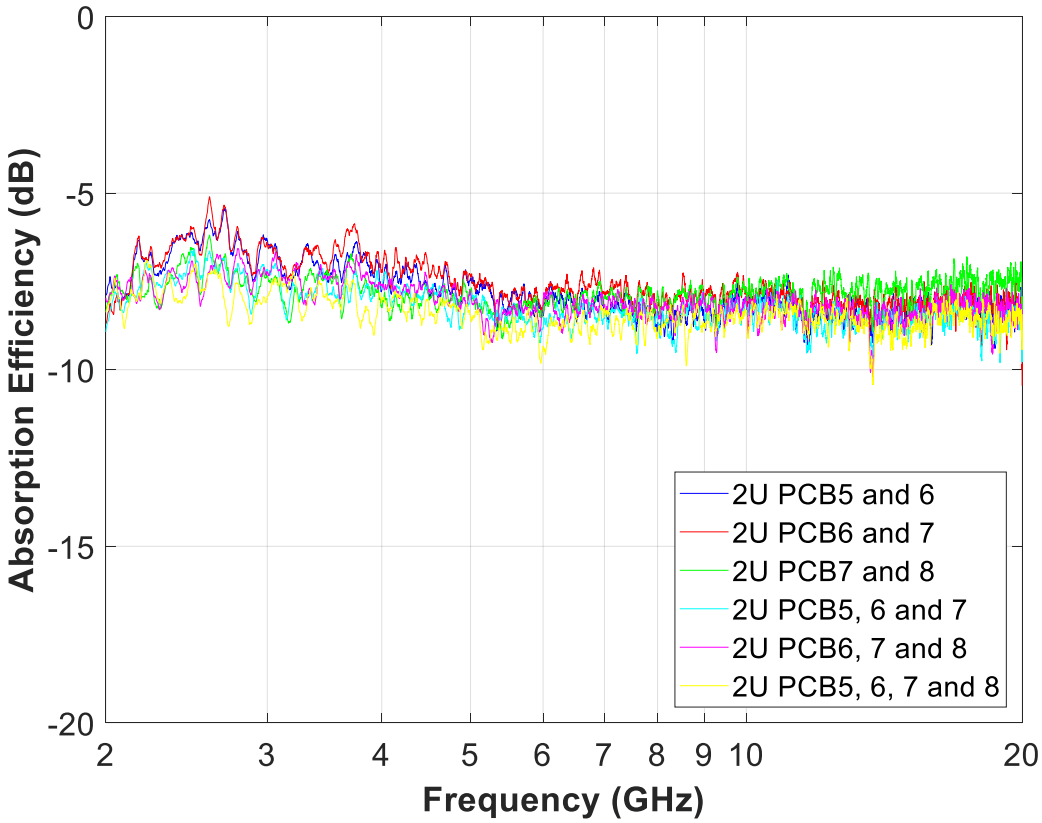

Figure 3.15: Measured absorption efficiency of all stacked configurations of the PCBs

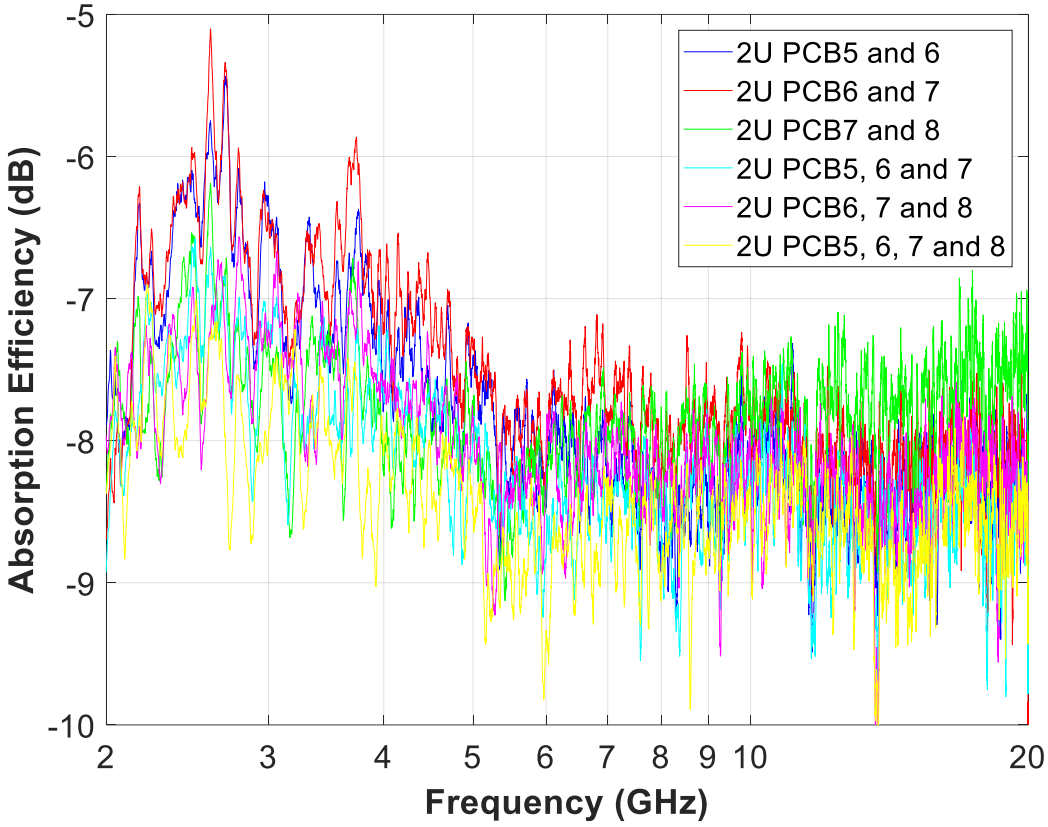

Figure 3.16: Detailed measured absorption efficiency of all stacked configurations of the PCBs

3.7. Shadowing Factor of Stacked PCBs

The ACS results for the stacked PCBs showed a reduction in ACS compared to the sum of the individual PCBs. It is clear that stacking the PCBs causes a 'shadowing' effect to occur where less energy is absorbed between the PCBs. This is because the average silhouette area of the stacked PCBs has been reduced.

A shadowing factor, γ, has been defined in [47] and shown in equation (3.4). A_s is the average silhouette area of the PCB and S is the surface area of the PCB. In (3.4), A_s is being reduced by the shadowing factor, γ. The shadowing factor is the factor which A_s is reduced by when PCBs are situated close together. In most cases, γ will be ≥ 0 and ≤ 1. As γ approaches zero a greater amount of shadowing is occurring. As it approaches one, the proximity between the PCBs has less effect. In the case of γ being greater than one this could either indicate a problem with the measurement or that the shadowing is having an adverse or unusual effect on the measurement, such as resonances forming between the PCBs.

$$A_s = \frac{\gamma S}{4} \tag{3.4}$$

The shadowing for each set of PCBs was calculated using equations (3.5) to (3.7). The full derivation of the shadowing factor can be found in [47]. These equations assume that, as the PCBs are the same size, the shadowing factor is the same for each PCB. If the PCBs were different sizes different shadowing factors would need to be calculated; this is outside the scope of this thesis.

In equations (3.5) to (3.7) $\langle\sigma_x\rangle$ is the absorption cross section of a single PCB or of a stack of PCBs. The x can refer to either a single PCB or a stack of PCBs. For example, $\langle\sigma_{5,6,7}\rangle$ is the ACS of a stack of three PCBs consisting of PCB5, PCB6 and PCB7.

For a stack of two PCBs:

$$\gamma = \frac{2\langle\sigma_{7,8}\rangle}{\langle\sigma_7\rangle + \langle\sigma_8\rangle} - 1 \tag{3.5}$$

For a stack of three PCBs

$$\gamma = \frac{2\langle\sigma_{5,6,7}\rangle - \langle\sigma_5\rangle - \langle\sigma_7\rangle}{\langle\sigma_5\rangle + 2\langle\sigma_6\rangle + \langle\sigma_7\rangle} - 1 \quad \textbf{(3.6)}$$

For a stack of four PCBs

$$\gamma = \frac{2\langle\sigma_{5,6,7,8}\rangle - \langle\sigma_5\rangle - \langle\sigma_8\rangle}{\langle\sigma_5\rangle + 2\langle\sigma_6\rangle + 2\langle\sigma_7\rangle + \langle\sigma_8\rangle} - 1 \quad \textbf{(3.7)}$$

The shadowing factor has been calculated for each stack of PCBs and the results shown in Figure 3.17. Figure 3.17 shows the shadowing factor for each set of stacked PCBs calculated from (3.5), (3.6) and (3.7). Generally, the shadowing factors show similar structure to each other throughout the frequency range and the values are between 0.5 and 0.9. These values mean that 10% to 50% less power is being absorbed in the stacks of the PCBs compared to the individual PCBs.

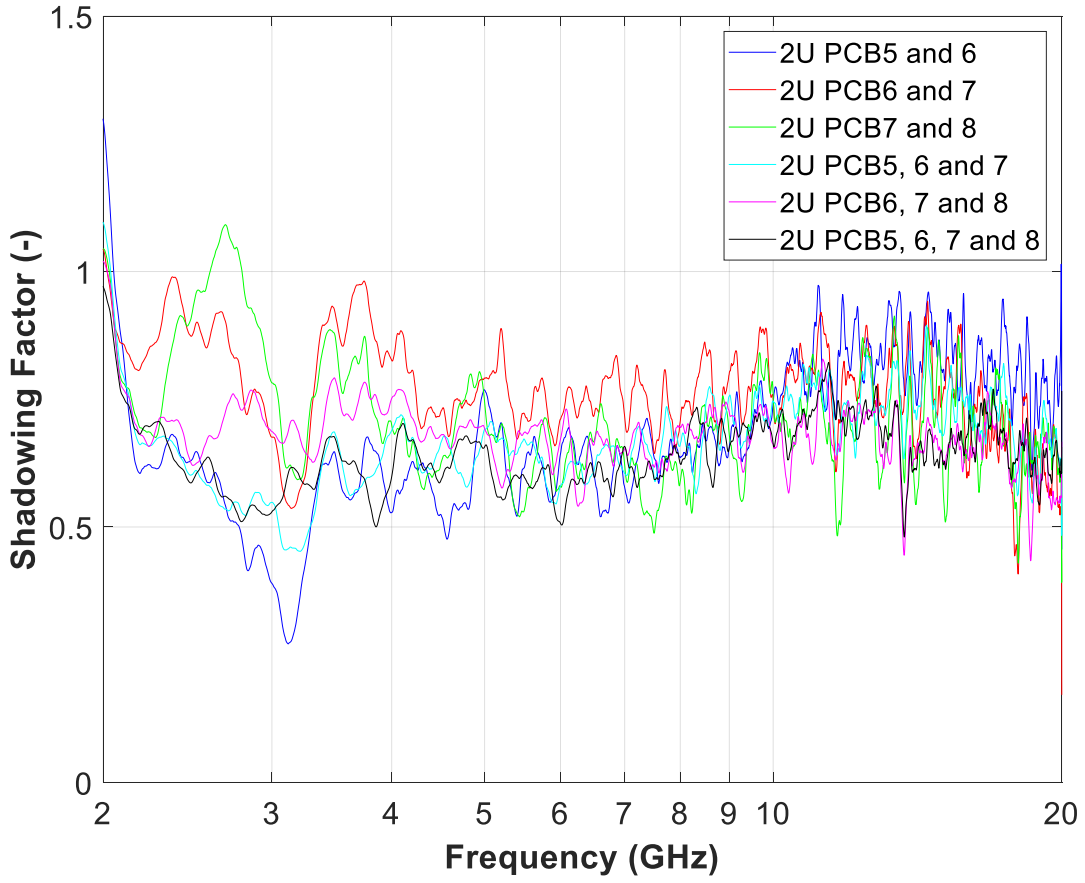

Figure 3.17: Shadowing factor of each set of stacked PCBs

3.8. Summary

In this chapter, the measurement and calculation of the ACS of individual and stacked PCBs has been looked at in detail. Measuring the ACS of a PCB in an RC, although time consuming, is a relatively easy measurement to make. It is important to consider the installation of the PCBs within their equipment enclosure. The results in this chapter have shown that when PCBs are stacked together, the ACS is reduced from what might be expected. Therefore, it is important to take factors such as this into account when calculating the SE of an enclosure populated by PCBs.

From looking at the individual PCB measurement results it can be seen that ACS is very dependent on the size of the PCB as well as the amount of components and metallic coverage the PCB has. When the PCBs are stacked together, as they may be in a real enclosure, the ACS is reduced from what might be expected. This is due to a shadowing effect. As the number of PCBs in the stack increases there is a greater reduction in ACS. This is because a larger proportion of the total PCB surface area is covered.

The next chapter of this thesis explores the changes in ACS when PCBs are placed in different positions inside an enclosure. This information will allow a more accurate prediction of SE.

Chapter 4

Changes in Absorption Cross Section due to Position in a Reverberant Environment

4.1. Overview

In the previous section, it is shown that stacking the PCBs together to better represent a realistic enclosure reduces the ACS. This is due to a 'shadowing' effect which is created as PCBs are positioned closer together. A similar situation to this is when the PCBs are close to the enclosure walls or in different positions throughout the enclosure.

In this chapter, it is shown how the ACS of PCBs changes depending on the location in a reverberant environment. As technology progresses enclosures are getting smaller and the contents, such as PCBs, are filling up a greater proportion of the enclosures. Therefore, in addition to looking at stacked PCBs it is also necessary to look at what happens when the PCBs get closer to the enclosure walls. Shielded enclosures and reverberation chambers are both reverberant environments; as discussed in Chapter 2. Therefore, it is possible to look at the effects of position in an enclosure by measuring the ACS in different positions in a RC.

4.2. Changes in ACS due to Position in Reverberation Chamber Measurements

The PCBs under test have been placed in several different locations in the RC including some with the PCBs close to the reverberation chamber walls, in both parallel and perpendicular orientations. If the ACS of the PCBs changes when positioned in different locations, this will change the internal EM field in an enclosure which will correspondingly change the enclosure SE.

4.2.1. Position of PCBs in the Reverberation Chamber

Three PCBs were measured and photographs of each are shown in Figure 4.1. The PCBs used were 6U_PCB1, 6U_PCB5 and 6U_PCB11 and they have been described previously in Section 3.2. In this chapter they will be referred to as PCB1, PCB5 and PCB11 for brevity. As a reminder, PCB1 and PCB5 have dimensions of 365 mm × 210 mm × 20 mm and 283 mm × 145 mm × 15 mm respectively. These two boards have a good coverage of components and metallic parts on them, including connectors, integrated circuits, passive components and heat sinks. PCB11 is a smaller board and has dimensions of 210 mm × 80 mm × 20 mm. It also has fewer components than the other two boards.

A number of measurements were made with the PCBs in different positions and orientations. These are shown in Figure 4.2. Each PCB was measured lying flat, with the component side of the board facing up, in the centre of the polystyrene. These measurements were used as reference measurements for comparison to the locations close to the walls and other measurement positions and orientations.

PCB1 was used for the majority of the measurements. It was measured lying flat on the polystyrene in different positions including component side up, component side down, rotated 90° and positioned with one of its edges next to the wall.

PCB1

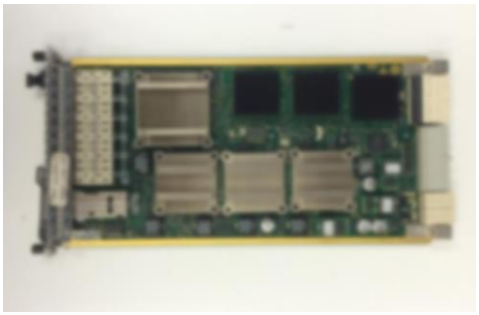

PCB5

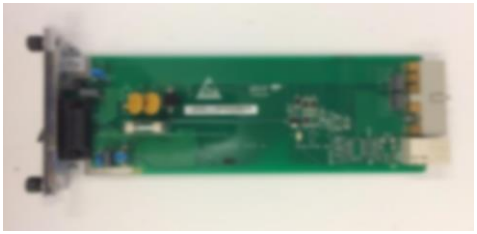

PCB11

Figure 4.1: Photographs of each of the PCBs tested. The photograph has been blurred, at the request of Huawei, to preserve design confidentiality.

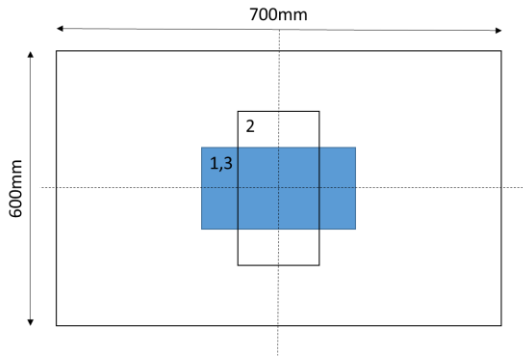

Positions 1-3, board on centre line

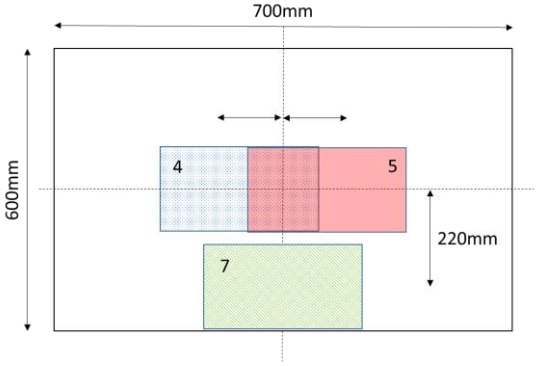

Positions 4,5 and 7, boards displaced 50mm from centre line and 220mm below centre line

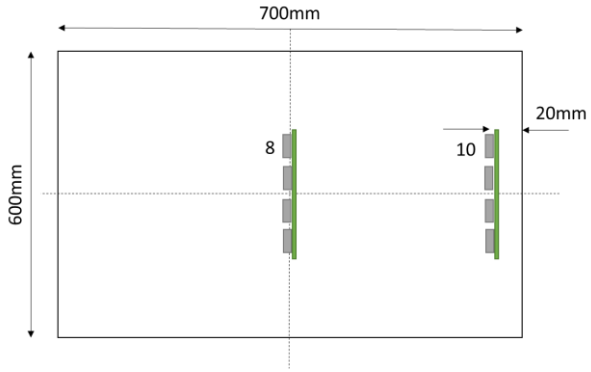

Positions 8 and 10 with board on edge

Figure 4.2: Plan view of the different PCB positions in the reverberation chamber

PCB11 was measured balanced on one edge in the centre of the polystyrene, away from the chamber walls in the centre of the RC. Two small pieces of polystyrene were placed either side of the board to keep it upright. This board was used rather than PCB1 as it could be balanced on its side without falling over due to the front plate's larger size.

PCB5 was used for the measurements where the PCB was placed parallel to the wall. This board was used as it has lower profile components on one side which allows the board to be slotted into a piece of polystyrene to keep the board in position during the measurements. PCB5 was measured positioned parallel to the chamber wall 10 mm from the wall and 20 mm from the wall. This was carried out with both the back of the PCB (flat side with fewer and smaller components) and front of the PCB (component side) facing the reverberation chamber wall.

A full list of measurement positions is given in Table 4.1; the positions are given relative to the central reference position described above.

Table 4.1: PCB measurement positions

Position Number	Position	PCB
1	Centre	PCB1 PCB5 PCB11
2	Centre 90° clockwise	PCB1
3	Centre upside down	PCB1
4	50 mm left	PCB1
5	50 mm right	PCB1
6	100 mm right, PCB edge against wall	PCB1
7	220 mm down, PCB edge against wall	PCB1
8	Centre on side, perpendicular to polystyrene sheet	PCB11
9	10 mm away from wall, back facing	PCB5
	10 mm away from wall, front facing	PCB5
10	20 mm away from wall, back facing	PCB5
	20 mm away from wall, front facing	PCB5

4.2.2. Changes in Measured ACS due to PCB Positioning

The measured ACS of PCB1 in different positions and orientations in the reverberation chamber is shown in Figure 4.3, Figure 4.4 and Figure 4.5. For the central reference measurement shown in these figures the ACS rises from 5×10^{-3} m^2 at 2 GHz to 8×10^{-3} m^2 at 3 GHz and then decreases to 5×10^{-3} m^2 at 5 GHz. From 5 GHz to 20 GHz the ACS remains relatively flat.

Figure 4.3 shows the ACS when the PCB is in different positions in the centre of the chamber; lying flat with the front side (component side) facing upwards, rotated 90° and lying flat with the back of the PCB facing upwards. The graphs show that there is minimal change in ACS between the central, reference position and the other measurement positions.

Figure 4.4 shows the ACS when the PCB is positioned lying flat on the polystyrene in the centre position and then in two positions with one edge just touching the reverberation chamber wall. For the position where the PCB is 100 mm to the right from the centre position, one short edge of the PCB is touching the wall. For the 220 mm down from the centre the front panel of the PCB is touching the wall. Again, it can be seen that there is little difference between the measurement positions even when the PCB is close to the reverberation chamber wall.

Figure 4.5 shows the ACS when the PCB is moved to the left of the centre position by 50 mm and to the right of the centre position by 50 mm and 100 mm, the latter in the touching the wall position. As before, the ACS does not vary significantly between measurement positions.

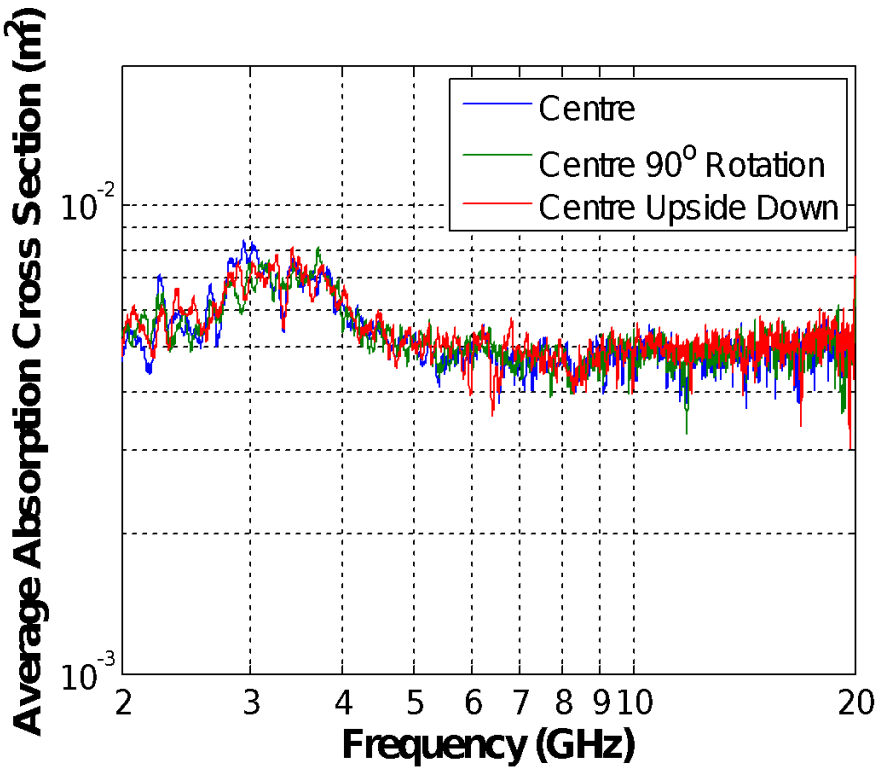

Figure 4.3: Measured ACS of PCB1 placed in the centre of the polystyrene, rotated 90° and turned upside down

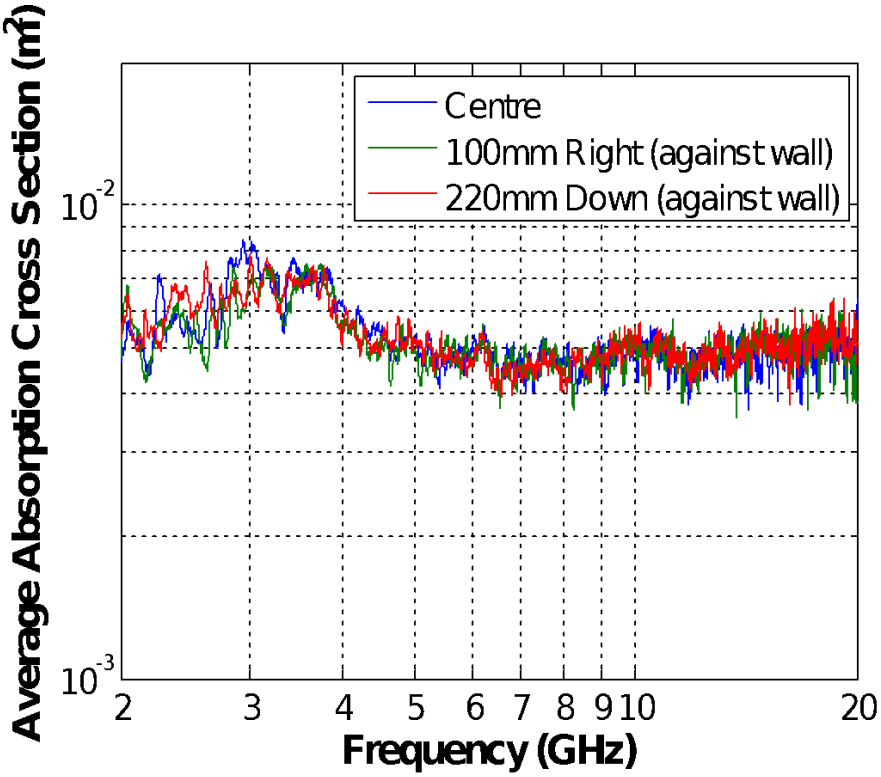

Figure 4.4: Measured ACS of PCB1 placed in the centre of the polystyrene and moved 100 mm right from the centre position so that the edge of the board is touching the reverberation chamber wall and 220mm down from the centre position so the front panel of the board is touching the chamber wall

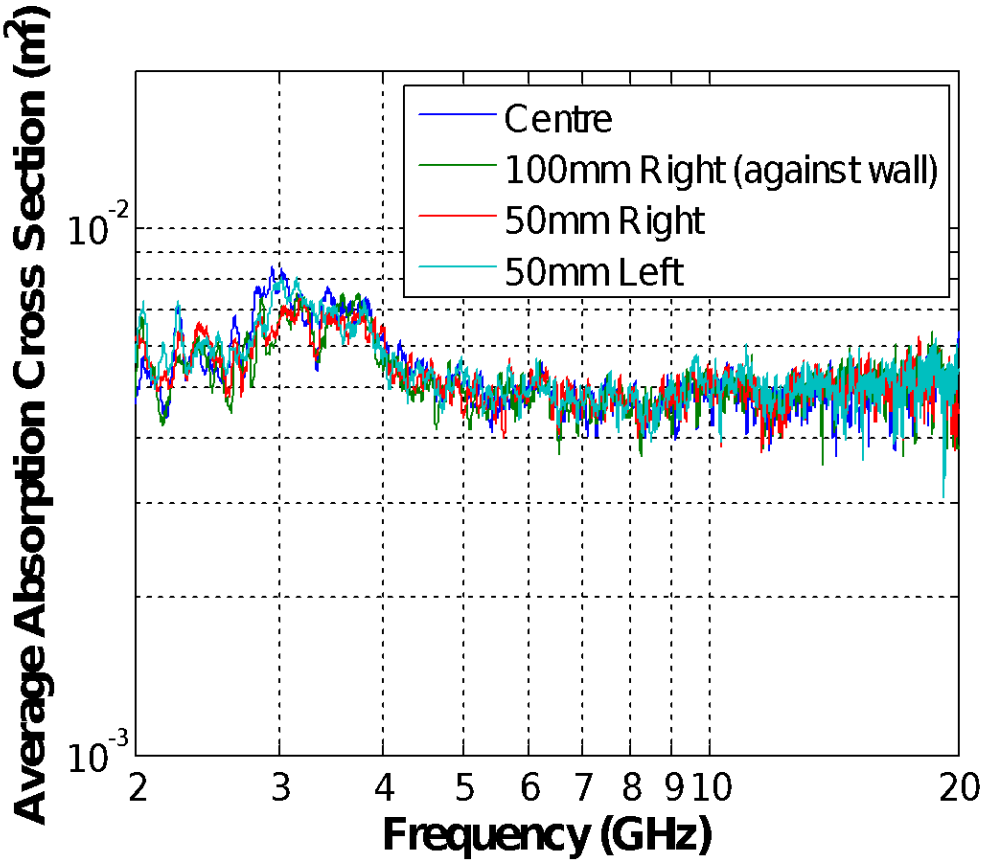

Figure 4.5: Measured ACS of PCB1 placed in the centre of the polystyrene and moved left 50 mm and right 50 mm and 100 mm

Figure 4.6 shows all results for PCB1 on one graph for comparison. The graphs show that putting this PCB in different measurement positions in the chamber produces little change in ACS even when moved against the chamber wall; the ACS is independent of position and orientation in the chamber when this PCB is perpendicular to the chamber walls.

This is because the PCBs are being measured in a reverberant environment. When mechanical and frequency stirring is used the EM field should be uniform in the working volume of the RC and the ACS would not be expected to change. However, when the PCBs are against the wall the part of the PCB nearest the wall is outside of the working volume. Therefore you might expect to see some change but this is not the case. This could be because only a small section of the PCB is outside the working volume and this is not enough to make a change.

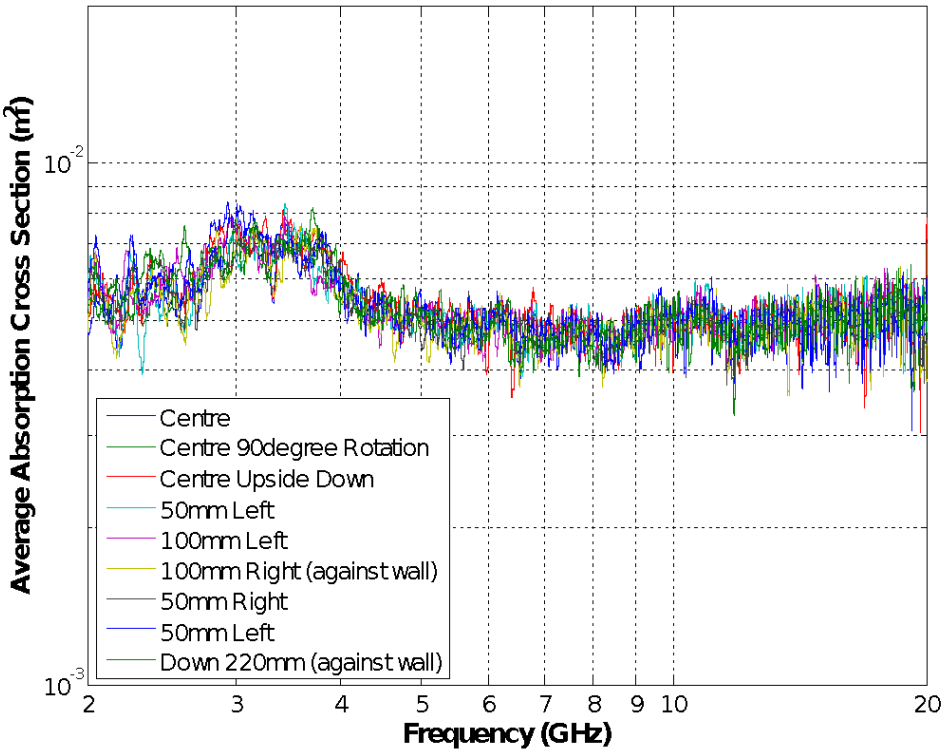

Figure 4.6: Measured ACS of PCB1 in all positions

Figure 4.7 shows the measured ACS of PCB11 when the PCB is stood on one of its long edges in the centre of the working volume of the chamber. The ACS for PCB11 in the centre position varies between 10^{-3} m^2 and 3×10^{-3} m^2. The ACS of this PCB is smaller than that of PCB1 as the size PCB is smaller. Again, the ACS of the PCB does not change significantly when positioned balanced on its side.

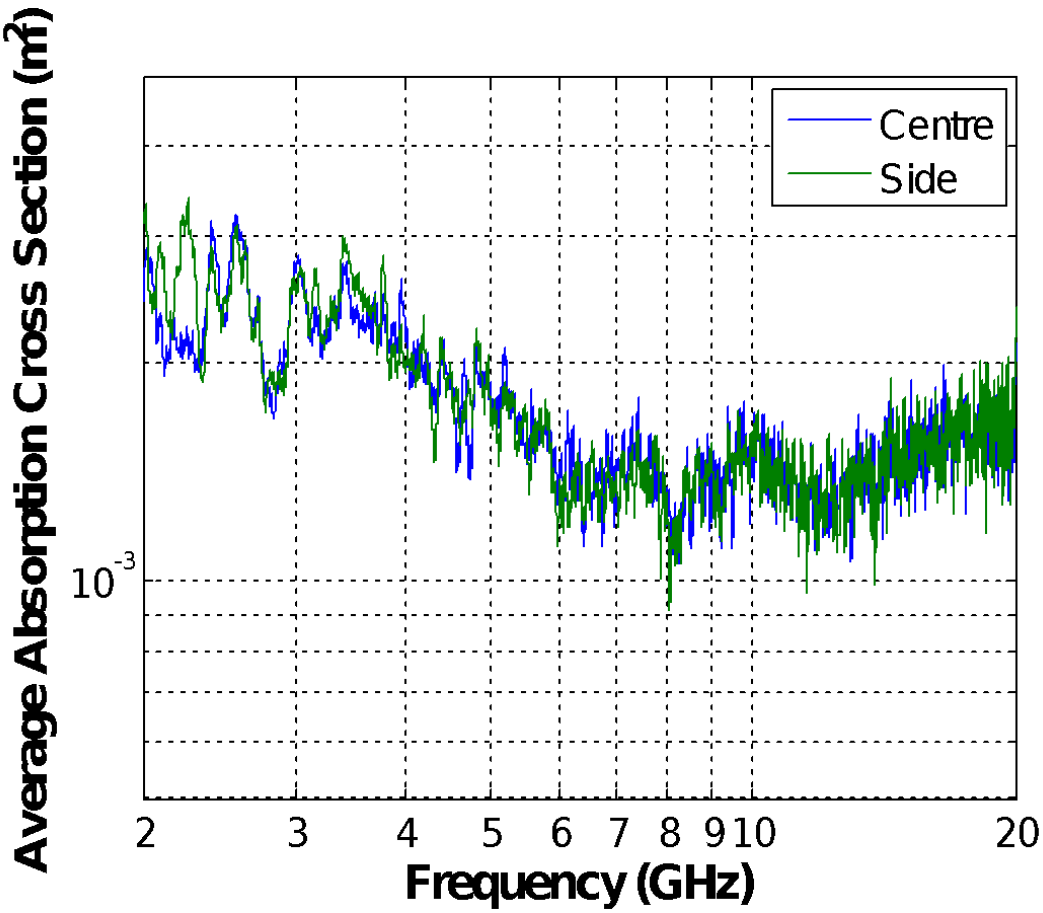

Figure 4.7: Measured ACS of PCB11 placed in the centre of the polystyrene horizontal (flat on polystyrene) and when the PCB is balanced vertically on its edge

Figure 4.8 shows the measured ACS of PCB5 in each of its measurement positions. The board was measured in the centre of the working volume of the reverberation chamber and then in four positions close to and parallel to the wall of the reverberation chamber. These positions were 10 mm and 20 mm from the wall with the back and the front (component side) of the PCB facing the wall.

For the case where the front of the PCB is facing towards the wall at a distance 20 mm away, the ACS is generally between 3×10^{-3} m^2 and 5×10^{-3} m^2 from 2 GHz to 4 GHz. This compares to between 3×10^{-3} m^2 and 8×10^{-3} m^2 when the board is in the centre position or with the back facing the chamber wall. This is a reduction in ACS of 10% to 50% in this frequency range. After 4 GHz the ACS is generally 10% less than the centre position.

When the PCB is 10 mm away from the chamber wall and with the front facing it the ACS is significantly lower than that of the centre and back facing positions from 2 GHz to 8 GHz. Between 2 GHz and 3 GHz it is reduced by between 20% to 50%. After 8 GHz the ACS becomes closer to the reference ACS but is still 10% to 20% lower. In both cases, the ACS is reduced by approximately 40% at 3 GHz and between 3 GHz and 8 GHz the 20 mm case is reduce by 30% from the ACS measured in the centre position.

Between 2 GHz and 3.5 GHz the front facing PCB ACS is approximately the same when the PCB is both 10 mm and 20 mm distance from the wall. After 3.5 GHz and up to around 8 GHz the difference between the ACS at 10 mm and 20 mm distance from the wall becomes more significant. A distance of 10 mm is a quarter wavelength at 7.5 GHz and a distance of 20 mm is a quarter wavelength at 3.75 GHz. These two frequencies are when the difference between the 10 mm and 20 mm ACS is greatest. It might be expected that this would actually occur at a difference of half a wavelength. As the reverberation chamber wall is a good conductor and the PCB side is absorbing this can be explained by image theory [50]. These results might be expected that as the measured ACS of a board changes as it is brought closer to the chamber walls. This is due to the change in field distribution and possible shadowing of one side of the PCB from the chamber. Usually it is advised to keep objects under

test at least a quarter wavelength (37.5 mm at 2 GHz) away from the chamber walls in order to remain within the working volume of the reverberation chamber [9].

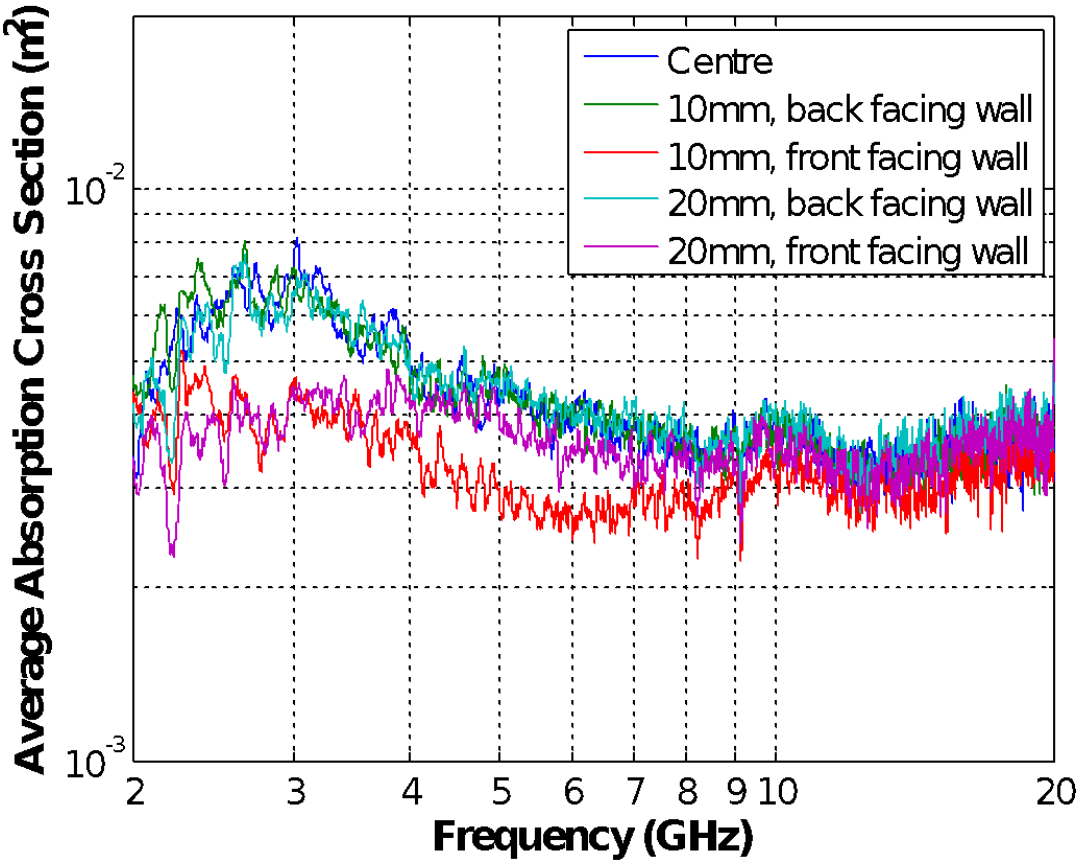

Figure 4.8: Measured ACS of PCB5 placed in the centre of the polystyrene and when board is parallel to the reverberation chamber wall at different distances from the wall and with different faces of the PCB facing the wall

4.3. Summary

The ACS of three different PCBs in a number of different positions and orientations in a reverberation chamber has been measured over the frequency range 2 GHz to 20 GHz. Generally, it has been found that when the PCB is perpendicular to the reverberation chamber walls different measurement positions have little effect on the ACS, even when the PCB is positioned close to the wall. However, placing the PCB parallel to the chamber wall did show some differences in ACS.

When the back of the PCB was facing the wall little difference was seen in ACS compared with the ACS in the centre positions for both the 10 mm and 20 mm distances from the wall. However, when the front of the PCB was placed facing the reverberation chamber wall the ACS was observed to be lower than both the centre and back facing measurements. In this situation the ACS is reduced up to 30% of the ACS of the board when placed in the centre of the chamber working volume. The distance between the PCB and RC wall also affected the measured ACS. At frequencies below which the distance between the PCB and the chamber wall is a quarter of a wavelength the ACS is most reduced. At frequencies above this the ACS becomes closer to the centre position PCB ACS.

In the previous chapter, stacks of PCBs were shown to have a lower ACS than expected due to 'shadowing'. This has been looked at in more detail in this chapter by looking at the effect of placing PCBs in different locations in a reverberant environment. The ACS does not change except when positioned close to, and with the components facing, the RC wall. As the ACS of one side of the PCB is reduced it is important to know the ACS of each, individual side of the PCB. The next chapter looks at how to measure and calculate the ACS of one side of a PCB.

Chapter 5

Absorption Cross Section of One Side of a PCB

5.1. Introduction

The previous chapter shows that when a PCB is not large enough to segment an enclosure into smaller cavities generally the ACS does not change depending on the PCB position inside the enclosure. However, when the PCB is close and parallel to an enclosure wall the ACS can change significantly. In this case, the ACS of one side of the PCB is greatly reduced and the side facing away from the wall is the predominant absorber. It is important to know the ACS of one side of a PCB so the reduction in ACS can be taken into account in any calculations carried out to predict the overall SE of an enclosure. The one sided ACS is also required if PCBs are stacked together or if considering an enclosure segmented into smaller cavities by PCBs. When considering the absorption in each cavity, the ACS of the side of the PCB in each cavity is needed, not the total ACS of the PCB.

This chapter investigates methods that could be used to extrapolate the ACS of a single side of a PCB by carrying out ACS measurements in the small RC. A set of representative contents (recos) have been measured as well as a selection of the PCBs previously measured (shown in Chapter 3). The single sided ACS of a PCB can then be used to model the PCB as an absorbing wall in a power balance model, or if PCBs are stacked together or close to an enclosure wall.

5.2. Using Representative Contents

A simplified representation of a PCB was required in addition to the actual PCBs. Previous work carried out by the AEG has developed sets of representative contents (referred to as 'recos') which have been both instrumented and un-instrumented [51][52]. A simplified version of a PCB is used in analytical models, such as a PWB model, as the structure of a real PCB is too complex to model easily. For example, due to the components that cover a PCB, the total surface area of a PCB would be time consuming to calculate.

The reco used for the work described in this thesis was developed by the AEG as part of the Huawei project [51]. The absorption of this reco was designed to be as close to the absorption of the majority of the PCBs from the 6U enclosure. The reco is shown in Figure 5.1. It consists of a sheet of aluminium with dimensions of 283mm x 144mm x 1mm and 16 pieces of LS22 RAM with dimensions of 40mm x 22.5mm x 9.5mm. A piece of polystyrene sheet, of depth 10mm, is taped to each side of the aluminium sheet. The polystyrene sheets have holes cut into them and are used to hold the RAM in place. The reco can be used with one absorbing side; with 8 pieces of RAM in place on one side of the aluminium sheet. The reco can also be used with two absorbing sides with 8 pieces of RAM on both sides of the aluminium sheet. The RAM can then be removed or replaced so the reco can be used either one or two sided. The two sheets of polystyrene on either side of the thin aluminium sheet also allow the reco to be placed on its edge when required for measurements.

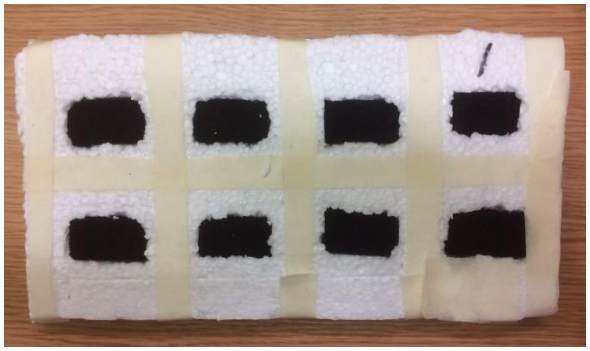

Photo of one face of the reco populated with RAM

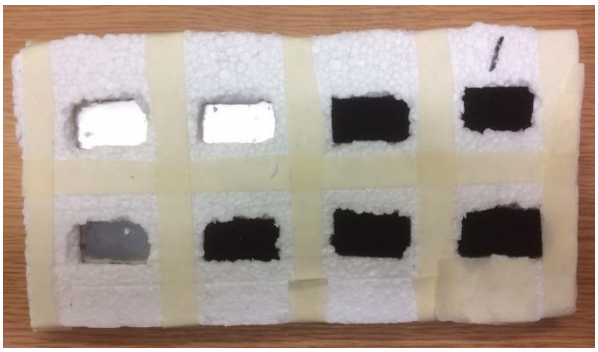

Photo of one face of the reco with some RAM removed showing the aluminium sheet beneath

Photograph showing the two layers of polystyrene with the aluminium sheet sandwiched between

Figure 5.1: Photographs of the reco

5.3. Measuring ACS Close to the RC Wall

Chapter 4 presented the ACS results of a PCB when positioned close to a RC wall. The following sections expand on these results by using a reco and measuring a greater number of distances from the wall. The results provide more detail about how ACS is reduced when close to the RC wall and the frequencies at which these changes occur.

5.3.1. Changes in ACS of a One Sided Reco Positioned Close to Wall

5.3.1.1. Measurement Methodology

The first ACS measurements described in this chapter were made using the same methodology as the previous measurements (see Chapter 2, Section 2.5.4). The S-parameters are measured between the two snake monopole antennas in the small RC with and without the object under test. The measurement parameters remain the same:

- Two port calibration
- Frequency range 1GHz – 20GHz
- Number of measurement points 10,001
- Number of stirrer positions 100
- Frequency stirring 50MHz

The ACS is calculated in the same way as previously. The equations used are shown again in equations (5.1) and (5.2).

$$< \sigma_a >= \frac{\lambda^2}{8\pi}\left(\frac{1}{G_{wo}} - \frac{1}{G_{no}}\right) \quad \textbf{(5.1)}$$

$$G = \frac{< |S_{21}|^2 >}{(1 - | < S_{11} > |^2)(1 - | < S_{22} > |^2)} \quad \textbf{(5.2)}$$

In these equations $\langle \sigma_a \rangle$ is the average ACS of the object, λ is wavelength, $G_{wo}$is the mean net transfer function with the PCB and G_{no} is the mean net transfer function without PCB (the reference measurement). S_{21} is the transmission coefficient

measured between two efficient antennas in the reverberation chamber and S_{11} and S_{22} are the reflection coefficients of the two antennas.

These measurements were taken with one side of the reco populated with absorber. The reco is positioned standing on its long edge parallel to the RC wall with the absorber facing the wall. Measurements were made with the reco at different distances from the wall. The distance is measured from the chamber wall to the aluminium sheet. At a distance of 10mm the polystyrene (with a depth of 10mm) is touching the RC wall; a distance 10mm is the closest measurement that can be made. The reco has also been measured in the centre of the RC as a reference.

A diagram showing the reco reference position and the reco in two different positions parallel to the RC wall is shown in Figure 5.2. The arrows in the diagram show that the distance between the RC wall and the reco is measured between the wall and the aluminium sheet in the centre of the reco. The measurements made are listed in Table 5.1.

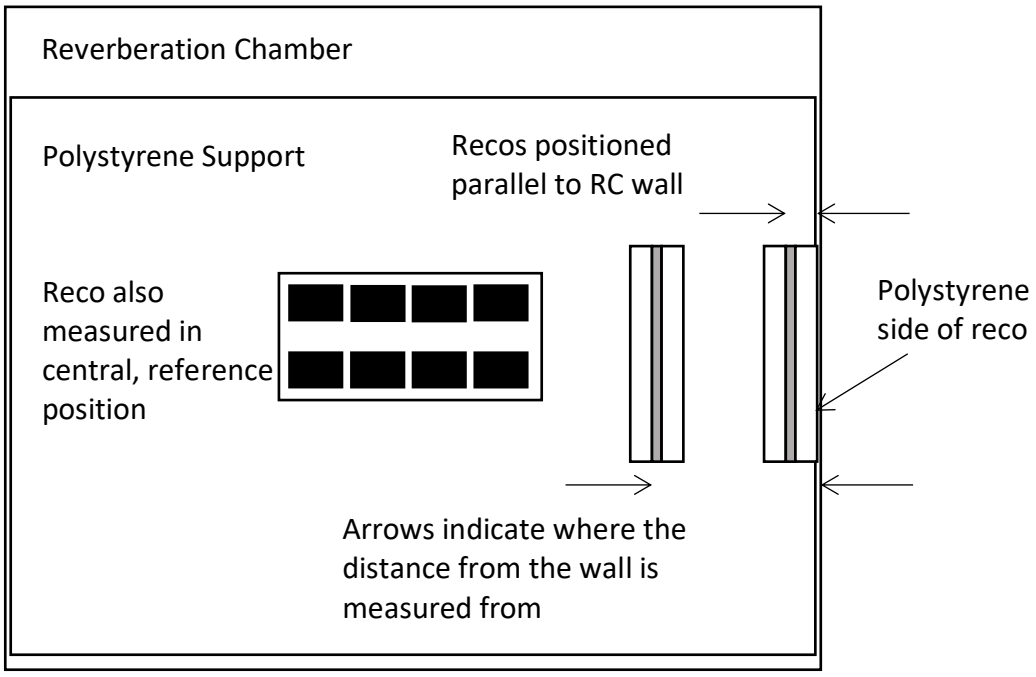

Figure 5.2: Diagram showing a top down view into RC with the reco in the central, reference position and two locations parallel to the RC wall. One of these is the closest positions to the wall, defined as 10mm position. The arrows show the distance between the RC wall and the reco is measured between the wall and the aluminium sheet in the centre of the reco.

Table 5.1: List of the ACS measurements of the one sided reco made at different distances from the RC wall.

Measurement	Distance from Wall	Comment
1	Empty chamber	Required for ACS calculation
2	Centre	Reference measurement
3	10mm	Against RC wall, shown in Figure 5.2
4	20mm	
5	30mm	
6	40mm	
7	50mm	
8	100mm	
9	200mm	
10	300mm	

5.3.1.2. Results

The changes in ACS observed by moving the reco away from the RC wall are shown in Figure 5.3 and in more detail in Figure 5.4.

Figure 5.3 shows the ACS of the different measurement positions over a frequency range of 1GHz to 20GHz. Below approximately 3GHz the measurement can be ignored as the RC is not working correctly at these frequencies, as has been seen previously. Figure 5.4 shows the same graph with the ACS results below $10^{-3}m^2$ removed from the graph. The ACS results at 10mm, 20mm and 30mm have been significantly reduced from the reference ACS result at the centre of the chamber. As the reco is moved further away from the wall the ACS increases up to the centre reference value. At 10mm the ACS is reduced to below $2x10^{-3}m^2$ at approximately 8.5GHz compared to the reference ACS of approximately $5x10^{-3}m^2$ at this frequency. Section 5.3.1.3 discusses this in more detail.

Figure 5.4 also shows that the minimum ACS is at different frequencies. The closer the reco is to the wall the higher the frequency the minimum ACS is at. This is discussed further in Section 5.3.1.4.

In

Figure 5.5 the ACS against the distance away from the RC wall is plotted for different frequencies. A general trend of a higher ACS for higher frequencies can be seen. When the reco is close to the RC wall the ACS is at its lowest. The black circle on the graph highlights that from 10mm to 20mm the ACS at these frequencies does not change significantly. At 30mm and above the change in ACS is greater. The frequencies which tend to change less are the lower frequencies. This could be because at these frequencies the RC is below its LUF and because there is less difference due to the wavelength (see Section 5.3.1.4). At the distances which are closer to the wall it is probable that any error in the position of the reco makes a bigger difference than at the positions further away from the RC wall.

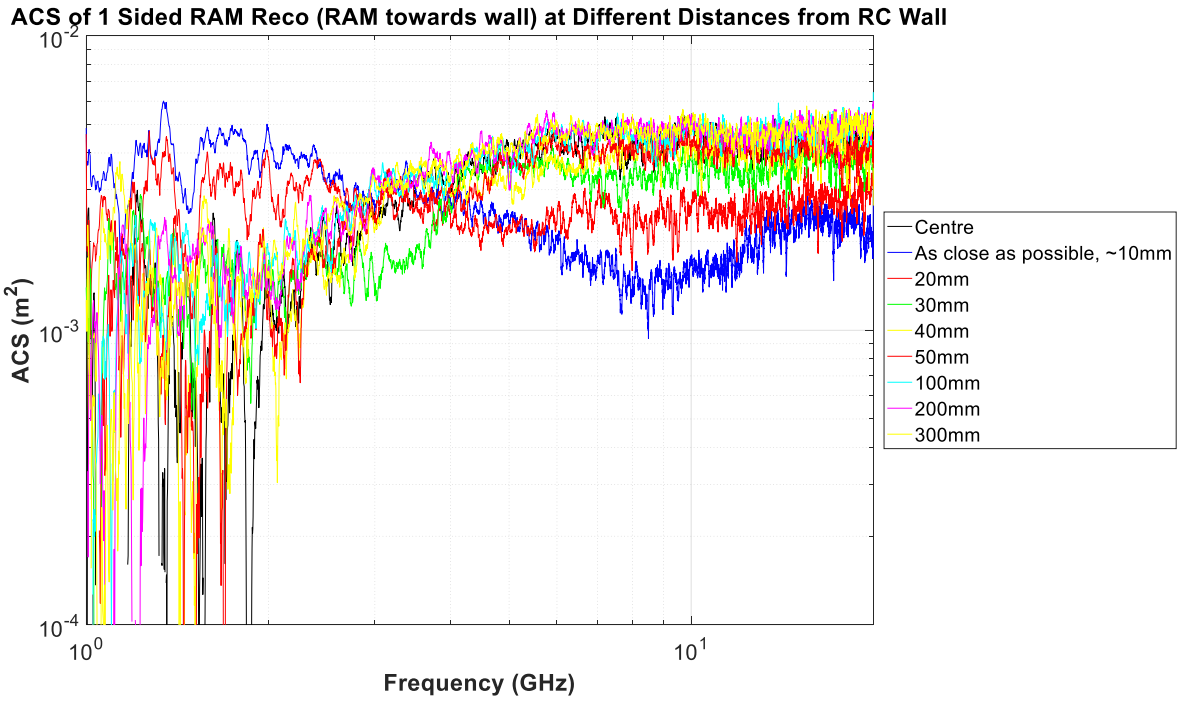

Figure 5.3: ACS of one sided reco measured at different distances from RC wall

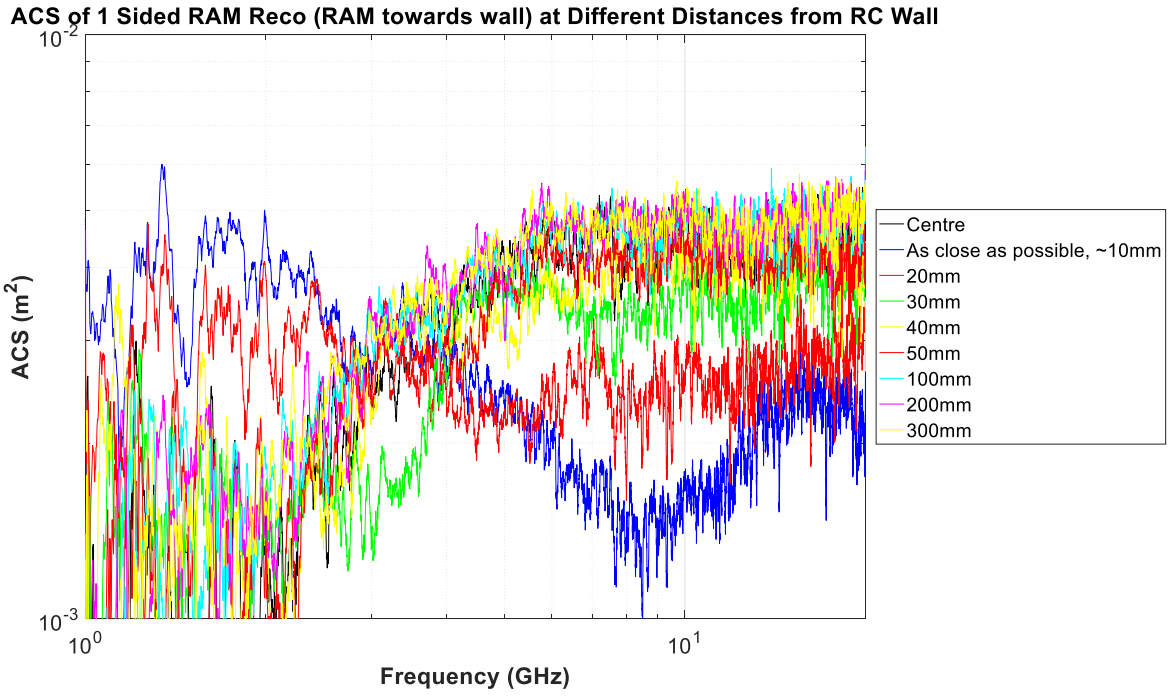

Figure 5.4: ACS of one sided reco measured at different distances from RC wall with spurious data below $10^{-3}m^2$ removed from the graph

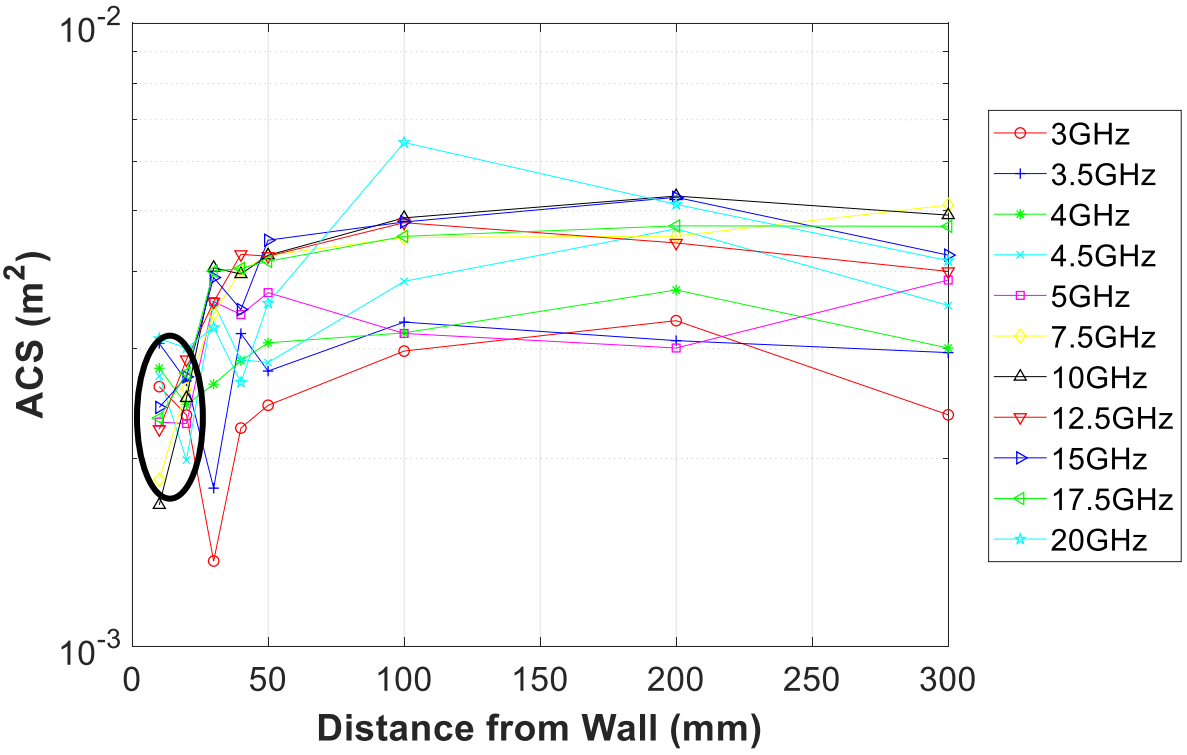

Figure 5.5: Graph showing how the ACS of the one sided RAM reco, with RAM facing towards the wall, changes with frequency at different distances from the wall

5.3.1.3. Reduction in ACS

Table 5.2 lists the approximate ACS above 5GHz for each measurement position away from the RC wall. Each of these ACSs has then been calculated as a percentage of the central reference value. For example, at 10mm the ACS levels out at approximately $2.45x10^{-3}m^2$ above 15GHz and for the reference ACS it is $4.5x10^{-3}m^2$. Therefore, the ACS at 10mm from the RC wall is 55% of the ACS in the centre of the RC. As the recos distance from the wall increases the ACS increases until above 50mm when it becomes comparable to the reference ACS. A graph of this increase is shown in Figure 5.6. Figure 5.4 shows that at approximately 8.5GHz the 10mm position ACS is $1.5x10^{-3}m^2$. This is 33% of the highest ACS.

Table 5.2: List of the measurement distances, the approximate ACS above 15GHz and this value as a percentage of the centre, reference ACS

Distance from Wall	ACS above 15GHz (m^2)	Percentage of Full ACS
Centre	4.50×10^{-3}	100%
300mm	4.50×10^{-3}	100%
200mm	4.50×10^{-3}	100%
100mm	4.50×10^{-3}	100%
50mm	4.25×10^{-3}	94%
40mm	4.00×10^{-3}	88%
30mm	3.75×10^{-3}	83%
20mm	2.75×10^{-3}	61%
10mm	2.45×10^{-3}	55%

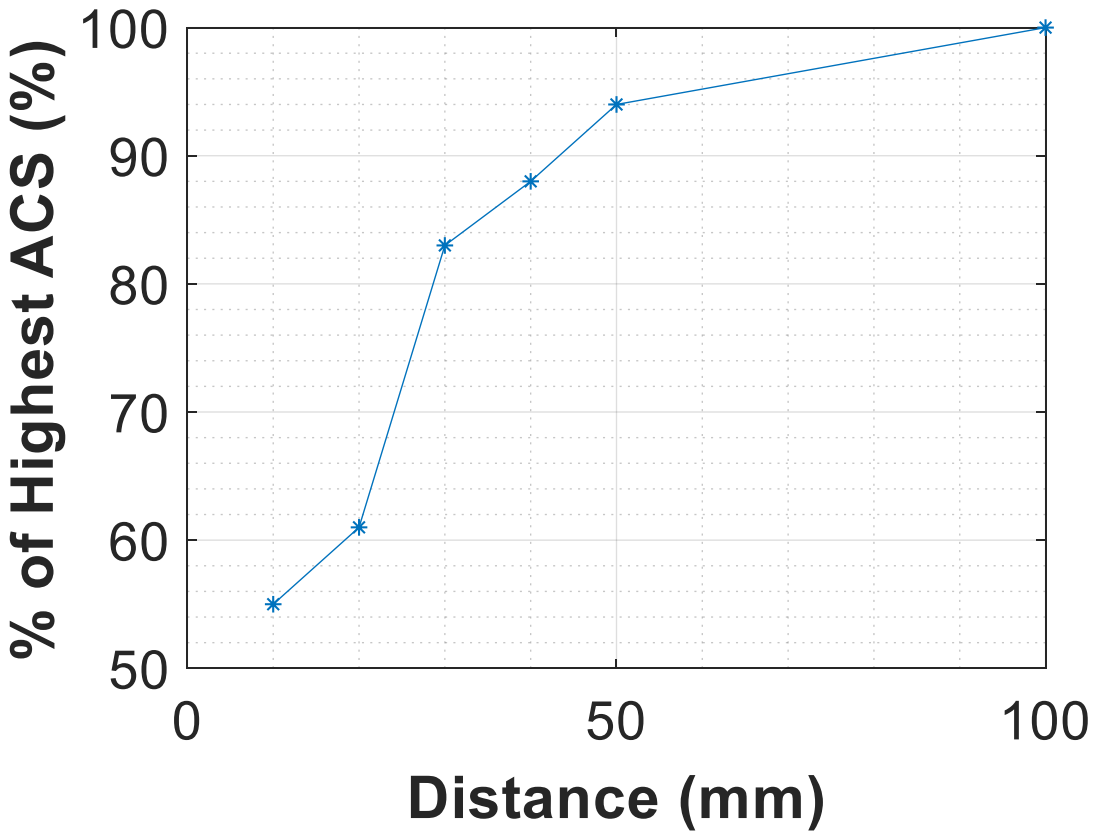

Figure 5.6: Graph showing the percentage of the highest ACS against the distance of the reco from the RC wall

Surface Area of the RAM

The reco has eight RAM pieces which have dimensions of 40mm x 20mm x 9mm. Each piece has a total exposed surface area of:

(40mm x 20mm) + 2 x (40mm x 9mm) + 2 x (20mm x 9mm) = **0.0019m^2**.

This exposed surface area value does not include one of the large faces of each RAM piece as this will be facing the aluminium sheet. The total exposed surface area of all eight pieces of RAM is **0.015m^2**.

When the reco is next to RC wall the exposed surface area of the RAM is reduced as the front faces of the RAM are blocked by the wall. In this case the surface area for each piece of RAM is:

2 * (40mm * 9mm) + 2 * (20mm * 9mm) = **0.0011m^2.**

For all eight pieces of RAM this is a surface area of 0.0086m^2. This value is 57% of the total surface area when the RAM is away from the wall.

Table 5.2 gives the reduction of ACS at 10mm as 55% of the ACS when the reco is in the centre of the RC. It is probable that the amount the ACS is reduced by is directly proportional to the reduction in exposed surface area.

5.3.1.4. Frequency Dependency

Figure 5.4 shows that the ACS of a reco positioned at different distances from the chamber wall differs from the centrally positioned reco as follows:

- At lower frequencies the ACS is significantly reduced from the ACS of the centrally positioned reco
- The ACS is at a minimum at a frequency which is dependent on how far away it is from the chamber wall

The ACS then increases until it levels out at a reduced ACS from the central position. The frequency at which the ACS levels out is also dependant on how far away the reco is from the chamber wall.

Table 5.3 shows various frequencies of interest that can be seen in Figure 5.4 and each column gives the following information:

- The first column is the distance from the reco to the RC wall.
- The second column is the wavelength frequency that each distance corresponds to (using $f = c_0/\lambda$).
- The third column is the frequency of the half wavelength of each distance
- The fourth column is the approximate frequency where the ACS levels out at its maximum ACS
- The final column is the frequency where the ACS is at its minimum.

At distances greater than 50mm these points become more difficult to read as they become similar to the reference value. At distances closer to the wall the ACS levels out at around the point where the frequency would be half a wavelength. The frequency at which the ACS is at its minimum corresponds to a wavelength of a quarter of the distance to the wall.

The reduction in ACS is minimal above 50mm. 40mm corresponds to a half wavelength of 3.75GHz. As seen in Figure 5.4, and in previous graphs of ACS, the results below 3GHz are unreliable. Therefore it makes sense that there is no observable reduction at 50mm and above as any reduction would be lost in the 'noise'. If this was to be investigated further an RC with a lower LUF would be required.

Table 5.3: Frequencies of interest for the ACS of the reco at different distances from the RC wall

Distance (mm)	Frequency	Frequency/2	Rejoining Point on Graph	Frequency of Minimum ACS
10	30GHz	15GHz	15GHz	8.5GHz
20	15GHz	7.5GHz	6-7GHz	3.5GHz
30	10GHz	5GHz	5GHz	2GHz
40	7.5GHz	3.75GHz	~3GHz	n/a
50	6GHz	3GHz	~2GHz	n/a
100	3GHz	1.5GHz	n/a	n/a
200	1.5GHz	750MHz	n/a	n/a
300	1GHz	500MHz	n/a	n/a

5.3.2. Two Sided Reco

The ACS measurements on the one sided reco at different distances from the RC wall have given an initial idea of how the ACS changes as the reco is moved away from the wall. In this section both sides of the reco are populated with RAM so that both the reco side facing the wall and the side facing away from the wall are absorbing. This is more representative of a PCB, although a PCB would have the different absorptions on each side.

5.3.2.1. Initial ACS Measurement of a Two Sided Reco

The first measurements using the double sided reco were carried out using the same method described in Section 5.3.1.1. Figure 5.7 shows the results for the one sided and two sided reco in two positions in the RC. Above 2GHz the measurements taken

with the reco in the centre of the RC have the same shape but are separated by a factor of two. As the two sided reco has twice the absorber of the one sided reco this is the expected result. When the recos are placed 10mm from the RC wall the ACS of the one sided reco is approximately a third of the two sided reco. The two sided reco has one side of absorber exposed and both recos have some absorption on the side facing the wall. This is why there is a greater difference in ACS.

From Figure 5.7 and the previous ACS results it can be seen that reducing the measurement error would allow smaller differences and changes to be seen in the results. A new method of measuring ACS in an RC was developed during the course of this work by another member of the AEG at the UoY [53][54]. This method reduces the error in the ACS measurement. The next section describes this method and how it is used in the work described in this thesis.

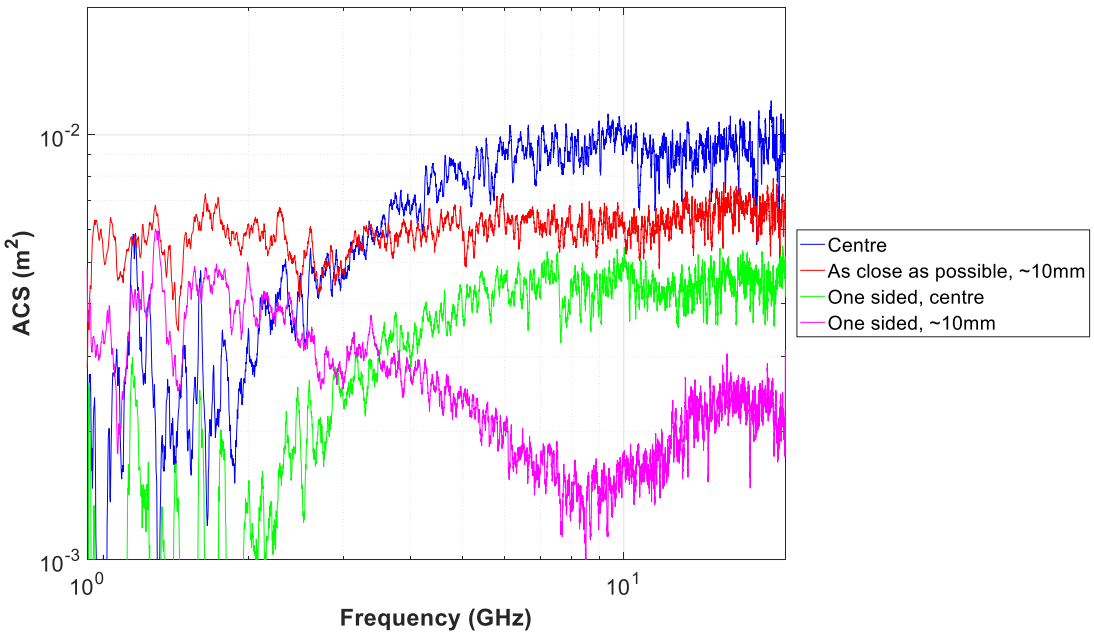

Figure 5.7: Comparison of the ACS of the one sided and two sided reco in two positions in the RC

5.3.2.2. Improved ACS Measurement Methodology

The new method was developed so that ACS measurements in a reverberation chamber can be made more quickly than with existing techniques [53][54]. This

makes ACS measurements of humans easier to carry out as the subject needs to be as still as possible during the measurement. The new technique calculates the energy decay time constant in the time domain by using a non-linear fitting method on the power delay profile [54]. Previously, linear fitting methods were used to do this but by using a non-linear method the number of samples required is reduced (a segmented sweep can be performed by the VNA) as well as removing the effect of the noise floor on the measurement and the effect of the window function used to select the frequency bands [54].

The physical set up of the experiment remains the same as shown in Figure 3.3 in Chapter 3. A two port calibration is carried out before beginning the measurement and the stirrer is stopped at 100 equally spaced positions in one full rotation of the stirrer. However, the VNA analyser is set up to do a segmented sweep from 1GHz to 20GHz. 189 segments were used with 51 points in each and 100MHz spacing between each segment. A reference measurement is made without an object in the RC and then with the object under test in the RC.

The data is processed by finding the Power Delay Profile (PDP) by carrying out the following functions:

$$\mathrm{PDP} = \langle |IFFT(S_{21} \cdot W)|^2 \rangle \quad \textbf{(5.3)}$$

Here, IFFT is an inverse fast Fourier transform and W is the window function that selects the required frequency bands. The chamber time constant can be found from the slope of the PDP by using the non-linear curve fitting technique [54]. This part of the analysis was carried out by Matlab code obtained from the author of [53][54]. Once the time constant has been obtained the Q-factor of the loaded and unloaded chamber can be calculated using (5.4).

$$Q = \omega\tau \quad \textbf{(5.4)}$$

The ACS of the loaded and unloaded chamber is then calculated using (5.5). The ACS of the object under test can then be found by subtracting the unloaded chamber ACS

from the loaded chamber ACS. A comparison between the old and new method of measuring the ACS is shown in Figure 5.8.

$$\langle \sigma \rangle = \frac{2\pi V}{\lambda Q} \qquad \textbf{(5.5)}$$

5.3.2.3. Results

Figure 5.9 and Figure 5.10 show the ACS results of the two sided reco at different distances from the RC wall using the new method of measurement. Both logarithmic and linear scales have been included so that differences in the structure of the plots can be seen. Above 3GHz, the ACS is showing similarities to the results seen with the one sided reco in Figure 5.4. The closer the reco is to the wall the more the ACS is reduced. At distances greater than 40mm it is difficult to distinguish the results from the reference ACS. When the reco is close to the wall the ACS is reduced until it eventually levels out at a value closer to the reference ACS. This happens at different frequencies depending on the distance of the reco to the RC wall. The most obvious difference is the two sided reco's greater ACS, which was seen in Figure 5.7.

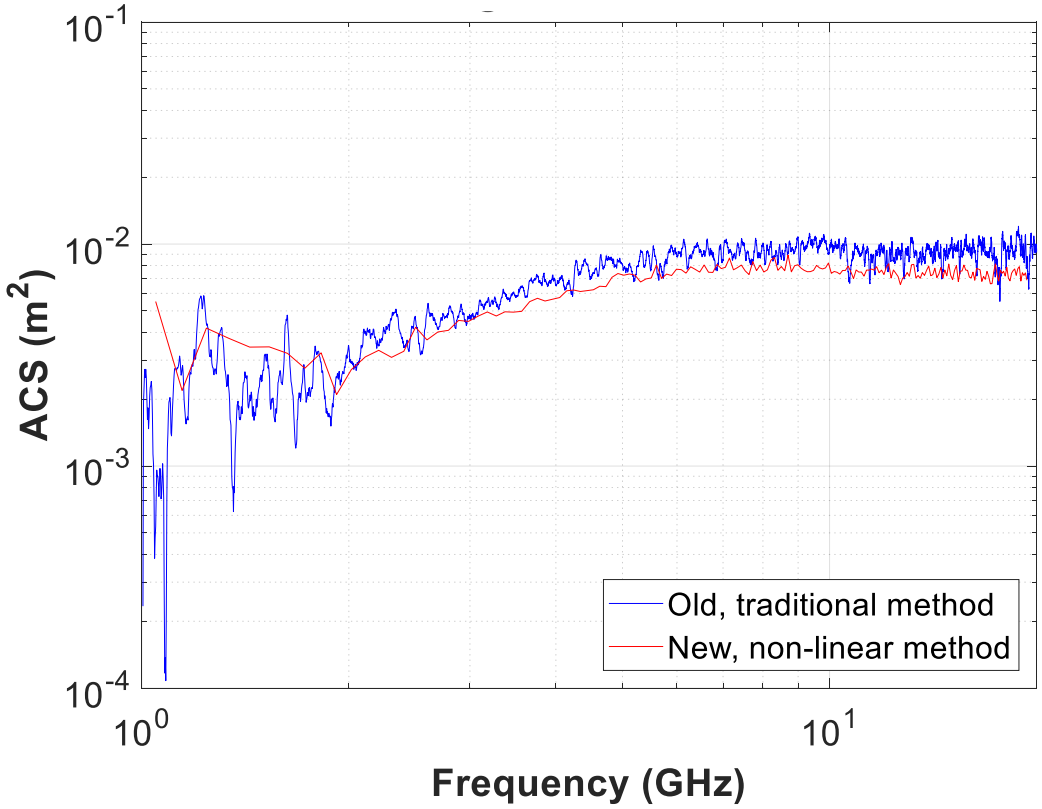

Figure 5.8: Comparison between the original ACS measurement method and the new, non-linear curve fitting method.

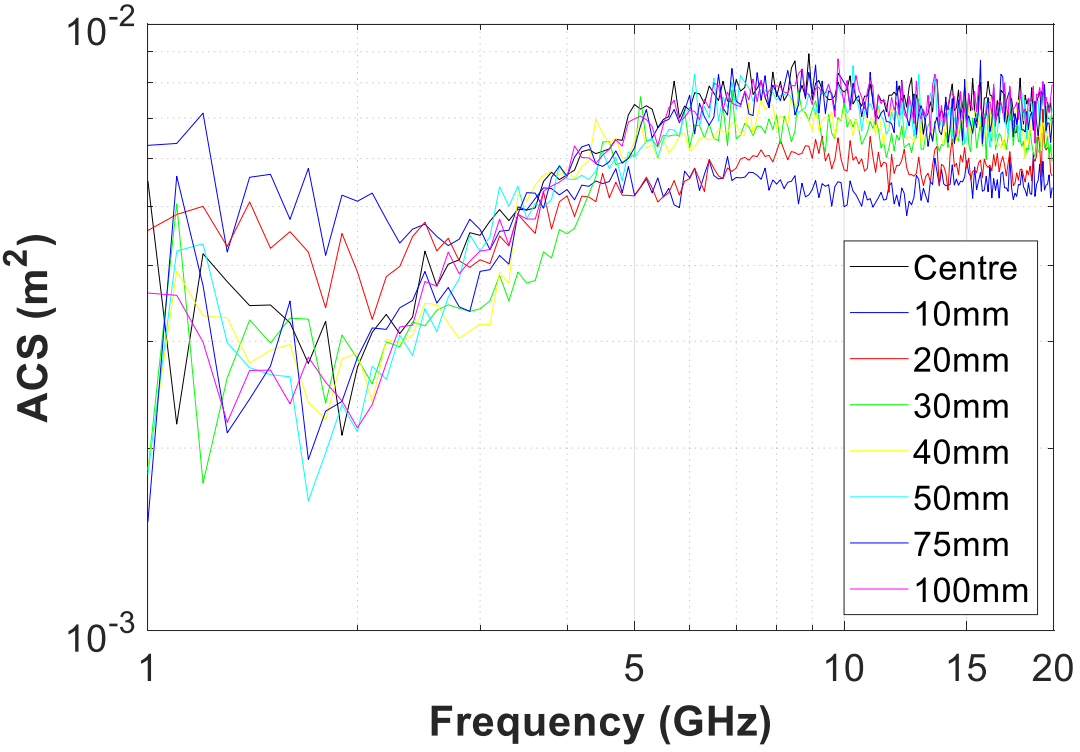

Figure 5.9: ACS of the two sided reco at different distances from the RC wall using the new method of measurement – logarithmic scale

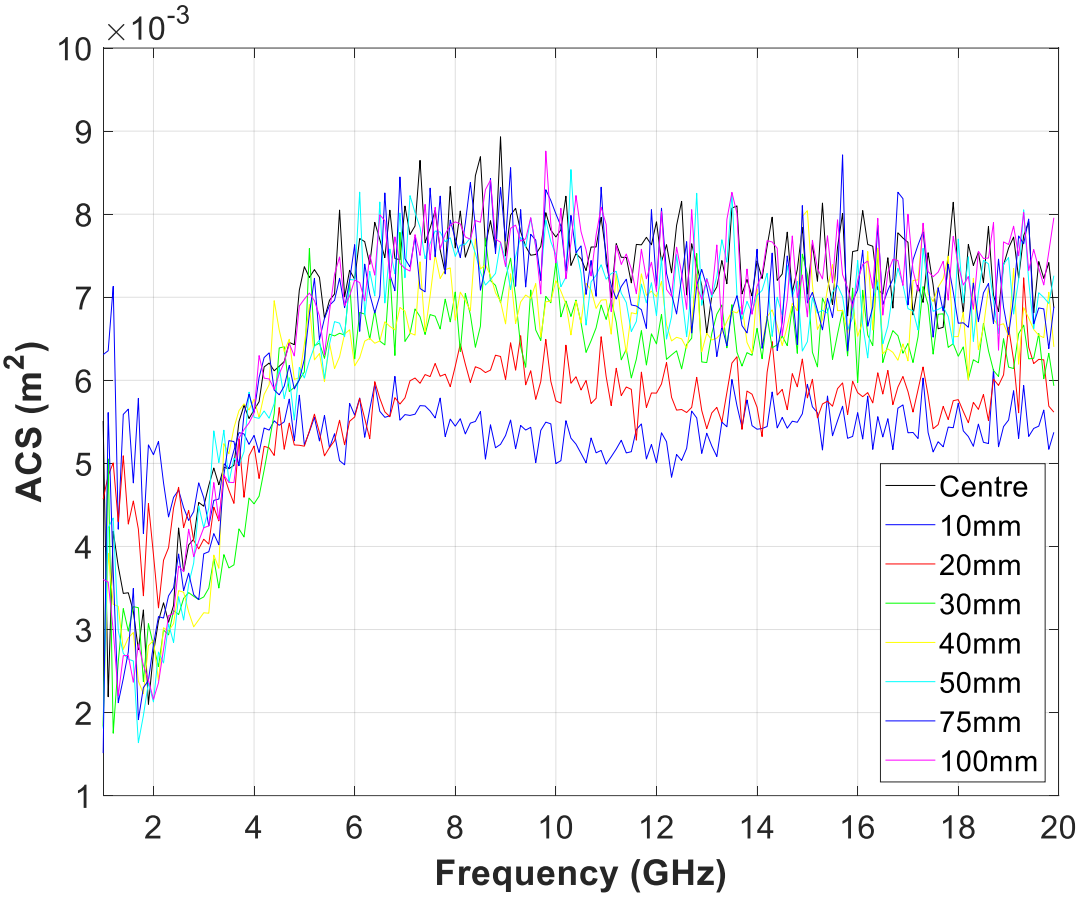

Figure 5.10: ACS of the two sided reco at different distances from the RC wall using the new method of measurement – linear scale

Figure 5.11 plots the ACS against the distance away from the RC wall for different frequencies. No results have been included for frequencies lower than 5GHz as this is lower than the LUF of the small RC. For the two sided reco the results seem to have less dependence on frequency compared to the one sided reco and the ACSs are all between $6.5 \times 10^{-3} m^2$ and $8 \times 10^{-3} m^2$ once the ACS is no longer affected by the RC wall (after 50mm).

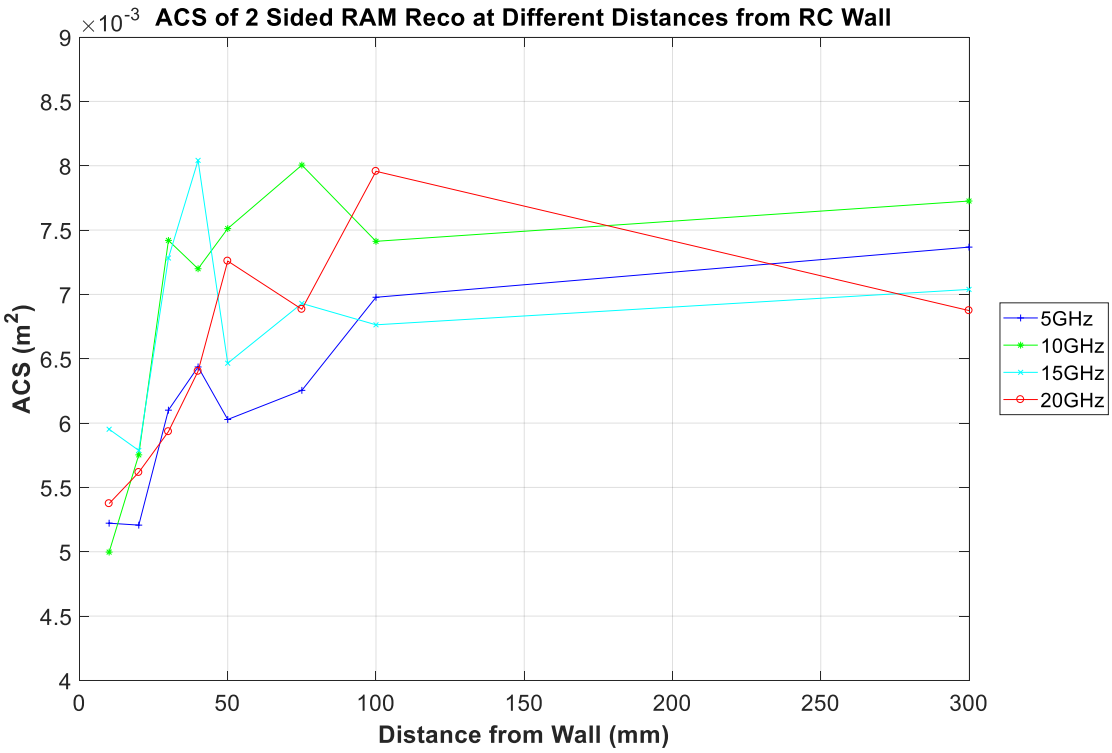

Figure 5.11: ACS of the two sided reco at different distances from the RC at different frequencies

5.3.2.4. Reduction in ACS

Table 5.4 lists the approximate ACS above 5GHz for each measurement position. Each of these ACSs has then been calculated as a percentage of the central reference value. For the 10mm position, the ACS levels out at approximately 5.5 x$10^{-3}$$m^2$ above 15GHz and for the reference ACS it is 9x$10^{-3}$$m^2$. This makes the ACS at the RC wall 75% of the ACS in the centre of the RC. As the reco is moved further away from the RC wall the ACS increases and at a distance greater than 50mm the ACS is approximately the same as the reference value.

A graph showing the reduction as a percentage (calculated for each frequency point from the actual measurement data) is shown in Figure 5.12. The data is fairly uniform showing that the structure of the reference and wall position ACSs are similar.

Figure 5.13 plots the reduction as a percentage against the distance away from the RC wall. This graph shows that the reduction is independent of the frequency it is

being measured at. It is apparent that between 10mm and 50mm from the wall the ACS is reduced quickly. When the reco is positioned 75mm and above from the wall there is little difference between those positions and the central, reference position.

Table 5.4: List of the ACS above 5GHz and as a percentage of the reference ACS at different distances from the wall

Distance from Wall	ACS above 5GHz (m^2)	Percentage of Full ACS
Centre	7.25×10^{-3}	100%
100mm	7.25×10^{-3}	100%
75mm	7.25×10^{-3}	100%
50mm	7×10^{-3}	96%
40mm	6.75×10^{-3}	93%
30mm	6.5×10^{-3}	90%
20mm	6×10^{-3}	83%
10mm	5.5×10^{-3}	75%

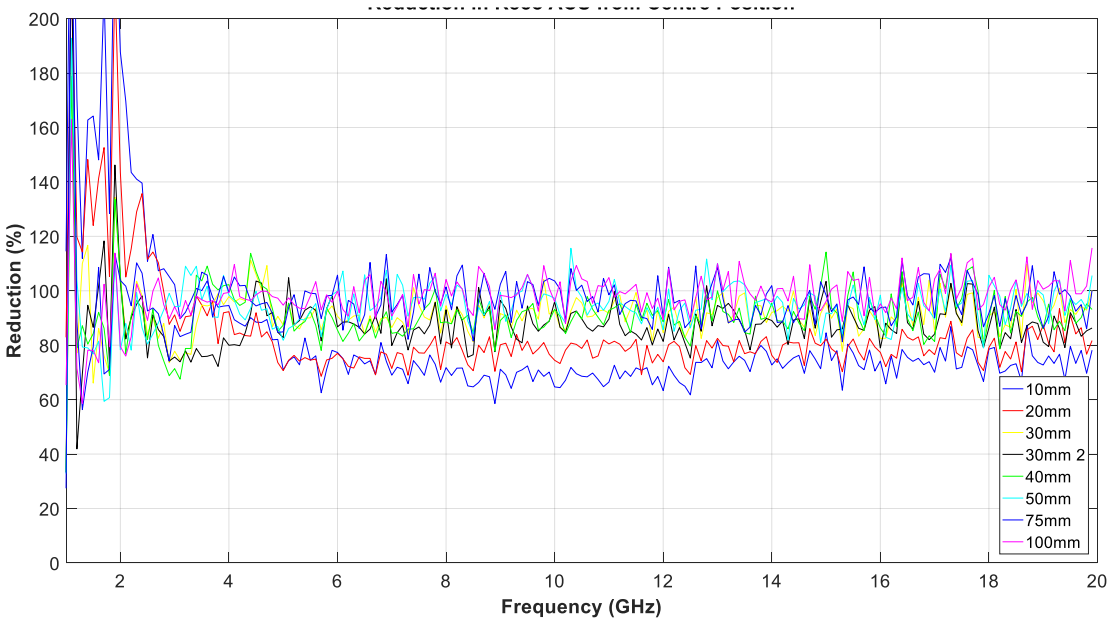

Figure 5.12: Reduction in ACS for the reco in different measurement positions

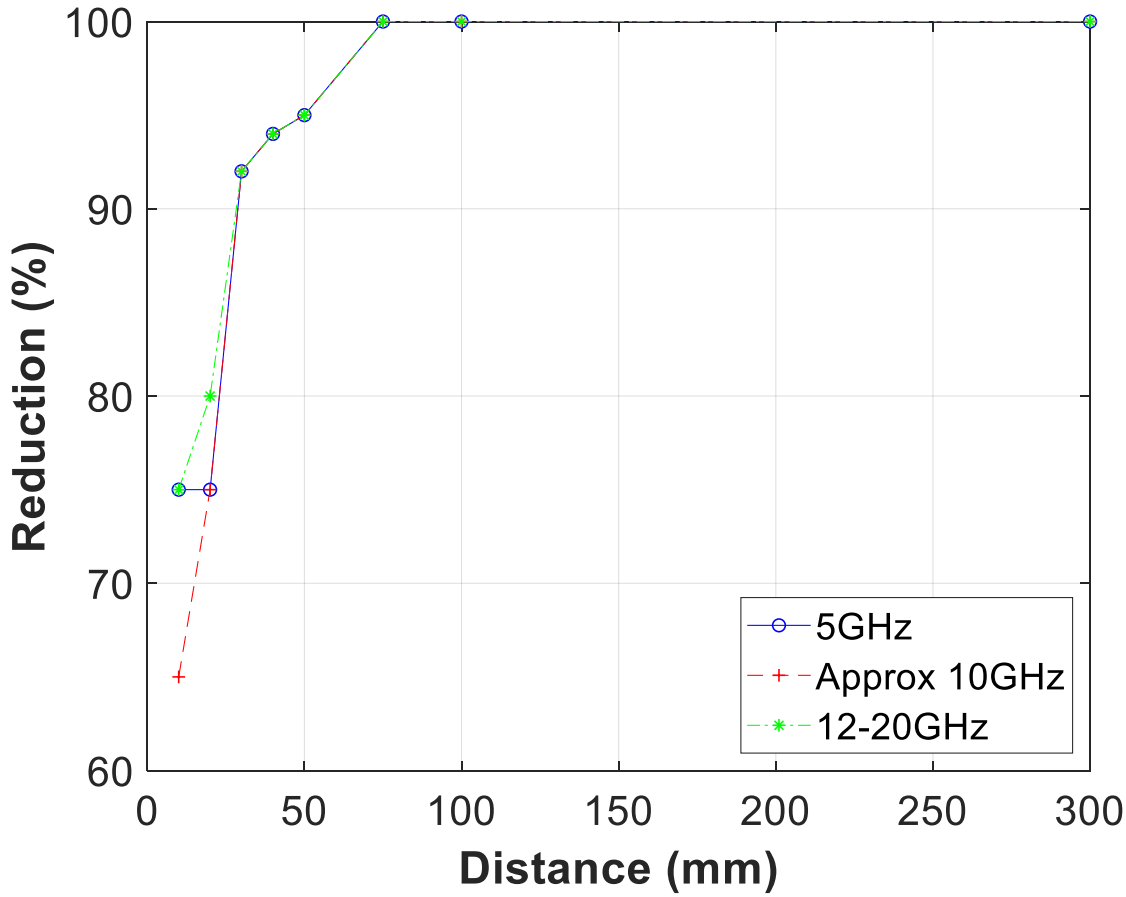

Figure 5.13: Graph showing the reduction of ACS as a percentage of the centre ACS against the distance of the reco from the RC wall

Surface Area of the RAM

The two sided reco has 16 pieces of RAM with a total exposed surface area of **0.03m^2**. When the reco is next to the wall the total exposed surface area is

$0.015 + 0.0086 = 0.0236m^2$

When next to the wall the exposed surface area is 78% of the total surface area of the exposed RAM. From Table 5.4 the ACS is reduced to 75% of the reference ACS. Like the one sided reco, the ACS has been reduced in line with the reduction in exposed absorbing surface area.

When the two sided reco is placed next to the RC wall the ACS is reduced to 75% of the total ACS. The one sided reco is reduced to 55% of the total value. This is to be expected as the absorbing RAM on the side facing away from the wall is still exposed and able to absorb energy.

5.3.2.5. Frequency Dependency

As there is a smaller reduction in ACS than for the one sided case, it is more difficult to see frequency points of interest in Figure 5.9.

5.4. Measuring ACS of Part of an Object

This section looks at the ACS of each individual side of two different PCBs. One side of the PCB is covered with foil and then the PCB is measured in the RC.

5.4.1. Methodology

The new method of measuring ACS, described in Section 5.3.2.2, was used for the measurements in this section. The same set up and test equipment parameters were used. For each measurement a sheet of foil was placed over one side of the PCB and the foil carefully pressed around the components. Due to the complexity of the PCB shape it was not possible for the foil to fit perfectly around all the components; there are some small gaps between the PCB and the foil. The foil was secured around the edge of the board using copper tape. The PCBs had various connectors which overlapped the edge of the board and some small gaps remained between the foil and the edges of the PCB. Photographs of the PCBs covered in foil are shown in Figure 5.14.

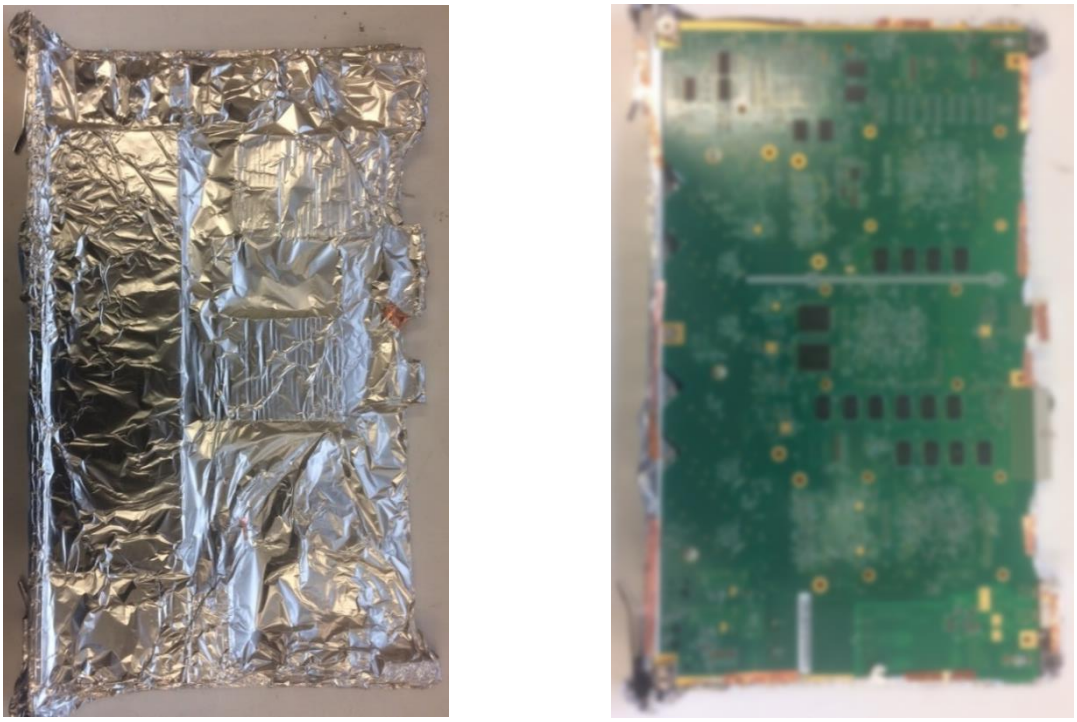

Figure 5.14: Photographs of a PCB its top side covered in foil (left) and its bottom side (right). The photograph has been blurred, at the request of Huawei, to preserve design confidentiality

5.4.2. Reco Measurements

The first measurements carried out using foil to cover one side of the object under test were performed on the double sided reco. Figure 5.15 shows the ACS of the two sided reco with no foil on it, the reco with one side covered in foil and the result with the reco 10mm from the RC wall. The majority of the ACS measurement with no foil falls between $7x10^{-3}m^2$ to $8x10^{-3}m^2$. When one side is covered by foil the result is between $4x10^{-3}m^2$ and $5x10^{-3}m^2$ and when positioned next to the wall between $5x10^{-3}m^2$ and $6x10^{-3}m^2$.

Figure 5.16 shows the two measurements with a reduction in ACS as a percentage of the total ACS. When the reco is half covered in foil the ACS is reduced to nearly half of the total ACS compared to the result next to the wall which is reduced to between 60% and 80% of the total. If covering one side of the reco with foil worked perfectly it might be expected that the ACS would be reduced to 50% of the total value. The reasons why it is slightly above this value could be errors in the measurement, the ACS could be different on each side or the foil is not covering the side of the reco fully so some energy is still getting absorbed on the covered side.

There is a difference of up to 30% between the foil and RC wall measurement. When measuring close to the RC wall the sides of the RAM pieces are still exposed and so more energy is absorbed so the ACS is reduced less. See Section 5.3 for the full explanation.

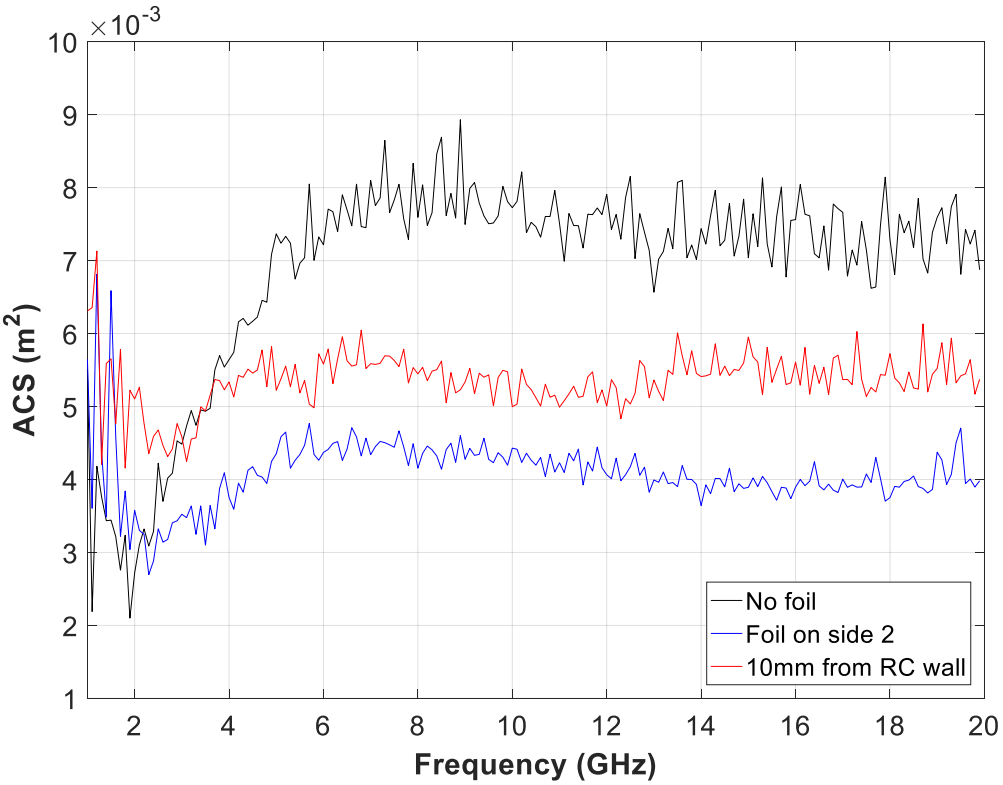

Figure 5.15: ACS of the two sided reco, one side of the reco covered in foil and the reco 10mm from the RC with no foil.

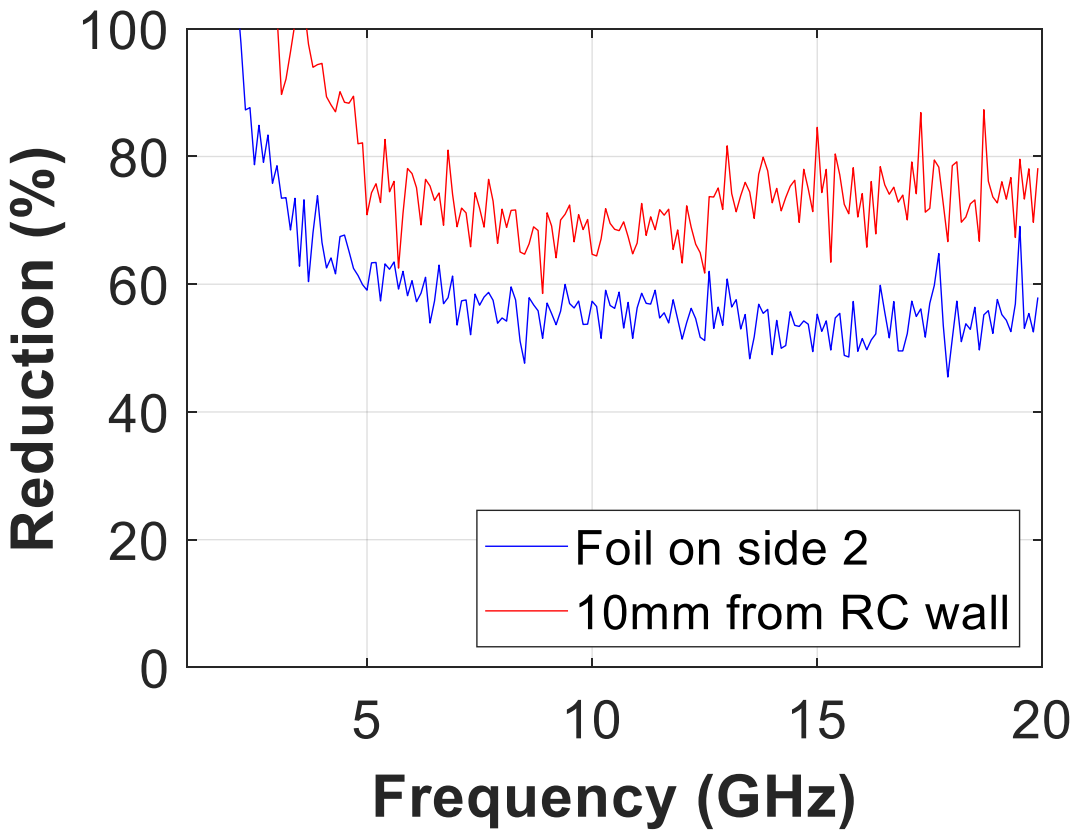

Figure 5.16: The reduction in ACS for the foil and RC wall measurement as a percentage of the total two sided reco ACS

5.4.3. PCB Measurements

The next sections describe the ACS measurements of PCBs partially covered in foil. The measurements show how the different sides of the PCBs have different levels of absorption. Chapter 6 presents a method to measure the transmission through a PCB. Two PCBs have been measured in this section; one with low transmission through it and one with higher transmission through it.

5.4.3.1. High Transmission PCB

The first results presented are for the PCB with higher transmission (6U_PCB2). The corrected transmission through this PCB was measured and will be described in Chapter 6; it was found to be between -50dB and -25dB. The top side and bottom side of the PCB are shown in Figure 5.17.

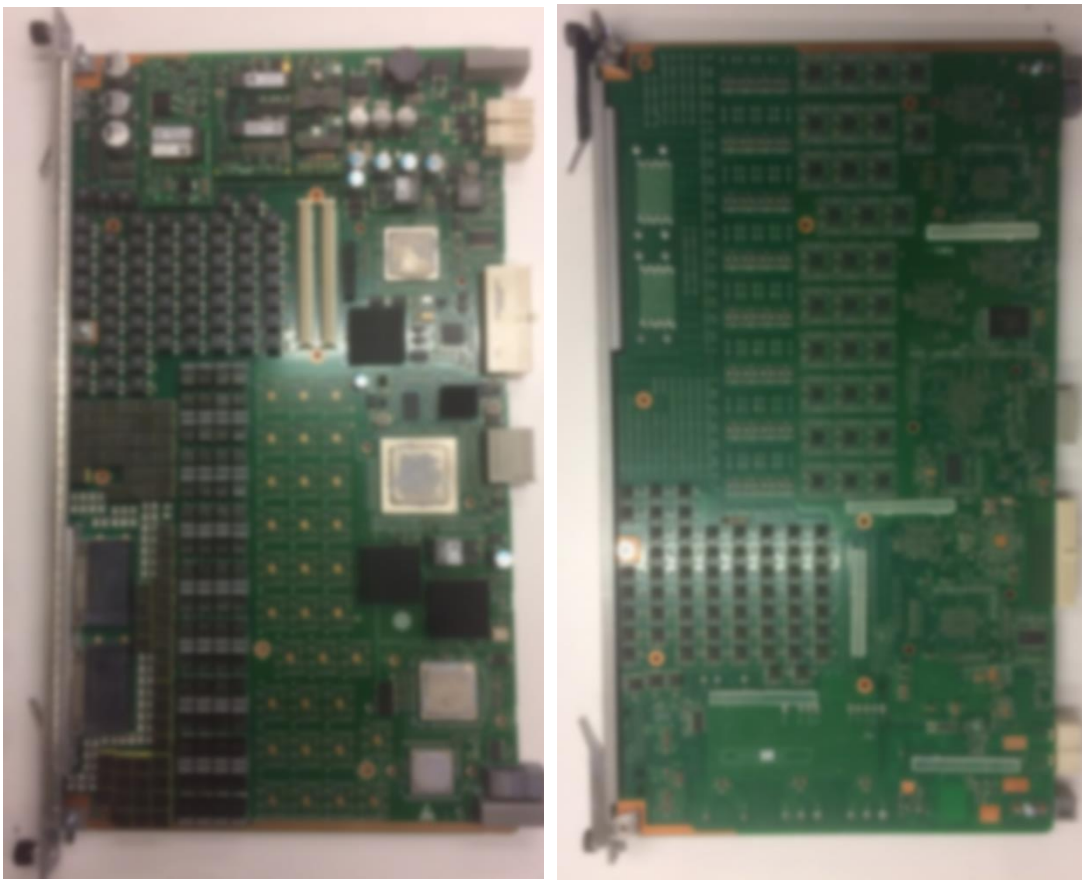

Figure 5.17: The top and bottom sides of 6U_PCB2. The photograph has been blurred, at the request of Huawei, to preserve design confidentiality.

The following measurements were carried out:

- The top of the PCB (with the majority of components on) covered in foil
- The bottom of the PCB (with a minimal amount of components on) covered in foil

Figure 5.18 and Figure 5.19 show each of the measurements listed above with a reference measurement where the PCB has no foil covering it. It is clear that the ACS of the top of the PCB (measured with the bottom of the PCB covered in foil) is greater than the ACS of the bottom of the PCB. The difference between the two sides is approximately $0.003m^2$ but varies over the frequency range. The top of the PCB is covered in components. This means there is far more surface area than the bottom side and that the different materials may absorb more energy than the mainly component-less bottom side. The graph also shows a plot of the ACS with the top covered and ACS with the bottom covered summed together. If the measurement was perfect and the foil allowed the individual sides to be measured completely separately then the sum would equal the reference measurement with no foil. However, the summed ACS is significantly higher than the reference value. Figure 5.19 shows that it is between approximately 120% and 150% of the reference ACS. There could be a number of different reasons for this:

- Due to the components on the PCB the foil isn't perfectly fitted around the PCB. Gaps around the foil might allow energy to be absorbed on the covered side
- The PCB might transmit energy through the substrate which can then be absorbed on the covered side
- The foil is absorbing a significant amount of energy
- Errors in the measurement – but not to the extent of the difference we see here.

Figure 5.20 shows the results with a measurement of the foil used to cover the PCB. The foil has a very low ACS which does not need to be taken into account; it is below $4\times10^{-4}m^2$ throughout the frequency range. The foil is not causing the summed ACS of the individual sides to be higher than the total ACS of the PCB.

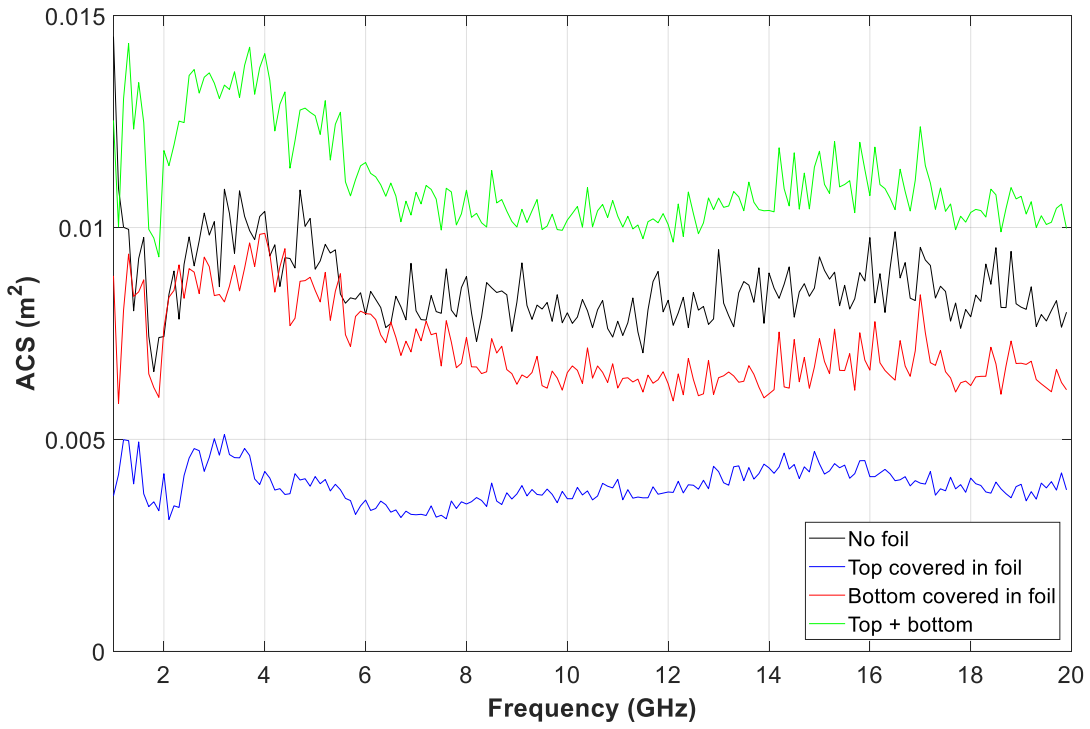

Figure 5.18: High transmission PCB ACS when it is uncovered, has each side covered in foil and the sum of the individual sides

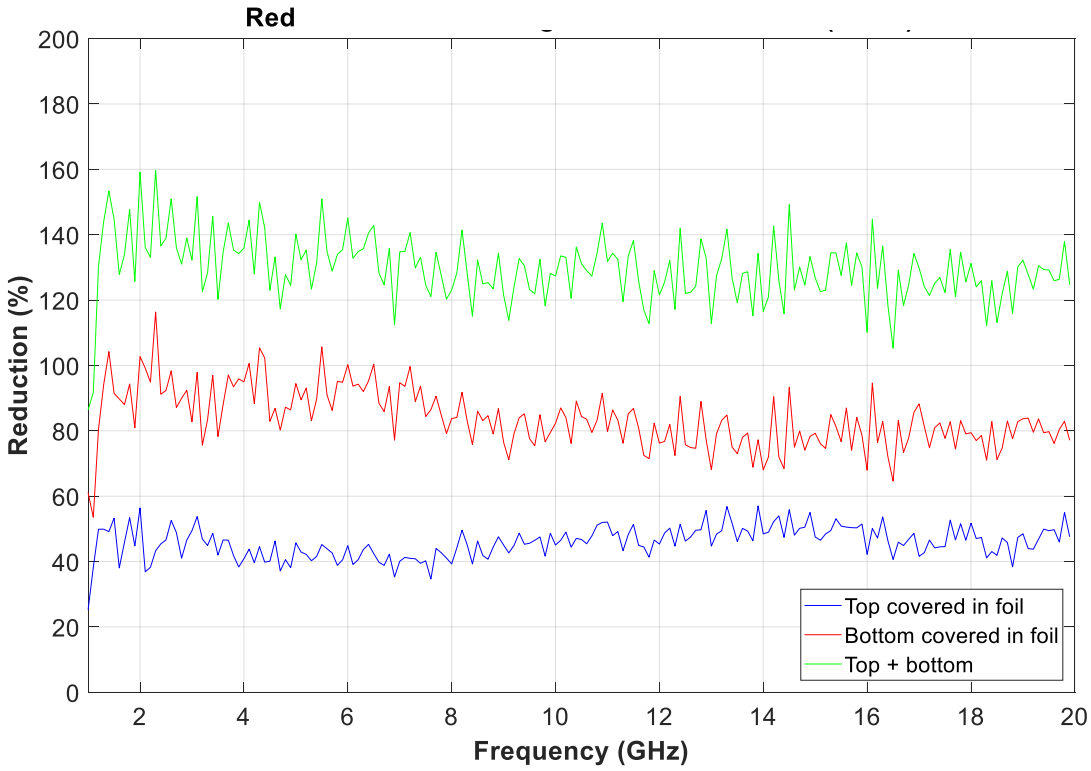

Figure 5.19: The reduction in ACS as a percentage of the partial and summed ACS compared to the reference ACS

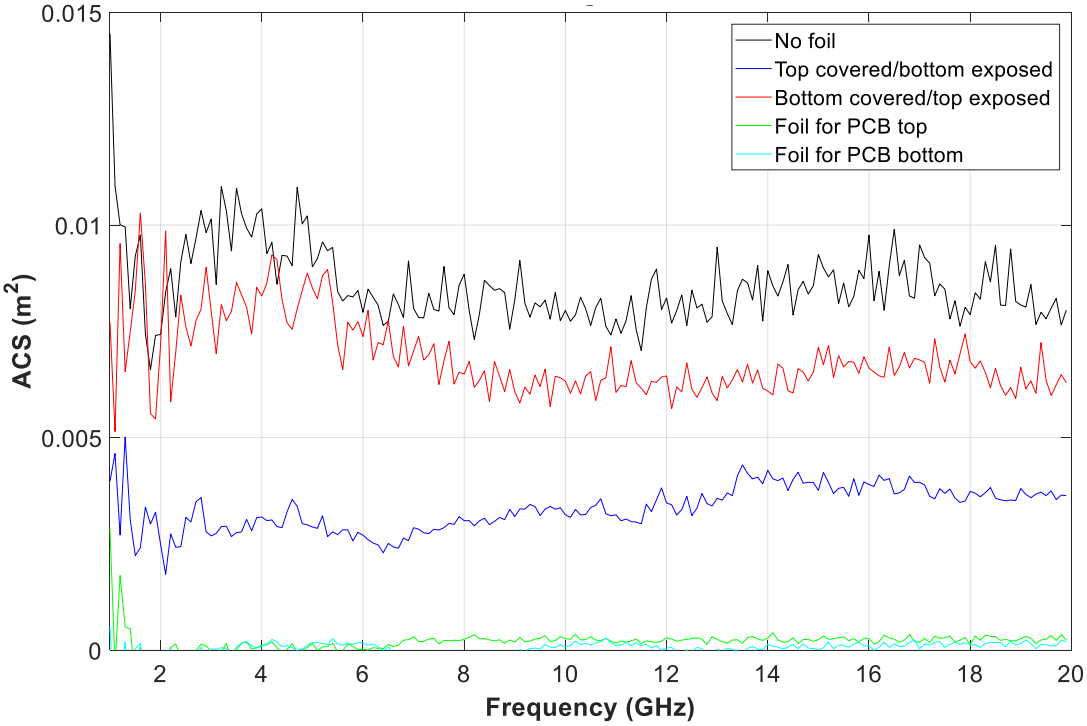

Figure 5.20: ACS of the PCB covered in foil measurements including the foil only ACS

5.4.3.2. Low Transmission PCB

The next results presented are for the PCB with lower transmission (6U_PCB1). The corrected transmission of this PCB was measured in Chapter 6 and is generally below -50dB. This is 25dB lower than the higher transmission PCB discussed in the previous section. The top side and bottom side of the PCB are shown in Figure 5.21.

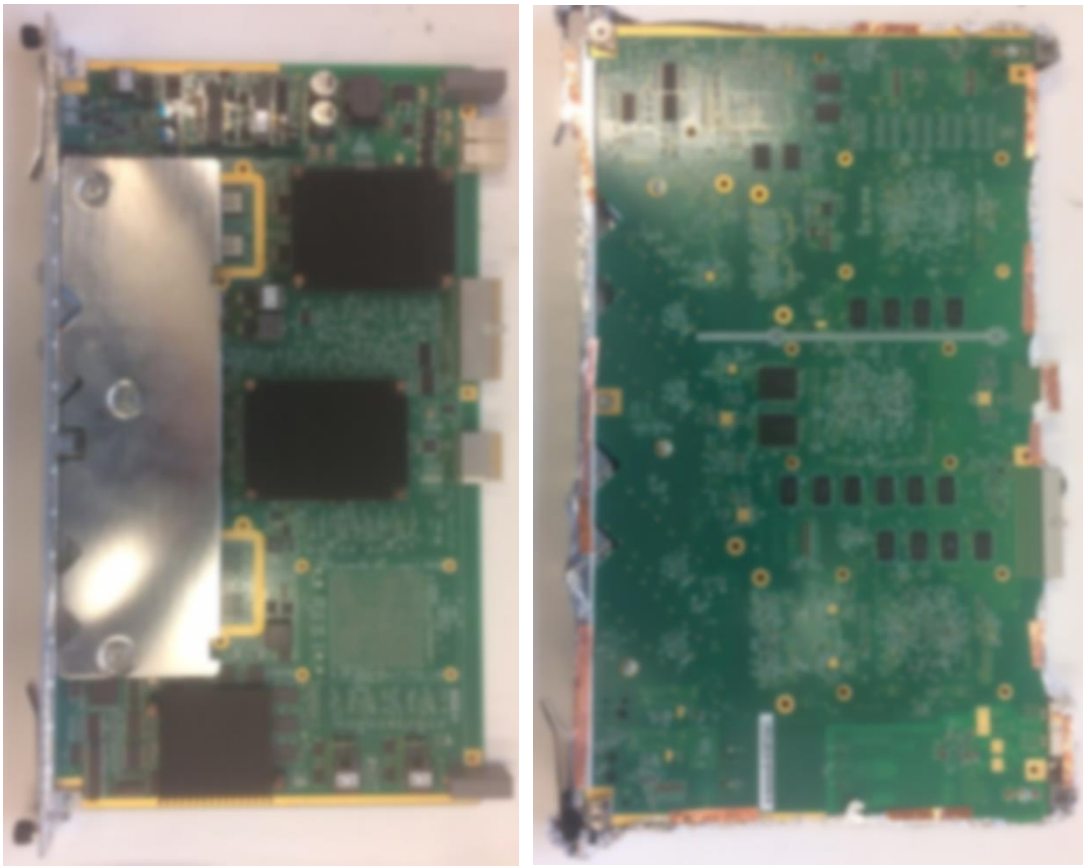

Figure 5.21: The top and bottom sides of 6U_PCB1. The photograph has been blurred, at the request of Huawei, to preserve design confidentiality.

The same measurements as for the high transmission PCB were carried out:

- The top of the PCB (with the majority of components on) covered in foil
- The bottom of the PCB (with a minimal amount of components on) covered in foil

Figure 5.22 and Figure 5.23 show each of the measurements listed above with a reference measurement with the PCB uncovered. As with the high transmission PCB, it is clear that the ACS of the top of the PCB (with components on) is greater than the ACS of the bottom of the PCB. The measured ACS of the top of the PCB is between

0.003m^2 and 0.005m^2 and the bottom of the PCB is between 0.002m^2 and 0.003m^2. In the frequency range of 10GHz to 20GHz the difference is approximately 0.001m^2; the ACS bottom of the PCB is around 70% of the top of the PCB.

Again the graph shows a plot of the ACS of the individual sides summed together. As before, this summed value of ACS is greater than the ACS of the PCB when measured uncovered with no foil. For the low transmission PCB the summed value is generally between 140% and 160% of the reference value.

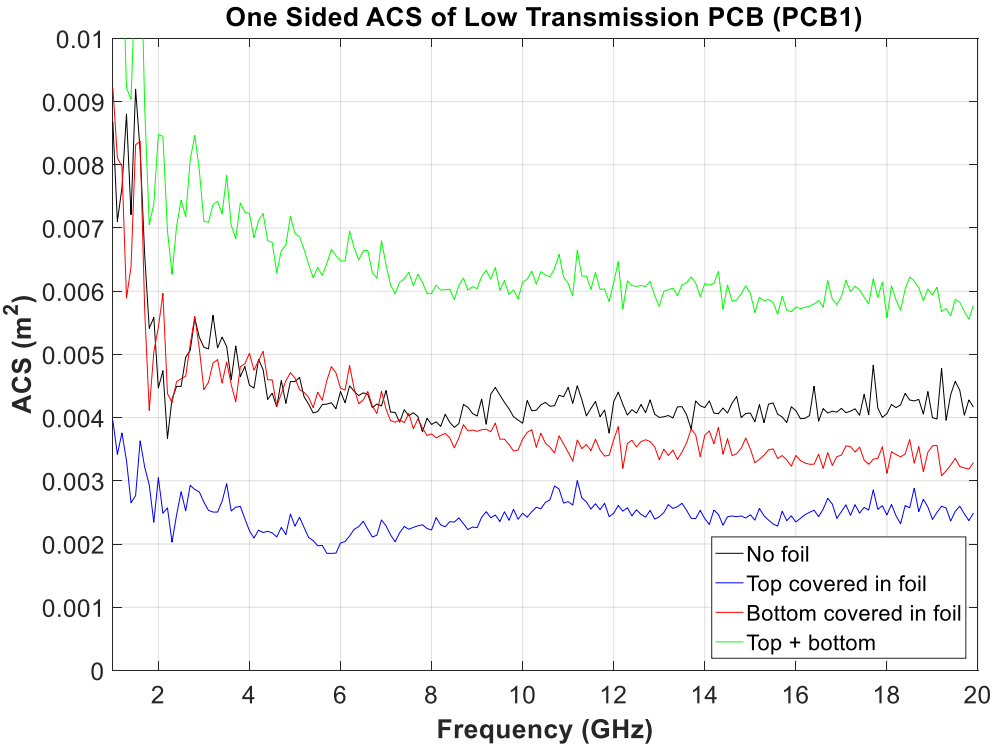

Figure 5.22: ACS of the low transmission PCB as a function of frequency when it is uncovered, has each side covered in foil and the sum of the individual sides

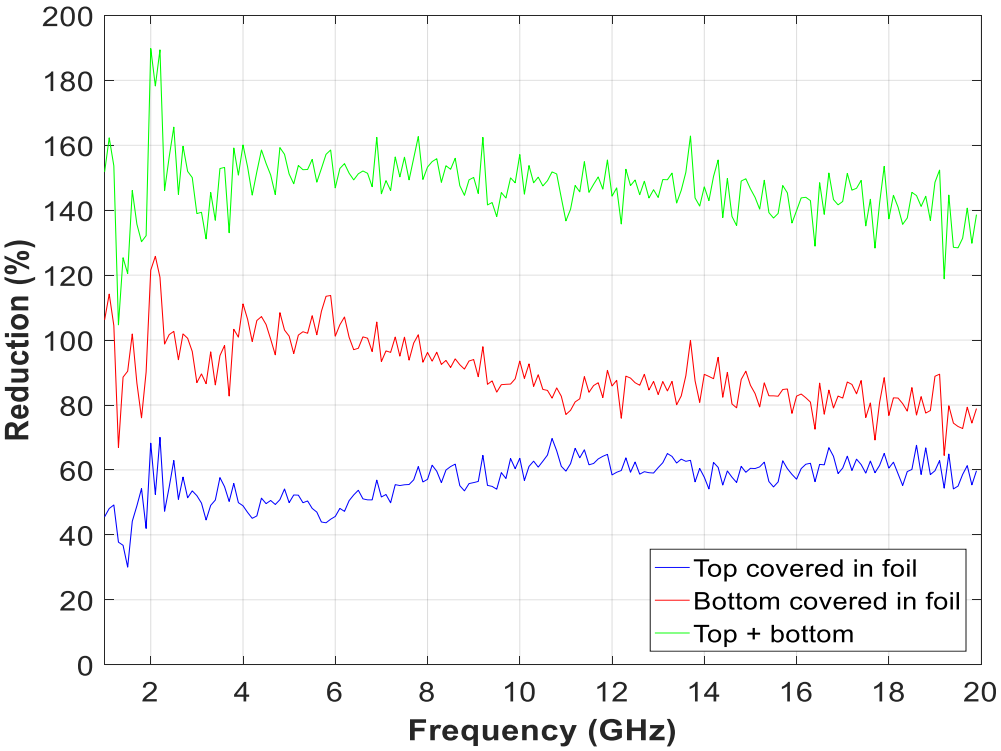

Figure 5.23: The reduction in ACS as a percentage of the partial and summed ACS compared to the reference ACS

5.4.3.3. Comparison between High and Low Transmission PCB

Figure 5.24 compares the reduction in ACS of each side of each of the PCBs to each PCB measured uncovered. When the top side of the PCB is uncovered then both the high and low PCB have been reduced to between 60% and 90% of the total ACS of each PCB and this reduction is similar for both PCBs. When the bottom of the PCB is measured both PCBs show a much greater reduction of generally between 30% and 60%. However, there is a difference of approximately 10% to 20% between the high and low transmission PCBs. The high transmission PCB has been reduced by a greater amount than the low transmission PCB.

The difference between the reductions in ACS of the bottoms of the PCBs could be explained by:

- Differences in how the foil was fitted around the PCB
    - If this was the case then it may also be likely that a difference would also be seen in the reductions in ACS of the tops of the PCB
- Differences in the components on the PCBs
- The difference in the transmission through each of the PCBs

Figure 5.25 shows the reduction in ACS when the individual sides of the PCB are summed together as a percentage of the ACS with the PCB measured as a whole. When each side of the low transmission PCB is summed there is a greater difference to the PCB measured uncovered result than that observed for the high transmission PCB. As the bottom of the low transmission PCB is reduced by less this is why the result in Figure 5.25 is seen.

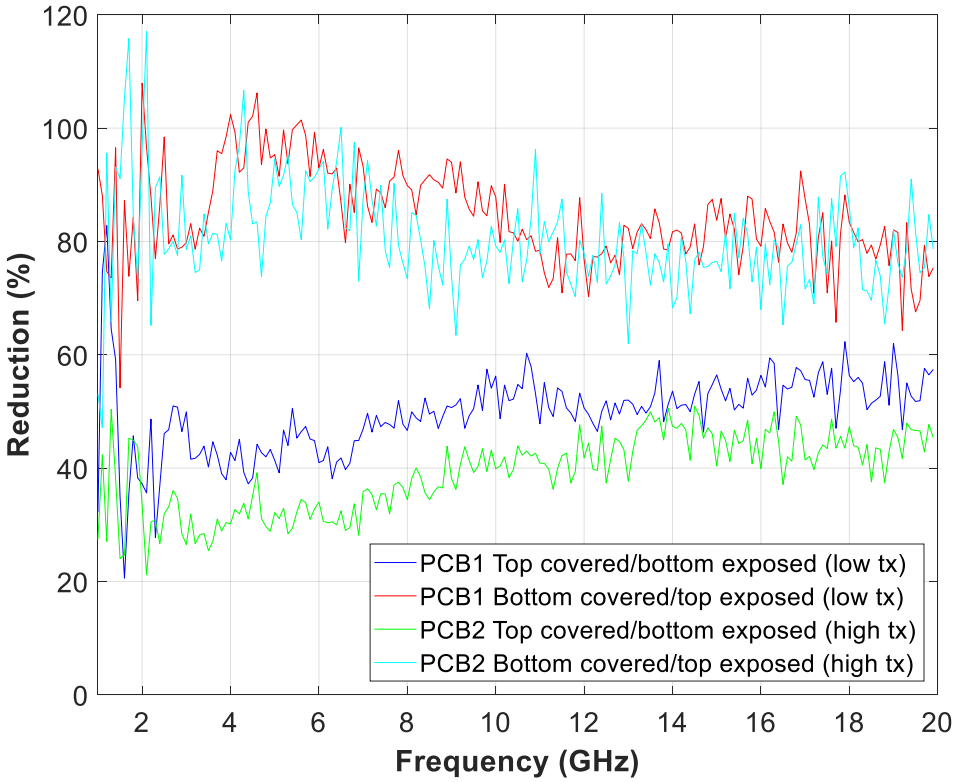

Figure 5.24: Reduction in ACS of each side of the PCBs to the PCB measured uncovered

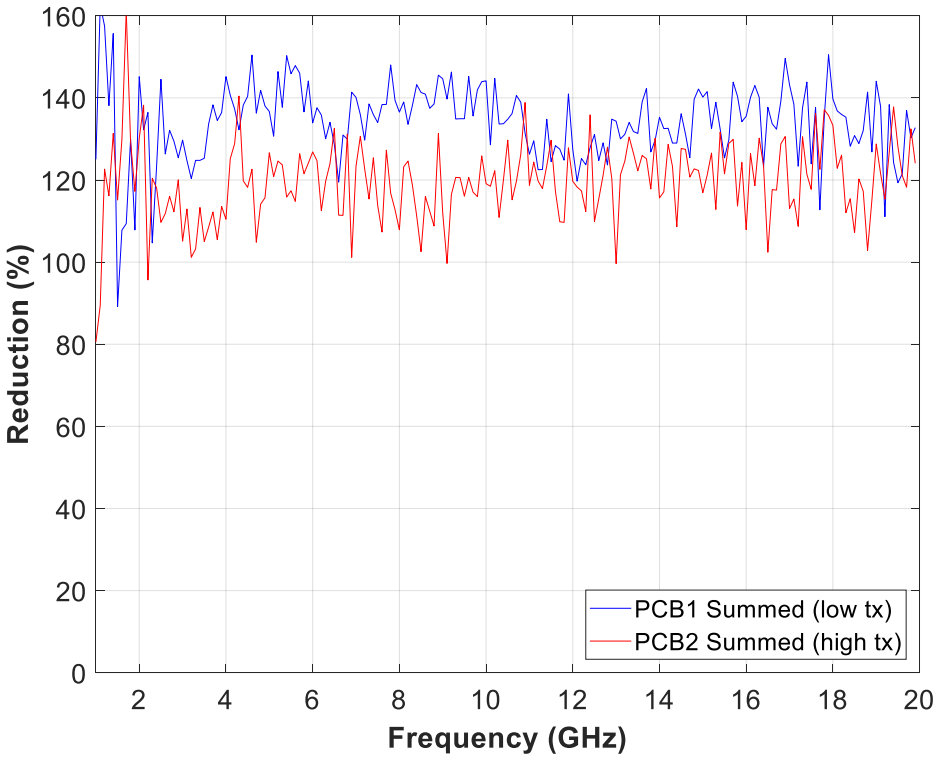

Figure 5.25: Reduction in ACS of the two sides of each PCB summed together compared to each PCB as a whole

5.5. Summary

If a PCB divides an enclosure into two cavities, only one side of the PCB should be considered in each cavity. Two sets of measurements have been presented in this chapter to attempt to measure the ACS of a single side of a PCB or reco.

The first set of measurements used a reco which was placed at different distances from the RC wall. When the reco was placed next to the RC wall its measured ACS was reduced by the same amount the surface area of the absorber was reduced by. As the reco was moved further away from the wall the ACS increased until being closer to the RC wall had no effect. This occurred at around 50mm from the wall.

The second set of measurements taken was of a PCB with one side covered in foil. The measurements showed that the top and bottom of the PCBs have different levels of ACS; this is expected as there are different components covering each side of the PCB. Covering one side of the PCB in foil reduced the ACS of the PCB but not as much as expected. When summed together the ACS of the individual sides of the PCB were greater than the ACS of the PCB measured without foil. There are a number of different reasons this is the case and these need investigating further to understand the results.

The next chapter looks at how the transmission through a PCB can be measured and whether it is significant enough to be considered when modelling enclosures.

Chapter 6

Transmission through Printed Circuit Boards

6.1. Overview

The previous chapters investigated the ACS of PCBs. In this chapter, the transmission through PCBs is considered. If a PCB segments an enclosure into different cavities the transmission through the PCB may need to be considered. This is in addition to the energy being transmitted through the apertures around the PCB and the energy that the PCB absorbs.

This chapter describes a method of measuring the transmission through PCBs. The problem is similar to that of measuring the SE of a planar sheet. Various techniques are available for the SE measurement of a planar sheet [55] but many require the edges of the sample to be quite flat and conductive. This is not possible with real PCBs as components are often mounted quite close to the edge of the PCB. Even when there are no components close to the edge, the surface of the PCB may not be conducting. The method of measuring the transmission through a PCB discussed in this chapter is based on a method developed by the AEG at the UoY. The SE of planar samples is measured using a piece of test equipment that minimises the requirement for edge conductivity; this is known as the absorber box method [57].

6.2. PCB Transmission Measurement Methodology

6.2.1. PCB Transmission Measurement Set Up

The absorber box measurement set up is shown in the diagram in Figure 6.1 and in the photographs in Figure 6.2.

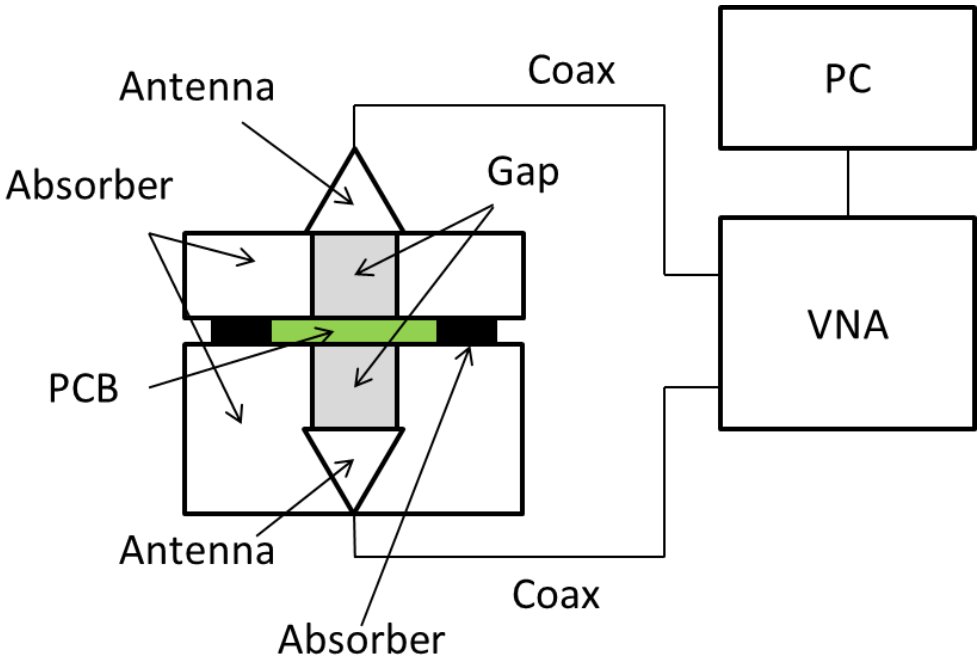

Figure 6.1: Diagram of the absorber box measurement set up

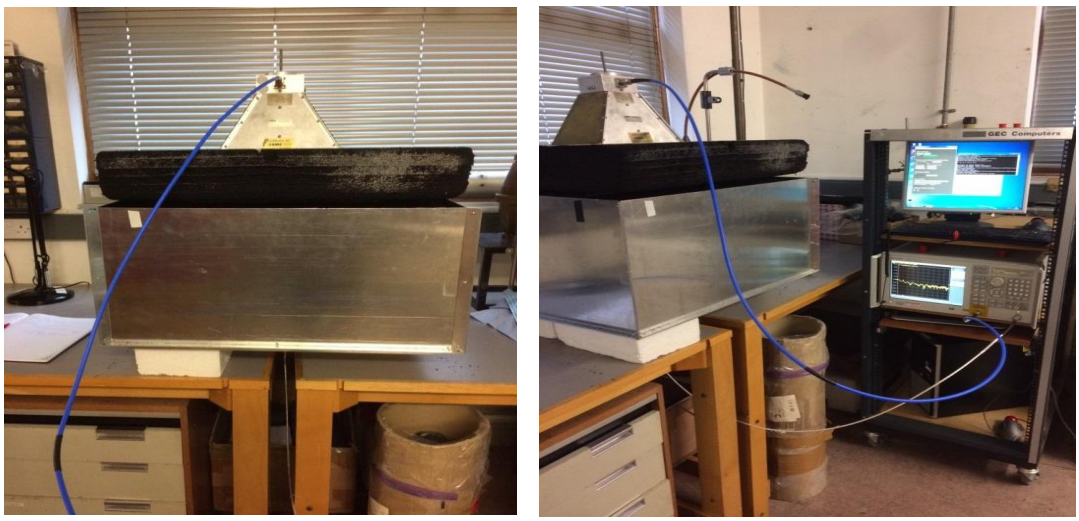

Figure 6.2: Photographs showing the absorber box with the top horn antenna on the left and the absorber box with the coaxial connections to the VNA on the right

The absorber box has dimensions of 600mm x 600mm x 330mm. The aperture in the absorber between the antennas is 140mm x 150mm. The sample is placed over the aperture between two blocks of layered absorber. The top absorber is made from AN79 layered absorber and the absorber inside the box is layered LS22 carbon loaded absorber. Two commercially available ridge horn antennas, ETS 3115 [55], are positioned above and below the sample under test which are connected to an Agilent E4404b VNA using coaxial cables. The absorber around the sample acts to terminate the sample so that the energy that would normally be diffracted around the sample is absorbed.

The VNA was used to collect a full set of S-parameters between 500MHz and 8GHz. The sweep time used was 5 seconds and 1601 frequency points were measured over this frequency range. The S-parameter data was collected and saved using the AEG measurement software. A moving average filter with a window covering 200MHz was applied to the data during post-processing.

The sample under test was placed between the two blocks of absorber material. The sample was placed so that the gap in the absorber was positioned centrally on the sample. As the height of the PCB causes the top block of absorber to be lifted away from the bottom block a gasket, using pieces of LS22 absorbing material, was placed around the sample. This is to ensure that the leakage around the sample is reduced as much as possible.

6.2.2. Calibration Measurement

In addition to the measurement of the sample under test a calibration measurement is required. This is in order to remove the effect of standing waves which may be set up in the absorber box cavity due to sample reflection coefficients being close to -1 [57].

The reference measurement is carried out with the circular brass plate shown positioned in the absorber box set up in Figure 6.3. The plate has an array of circular holes spaced 10mm apart each with a 3mm diameter to create a sheet of material with a known SE [57].

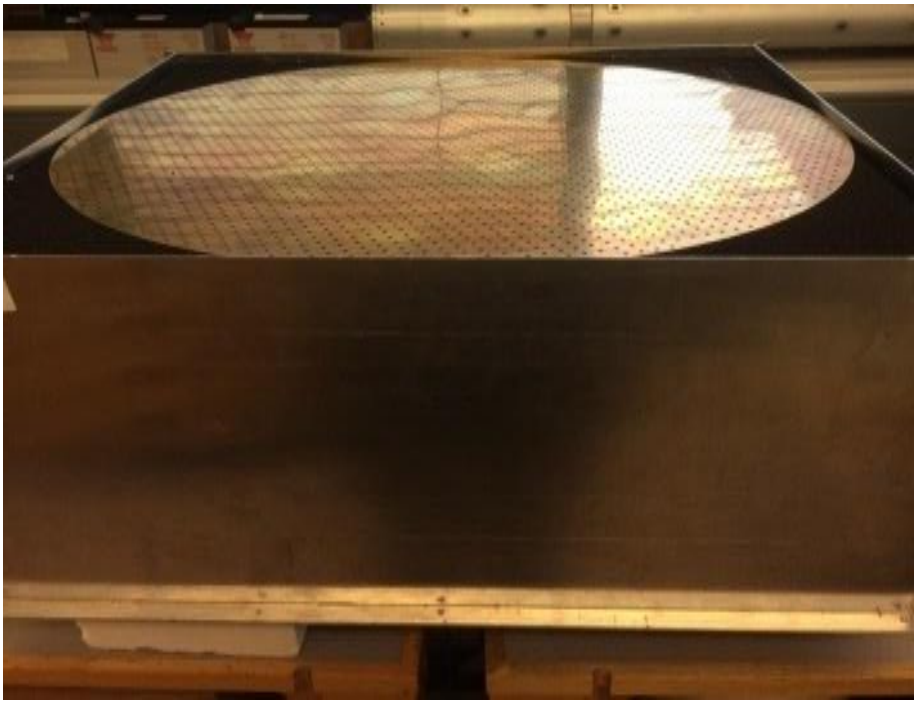

Figure 6.3: Photograph of the brass reference sample in the absorber box

6.3. Calculation of Corrected Transmission

The transmission of each measured sample can be calculated using Equation (6.1) [57].

$$T_C^{sample} = S_{21}^{sample} \frac{T^{ref}}{S_{21}^{ref}} \quad \textbf{(6.1)}$$

Where T^{ref} is the known transmission through the reference sample, S_{21}^{ref} is the measured transmission through the reference sample and S_{21}^{sample} is the measured transmission through the sample under test. The known transmission of the reference sample is calculated using Equation (6.2),

$$SE = 117 - 20 \times \log(f)\, dB \quad \textbf{(6.2)}$$

where f is frequency in MHz.

6.4. Samples under Test

The transmission of three types of sample has been measured using the absorber box. The first sample was a plain sheet of aluminium with dimensions of 395mm x 240mm and thickness of 1mm. The second was a sheet of plain, undeveloped PCB substrate with a layer of copper on one side. This sample has dimensions of 300mm x 227mm and thickness of 1mm. These samples are shown in Figure 6.4.

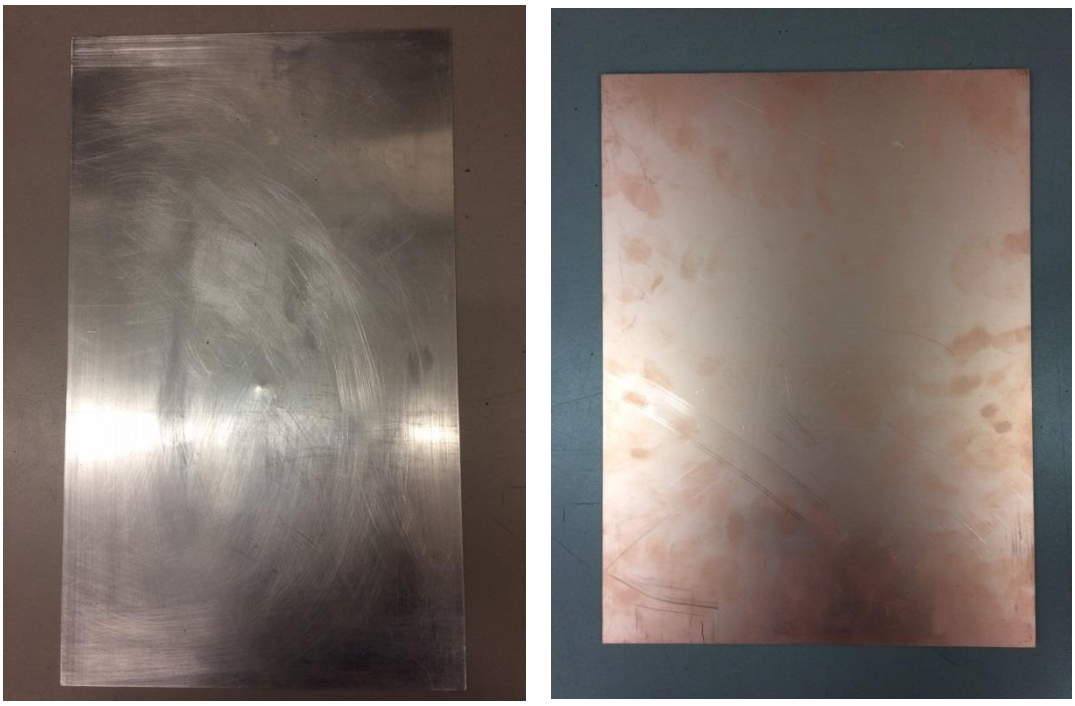

Figure 6.4: Photographs of the aluminium sheet on the left and the PCB substrate with the copper facing up on the right.

Three PCBs taken from the 6U Huawei enclosure were measured. These PCBs are shown in Figure 6.5 and are 6U_PCB1, 6U_PCB2 and 6U_PCB5. For brevity, the '6U_' will be removed throughout this chapter. Each PCB has dimensions of 365mm x 210mm and has a variety of different components on them including heat sinks, connectors, ICs and passive components. PCB1 and PCB5 have the largest amount of metal on their surface. PCB2 has significantly less metal on its surface and also has a larger amount of ceramic and plastic components on it. The underside of each PCB also has some low profile components on which cause the board to be lifted slightly from the surface the PCB is lying on. This distance was measured using a pair of

callipers as 3mm ± 0.05mm. This distance varies only slightly around each of the PCBs. All three of these PCBs have had their ACS measured in the RC.

Figure 6.5: The photograph shows each of the PCBs under test. From the top: PCB5, PCB2, PCB1. The photograph has been blurred to preserve design confidentiality at the request of Huawei.

6.5. Measured Transmission through the Sheet Materials

The aluminium and substrate sheet were each measured in four different configurations. The sheets were measured flat on the block of absorber and then lifted 1mm, 2mm and 3mm from the block using 1mm plastic spacers. This is to see the effect the 3mm gap under the PCB has. The aluminium sheet should have negligible transmission. Therefore, measuring the aluminium sheet flat on the absorber will show the minimum transmission, or maximum SE, that can be measured using this set up.

Figure 6.6 and Figure 6.7 show the corrected transmission measurements of the aluminium and substrate sheet respectively.

Figure 6.6 shows that the minimum measurable transmission is approximately -70dB from 2GHz to 8GHz. As the aluminium sheet is lifted further from the absorber the transmission increases to a maximum of around -55dB above 2GHz but still has approximately the same structure as when there is no gap between the absorber and sample under test. As the sheets are lifted above the absorber the size of the gap increases which causes more leakage around the sample thus increasing the measured transmission.

Figure 6.7 shows a similar result for the PCB substrate. In this case the transmission is higher at the lower end of the frequency range but decreases to roughly the same transmission as the aluminium sheet between 6GHz and 8GHz for the 0mm case. The reason for this is most likely due to the slightly smaller sample size. This causes more leakage around the sample at the lower frequencies.

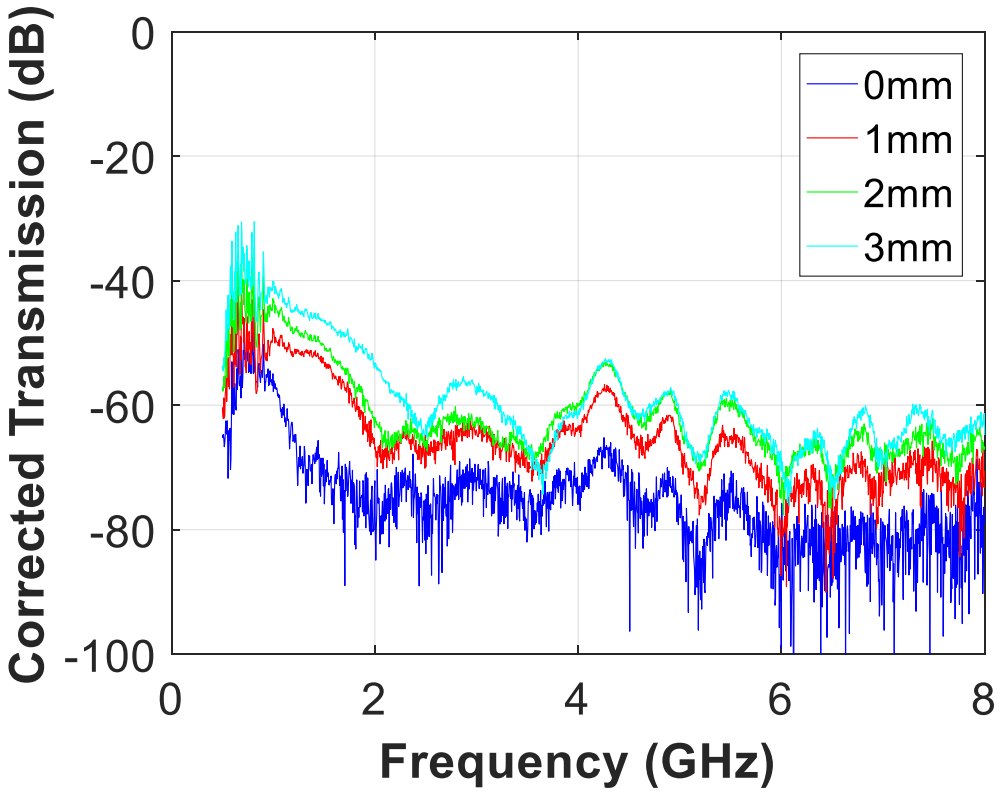

Figure 6.6: Measured corrected transmission of the aluminium sheet flat on the bottom of the absorber block and lifted 1mm, 2mm and 3mm from it

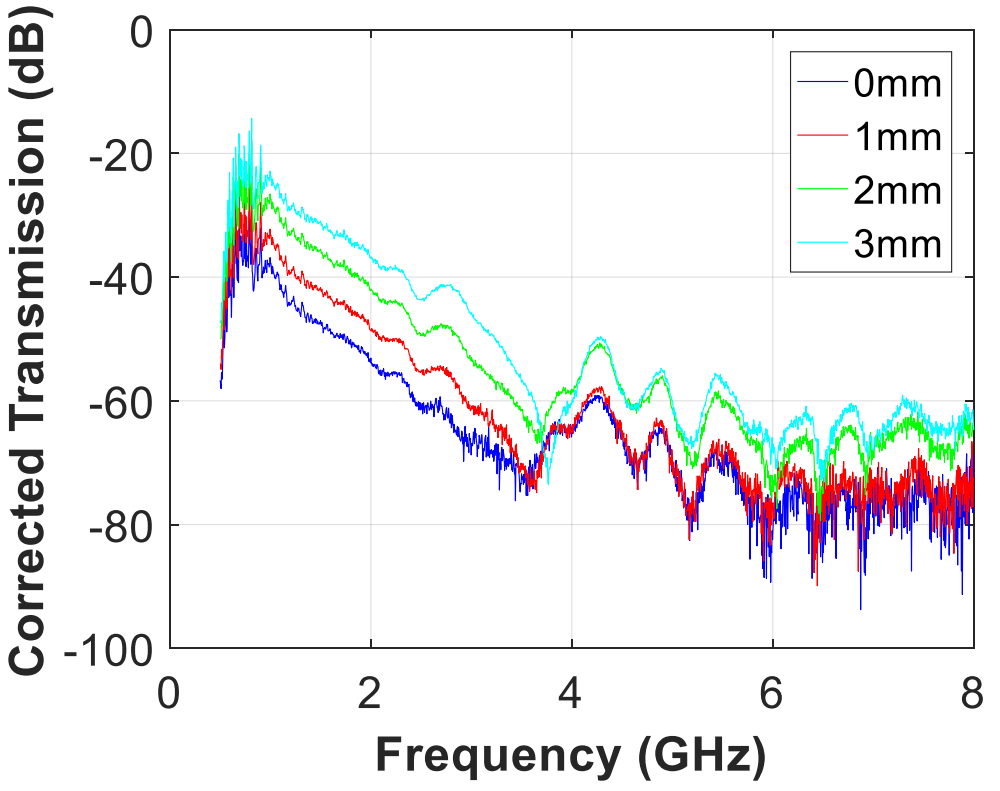

Figure 6.7: Measured corrected transmission of the substrate sheet flat on the bottom of the absorber block and lifted 1mm, 2mm and 3mm from it

6.6. Transmission through the PCBs

Figure 6.8 shows the measured corrected transmissions for the three PCBs. PCB1 and PCB5 have a transmission of between approximately -70dB and -45dB over the frequency range 2GHz to 8GHz. This corresponds to a transmission cross section (TCS) (see Section 2.5.2), $\langle \sigma^{t}_{21,pcb} \rangle$, between $3\text{x}10^{-5}$ m^2 and $5.3\text{x}10^{-4}$ m^2. This TCS can now be used in the PWB. There are a number of different minima that are below -80dB, which reach the minimum measurable transmission for this set up. PCB2 has a significantly higher transmission than the other two PCBs and is between -25dB and -55dB between 2GHz and 8GHz. This corresponds to a TCS between $5.3\text{x}10^{-3}$ m^2 and $1.6\text{x}10^{-4}$ m^2. As discussed in Section 6.4 of this chapter PCB2 has a smaller number of metallic components on compared to PCB1 and PCB5. This additional shielding on PCB1 and PCB5 may be causing their decreased transmission compared to PCB2.

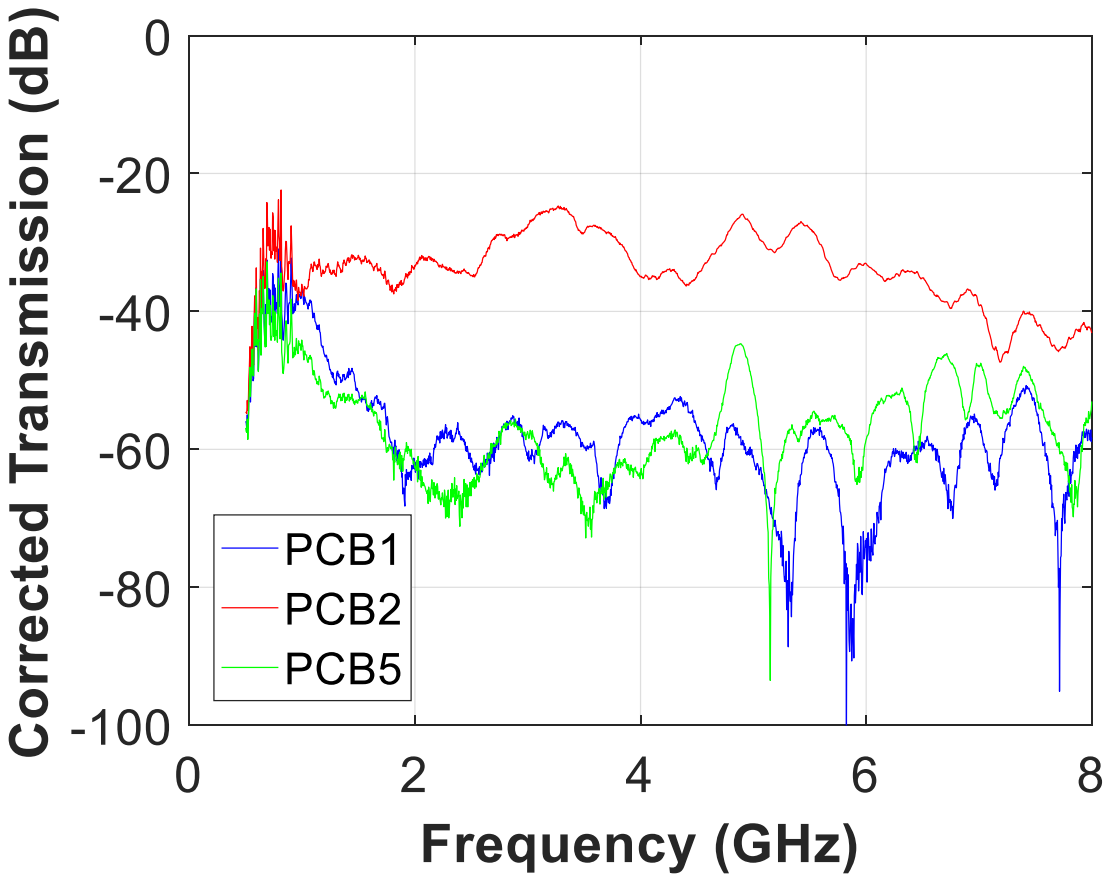

Figure 6.8: Measured corrected transmission of PCB1, PCB2 and PCB5 using the absorber box

Figure 6.9 shows the measured ACS of the three PCBs which have previously been presented in Chapter 3. The figure shows that PCB1 and PCB5 have a similar ACS in addition to similar transmission through the PCBs. As these two PCBs have the most metallic components on, it could be reasoned that the metal is causing a significant amount of energy to be reflected from the surface of the PCB rather than be transmitted or absorbed. PCB2 has a higher transmission through it and also has a higher absorption. As there are fewer metallic components on this PCB, less energy may be reflected away and so more energy is available to be absorbed or transmitted through the PCB.

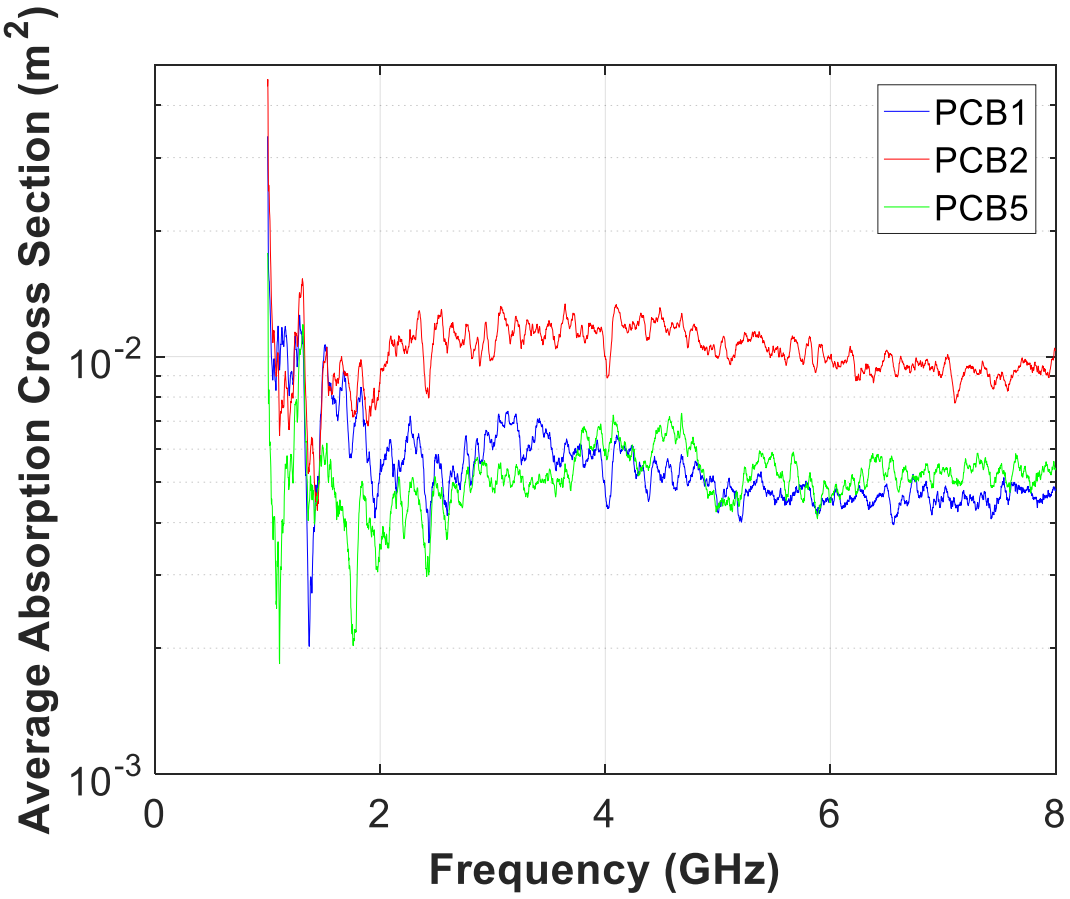

Figure 6.9: Measured ACS of PCB1, PCB2 and PCB5

Figure 6.10 compares the main corrected transmission results in this chapter. The aluminium sheet lying flat on the absorber demonstrates the limits of this measurement. The aluminium sheet lifted 3mm, PCB substrate lifted 3mm, PCB1 and PCB5 all have a similar corrected transmission of around -60dB above 3.5GHz. This likely indicates that the measurement is limited by the 3mm distance that the samples are lifted from the absorber block. The amount of energy being transmitted through these two PCBs is similar to that of the aluminium sheet and is at the limit of the measurement method.

The low transmission through these PCBs is likely to be insignificant compared to the transmission through any apertures between cavities in the enclosure. In this case, this transmission mechanism may not need to be included in the PWB. However, PCB2 has a higher TCS which is comparable with the ACS of a typical PCB and so this would need to be included in the PWB. This is explored further in the next chapter.

The size of PCB2 is the same as PCB1 and PCB5 and they all have the 3mm gap between the board and absorber block. The main difference between them is the smaller amount of metal and a greater amount of ceramic components on PCB2. As previously discussed this accounts for the difference in transmission.

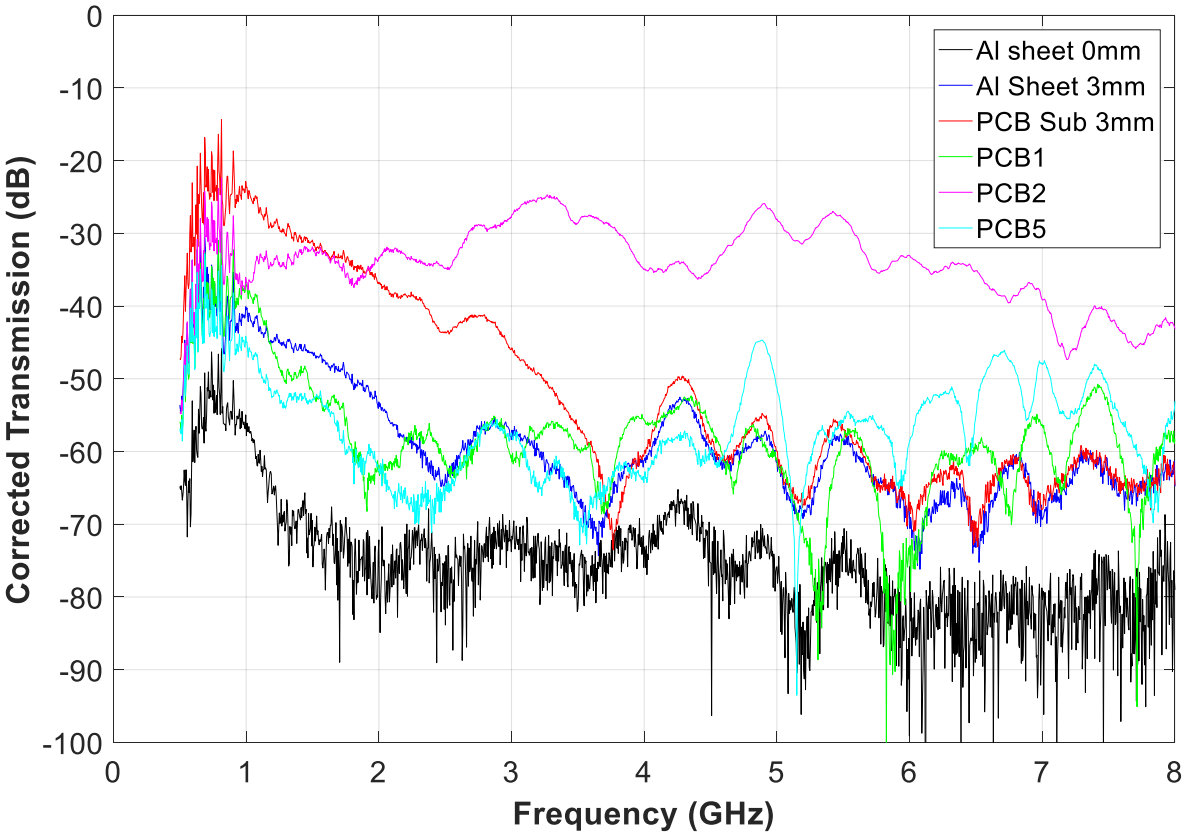

Figure 6.10: Comparison of the measured corrected transmission of the aluminium sheet flat on the absorber block (0mm), lifted 3mm from the absorber block, the substrate lifted 3mm from the block, PCB1, PCB2 and PCB5

6.7. Summary

In this chapter, a measurement has been described which allows the transmission through PCBs to be calculated using the absorber box method. By measuring an aluminium sheet and PCB substrate sheet it can be seen that the measurement is limited by a 3mm gap underneath the PCBs. A minimum transmission of -60dB for these PCBs can be measured at frequencies over 2GHz. Of the three PCBs measured, two of the PCBs had a transmission low enough to be limited by this factor. This may mean that the transmission through these PCBs does not need to be considered in the PWB. The third PCB has a higher measured transmission of between -20dB and -50dB which is high enough that that its effect may need to be considered in any PWB model. A possible reason for this is that PCB2 has significantly less metal on it.

Using the absorber box method is a quick and efficient way to measure the transmission through PCBs. The data collected using this method can be used in methods such as computational modelling as well as the PWB method [58][59]. As with the other work described in this thesis, this information allows a more accurate prediction of the SE of an enclosure with contents such as PCBs in. The next chapter shows how the ACS and TCS of PCBs can be used to predict the SE of a populated enclosure.

Chapter 7

Predicting Shielding Effectiveness using Power Balance Models

7.1. Overview

In this chapter, the absorption and transmission cross sections of PCBs and recos are used in power balance models (PWB) to show that this method can be used to predict the SE of an enclosure. The PWB models use the information on PCB and reco ACS and TCS detailed in the previous chapters including the ACS of stacked PCBs and one sided PCBs and recos. The results from the PWB models are compared with SE measurements made in an RC.

The first set of models is of a single cavity enclosure with and without PCBs inside. These models are then expanded on by showing how the SE of an enclosure split into two cavities can be measured and calculated. For each enclosure configuration, a comparison is made between the SE results of the model and of the measurement.

7.2. Shielding Effectiveness Measurements of an Enclosure in a Reverberation Chamber

7.2.1. Methodology

In Chapter 2 of this thesis, the measurement methodology and example measurement of enclosure SE in a RC was described. The same enclosure and measurement method was used to produce the results discussed in this chapter. The next paragraphs summarise the methodology and confirm the measurement parameters used. The setup of each measured enclosure configuration is described.

The measurement set up is shown diagrammatically in Figure 7.1 and Figure 7.2 shows a photograph of the set up taken from inside the RC.

The measurement was carried out in the UoY AEG large RC. The mechanical stirrer, controlled by a PC external to the chamber, was rotated and stopped at 100 equally stepped positions over one full rotation. A VNA was used to collect a full set of S-parameters between the blade and monopole antenna. The measurement was carried out over the frequency range 1GHz to 20GHz at 10,001 measurement points. The sweep time was 2.5s. A moving average with a BW of 100MHz was applied to the data after it had been collected.

At the beginning of each measurement day, a reference measurement was carried out with the enclosure removed from the set up; the antenna remained attached to the enclosure lid. Measurements with the enclosure were then made.

The S-parameter data is then used to calculate the SE using the following equation.

$$\boldsymbol{SE = 20\log_{10}\frac{|\langle S_{21\,ref}\rangle|^2}{|\langle S_{21\,enc}\rangle|^2}} \qquad \textbf{(7.1)}$$

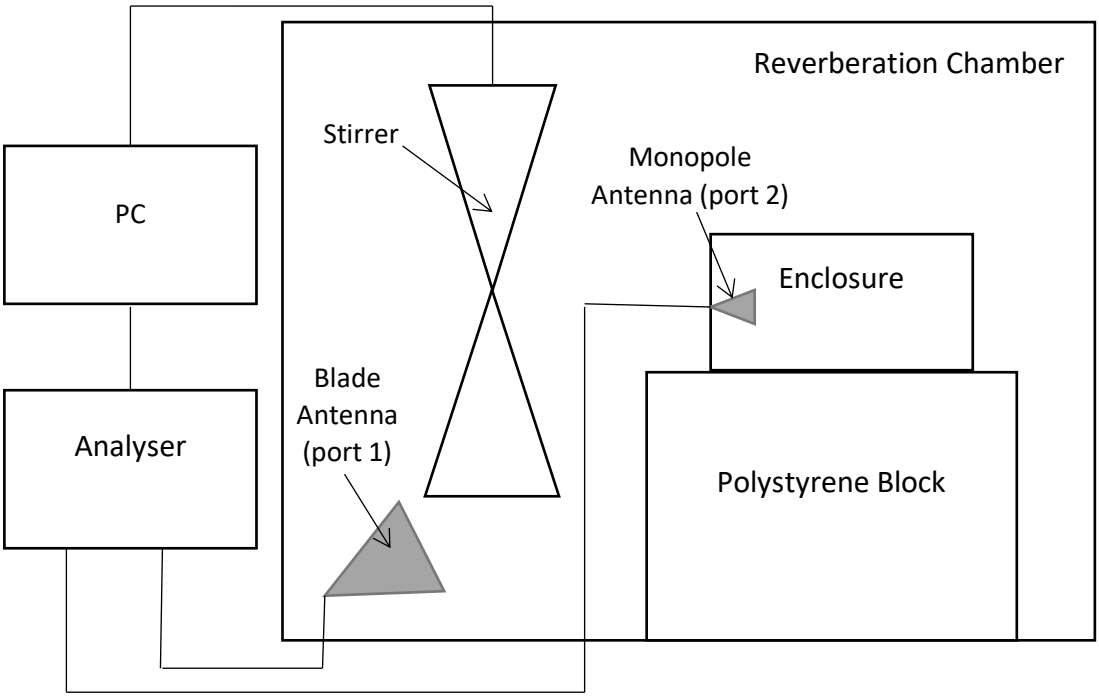

Figure 7.1: Diagram of the SE measurement setup of an enclosure in the large reverberation chamber

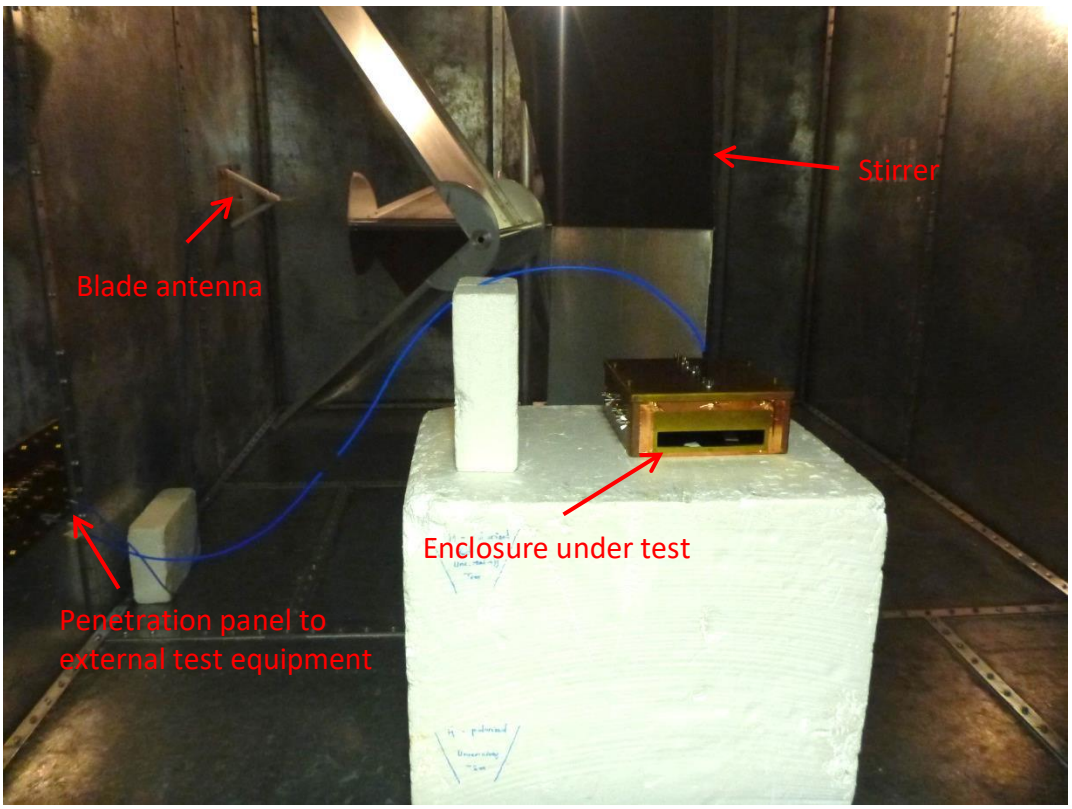

Figure 7.2: Photograph of the enclosure SE measurement set up in the large reverberation chamber

7.2.2. Enclosure under Test

The enclosure under test is same enclosure described in Section 2.3.3.2 and is shown in the RC in Figure 7.2. For all measurements described in this chapter, the front plate used on the enclosure is with a large aperture with dimensions of 200mm x 20mm. The aperture was positioned at the bottom of the front plate when attached to the enclosure. The front plate is shown in Figure 7.3.

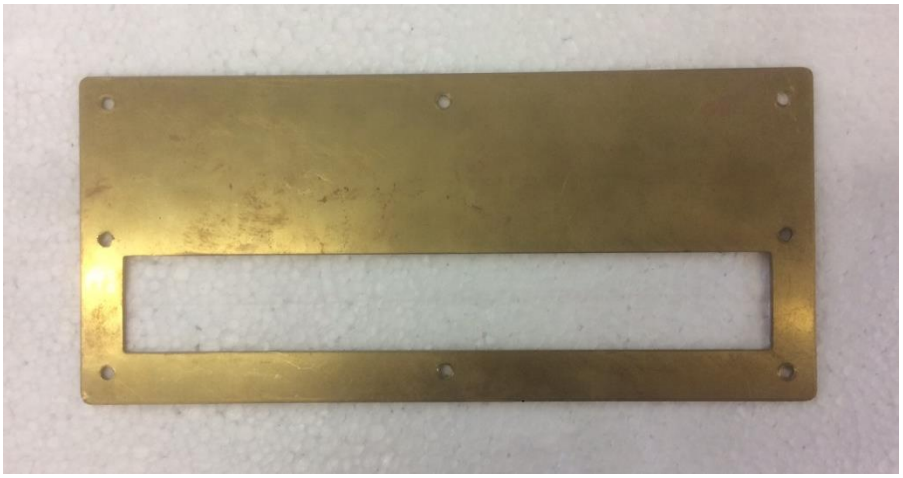

Figure 7.3: Front plate with large aperture.

In addition to being used as a single cavity enclosure, the enclosure has been used as a two cavity enclosure for some measurements detailed in this chapter. To create a two cavity enclosure two dividers were manufactured from a sheet of aluminium with a thickness of 1mm. The dividers have dimensions of 290mm x 104mm and 290mm x 114mm. When the larger divider is positioned in the enclosure there is a gap of 3mm between the top of the divider and the wall of the enclosure and the bottom of the divider and the wall of the enclosure. The smaller divider gives a gap of 8mm either side. This is shown diagrammatically in Figure 7.4.

The dividers can be used as a reco and are shown in Figure 7.5. These reco dividers can be used to show what happens to the enclosure SE if divided by an absorbing object, such as a PCB. Two sheets of polystyrene (of thickness 10mm) have been fitted to the divider sheets. The divider can be used with no absorber (referred to as metallic divider) or absorber can be placed in the polystyrene sheet to convert it into

a reco as described in Chapter 5. This is referred to as the reco divider and can be made one sided or two sided. The absorber used is the same as in Chapter 5.

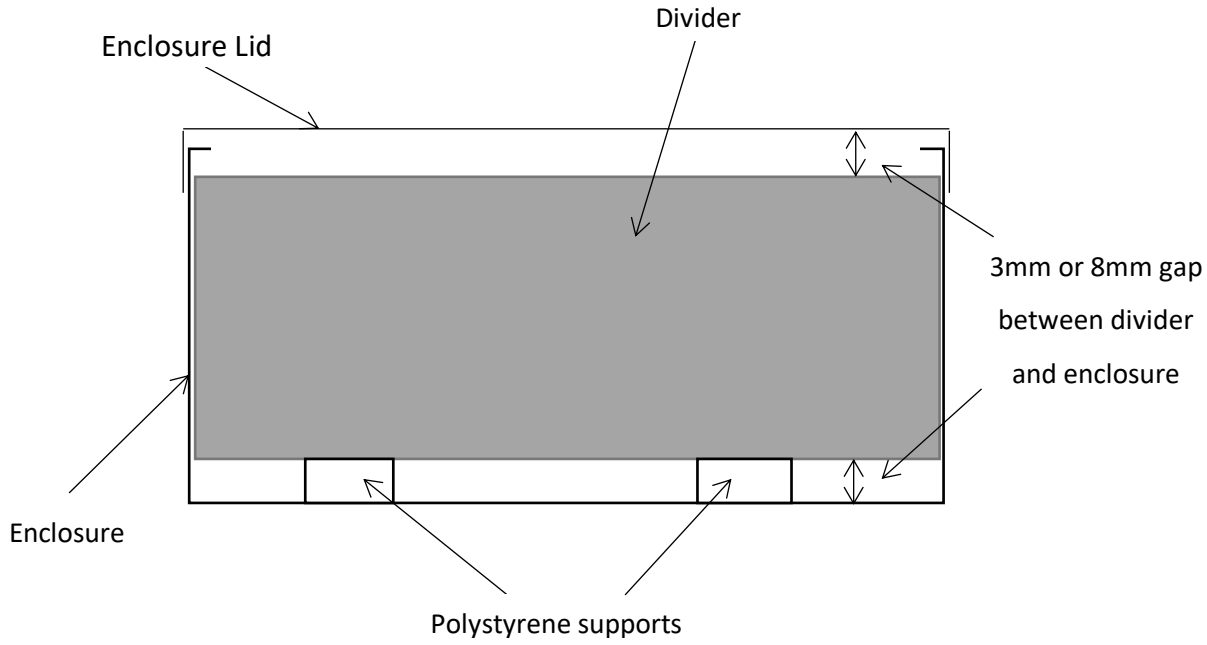

Figure 7.4: Diagram of the cross section of the enclosure to show the gap of 3mm between the top of the divider and the wall of the enclosure and the bottom of the divider and the wall of the enclosure

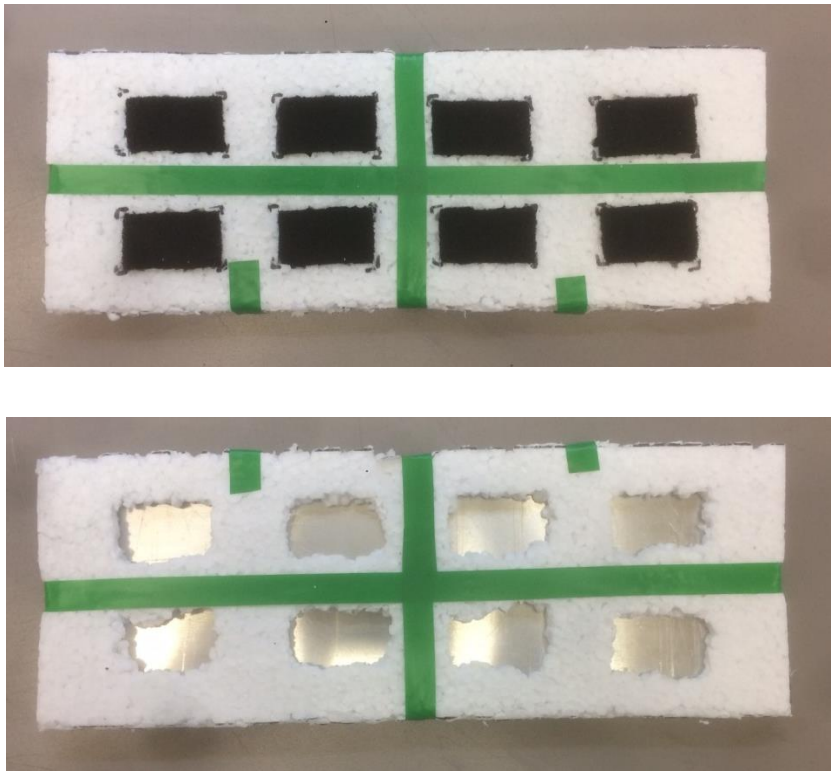

Figure 7.5: The reco divider with absorber in position in the top photograph and without absorber in the bottom photograph

7.3. Single Cavity Enclosures

7.3.1. Empty Single Cavity Enclosure

In Chapter 2 a PWB of an empty single cavity enclosure was presented along with measurements of the enclosure for comparison. The model, SE equation and results are presented here as a reminder.

7.2.1.1. Empty Single Cavity Enclosure Model

The power balance model of the empty single cavity enclosure was shown diagrammatically in Figure 2.11 and repeated in Figure 7.6 for convenience. The walls of the enclosure are metallic with a small amount of loss and there is an aperture in the centre of one wall of the enclosure. An antenna is located inside the enclosure as this is the case when performing the measurement.

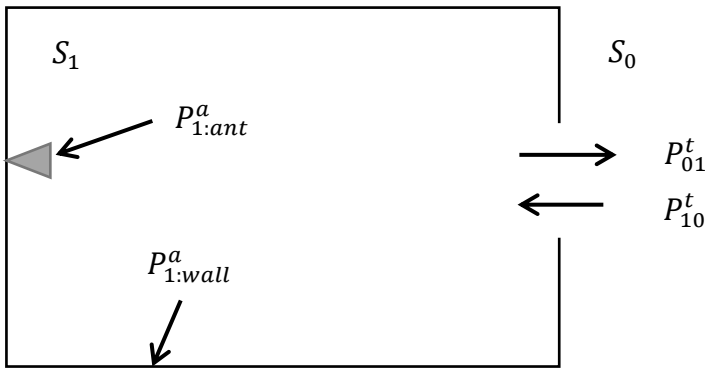

Figure 7.6: Power balance model of an empty metallic enclosure with a single aperture

InFigure 7.6, the symbols refer to the following:

- S_0 power density external to the enclosure
- S_1 power density internal to the enclosure
- $P^a_{1:wall}$ power absorbed by the inside of the enclosure wall
- $P^a_{1:ant}$ power absorbed by the antenna
- P^t_{01} power transmitted internal to external of the enclosure
- P^t_{10} power transmitted external to internal of the enclosure

The full derivation of the equation used to calculate the SE of the enclosure is given in Section 2.5.5.1. The equation is repeated here:

$$SE = \frac{S_0}{S_1} = \frac{\sigma^a_{1:wall} + \sigma^a_{1:\text{ant}} + \sigma^t_{10}}{\sigma^t_{10}} \quad \textbf{(7.2)}$$

The parameters used in the model are based on the enclosure discussed in Section 7.2.2. The equations used to calculate the losses for the wall, antenna and aperture are discussed in Chapter 2 Section 2.5 and are repeated below.

Wall losses in a metallic cavity:

$$\sigma_{walls} = \frac{4A}{3c}\sqrt{\frac{\pi f \mu_r}{\mu_0 \sigma_w}}\left[1 + \frac{3\lambda A}{32V}\right] \quad \textbf{(7.3)}$$

Transmission Cross Section of an Aperture:

$$\sigma^t_{aperture} = \frac{A_{aperture}}{4} \quad \textbf{(7.4)}$$

Absorption Cross Section of an Antenna:

$$\sigma_{ant} = \frac{\lambda^2}{8\pi}(1 - |S_{11}|^2) \quad \textbf{(7.5)}$$

7.2.1.2. Empty Single Cavity Enclosure Measurement

As discussed in the introduction section of this chapter a measurement of an equivalent enclosure for each model has been carried out. Photographs of the empty single cavity enclosure with large aperture are shown in Figure 7.7. The SE of the enclosure was measured using the method described in Section 7.2.1.

7.2.1.3. Empty Single Cavity Results

Figure 7.8 shows the PWB and measured SE results for the empty single cavity enclosure. These results have been discussed previously in Chapter 2 Section 2.5.5. The results will not be discussed further in this section but are repeated for comparison to the following PWBs.

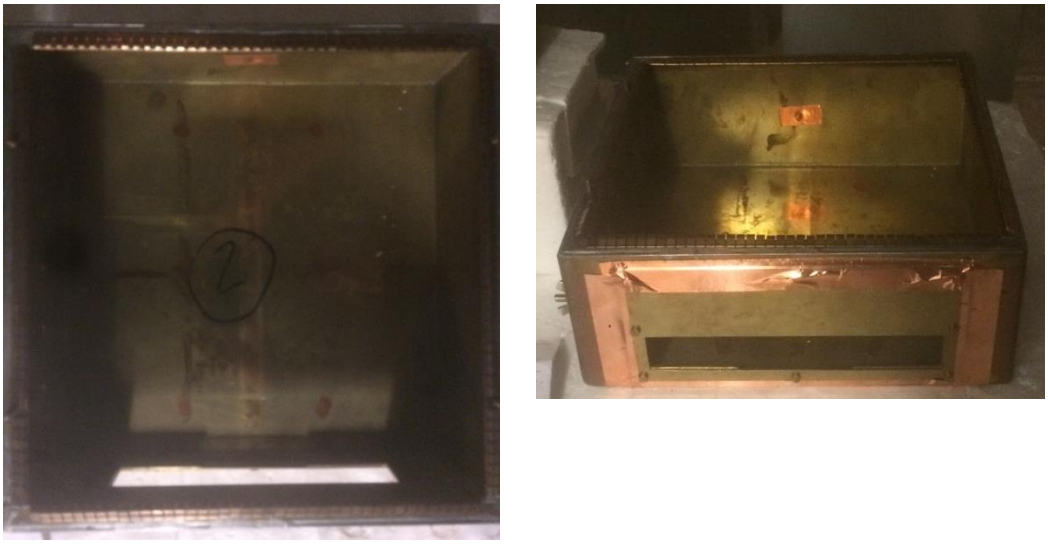

Figure 7.7: Photographs of the empty enclosure taken from the top (left photo) and from the front (right photo)

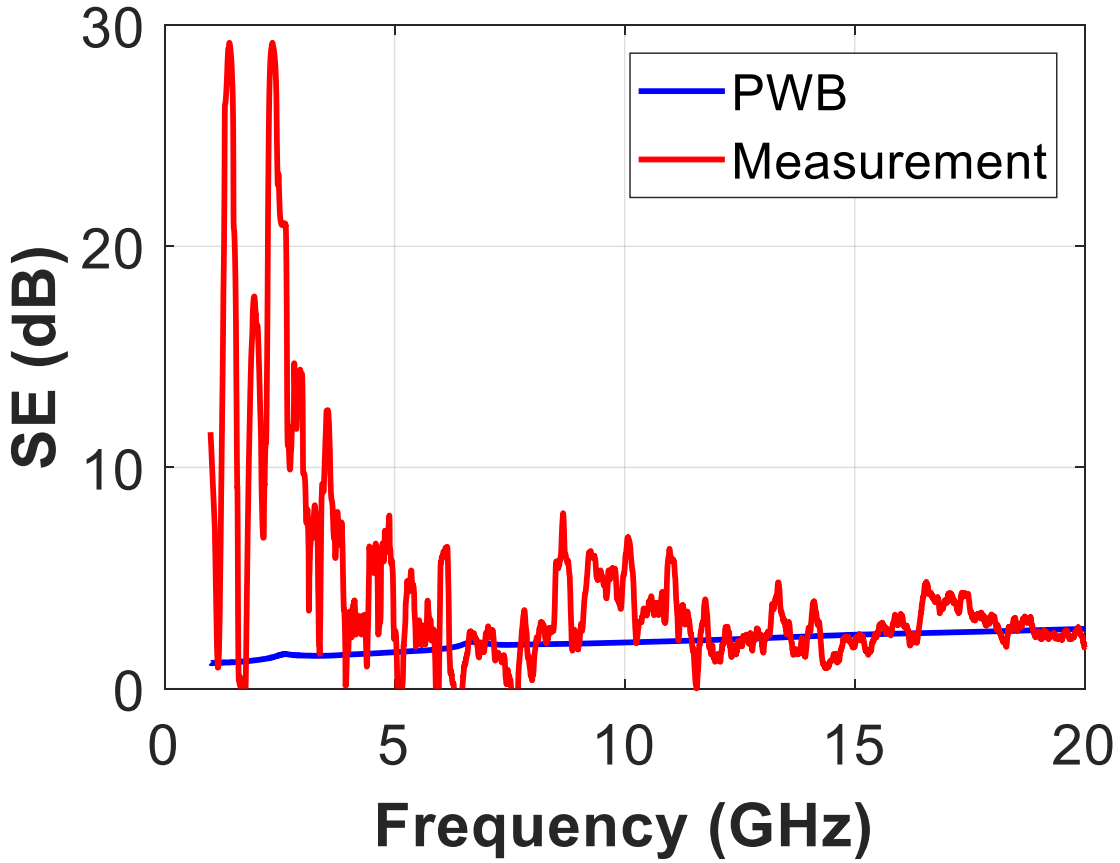

Figure 7.8: Comparison of modelled and measured SE of a single cavity empty enclosure with an aperture

7.3.2. Single Cavity Enclosure with Single Reco

In Chapter 2 Section 2.5.5 a model was presented of a single cavity enclosure with a single reco positioned in the centre of the enclosure. A summary of the model and the SE equation is given below. The modelled SE can now be calculated as more is now known about the ACS of PCBs and recos.

7.2.1.4. Single Empty Cavity with Central PCB Model

A diagram of the PWB is shown in Figure 2.14 and repeated in Figure 7.9 for convenience. In this model $P^a_{1:reco}$ is the power absorbed by the reco and $\sigma^a_{1:reco}$ is the ACS of the reco.

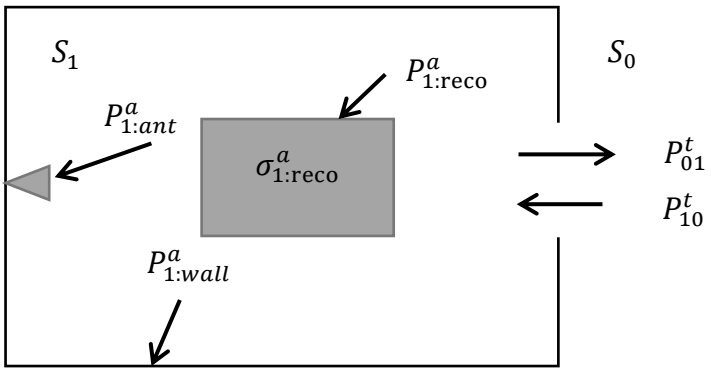

Figure 7.9: Power balance model of an enclosure with aperture and single, central reco positioned centrally

The SE of this configuration can be calculated using the following equation. The ACS of the reco is summed into the numerator of the equation.

$$SE = \frac{S_1}{S_0} = \frac{\sigma^a_{1:wall} + \sigma^a_{1:\text{ant}} + \sigma^a_{1:\text{reco}} + \sigma^t_{10}}{\sigma^t_{10}} \quad \textbf{(7.6)}$$

The ACS of the recos measured in Chapter 5 are used to calculate the SE of the enclosure; although the size of the aluminium sheet is different the absorber used is the same. Equations (7.3), (7.4) and (7.5) were used to calculate the absorption of

the enclosure walls, TCS of the aperture and absorption by the antenna. Like the antenna reflection coefficients, it was necessary to interpolate the measured ACS of the PCB in order to match the PWB frequency points.

The losses due to the enclosure walls, antenna and reco and the TCS of the aperture are shown in Figure 7.10. Above 5GHz, the ACS of the reco is between approximately $4x10^{-3}m^2$ and $6x10^{-3}m^2$. This is around three times greater than the next biggest loss mechanism, the aperture. The reco is the dominant loss mechanism in this configuration and this will have a significant effect on the enclosure SE.

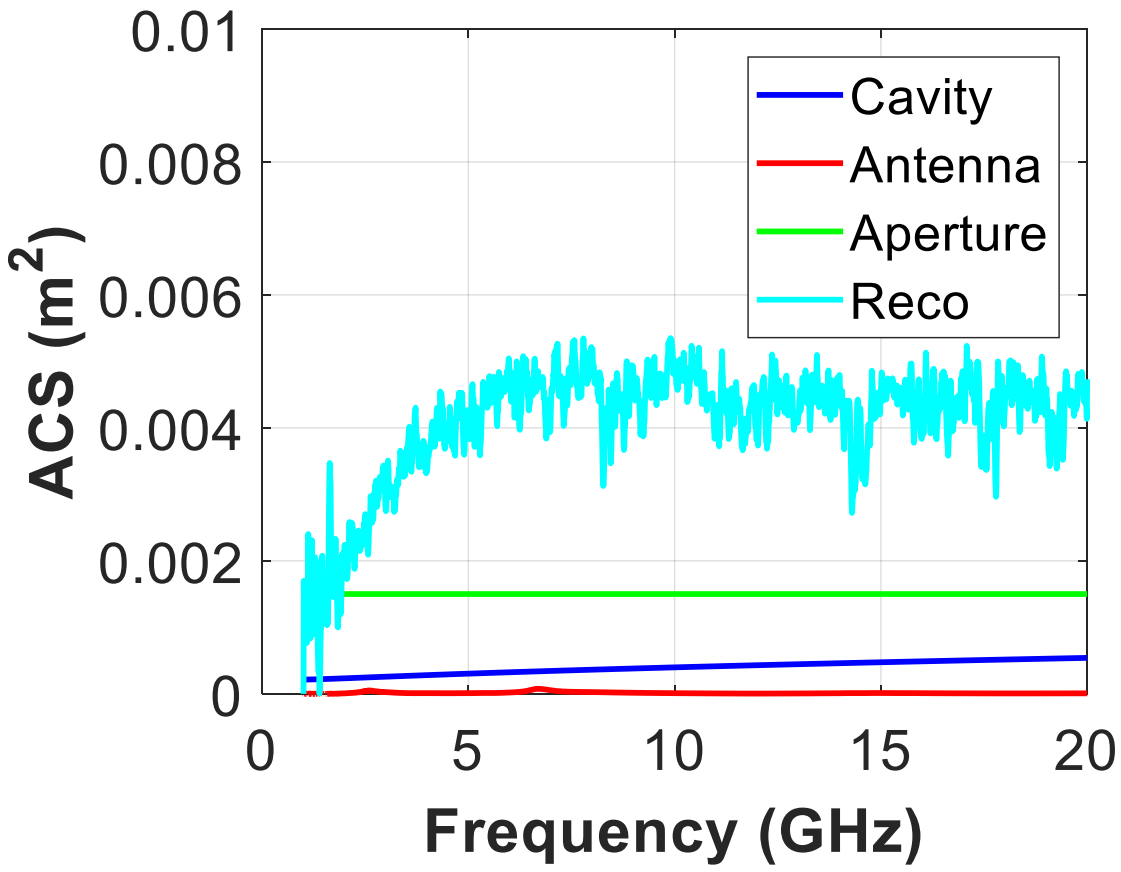

Figure 7.10: Losses in a metallic enclosure with a single aperture and containing an antenna and a single PCB in its centre

7.2.1.5. Single Cavity Enclosure with Reco Measurement

Photographs of the enclosure with the reco in are shown in Figure 7.11. The reco was placed 40mm from the bottom of the enclosure on four sheets of polystyrene of 10mm thickness. This was to keep the reco away from the enclosure walls.

The SE of the enclosure was measured using the method described in Section 7.2.1.

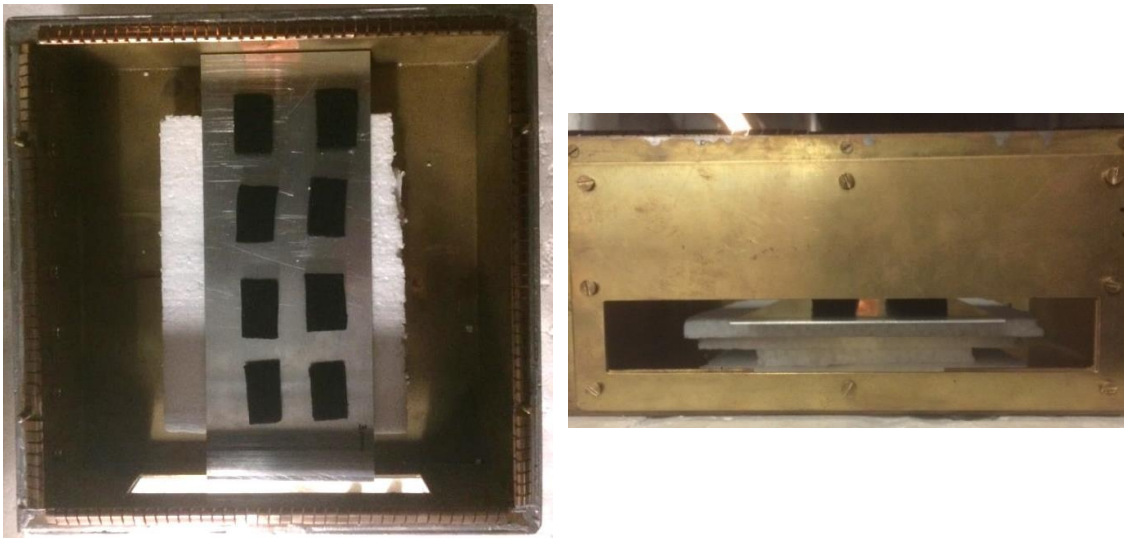

Figure 7.11: Photographs of the single cavity enclosure with the reco inside taken from the top (left photo) and from the front (right photo)

7.2.1.6. Single Cavity Enclosure with Reco Results

Figure 7.12 shows the PWB and measured SE results for the single cavity enclosure with reco inside.

The SE of the modelled enclosure increases from approximately 5dB to 12dB from 1GHz to 5GHz. Above 5GHz, the SE remains at 12dB. The greater variation in SE, compared to the empty enclosure configuration, over the frequency range is caused by using the measured ACS of the reco. The measured SE of the enclosure lies between 10dB and 16dB above 5GHz.

The measured and modelled results are of a similar magnitude and lie between 10dB and 15dB over most of the frequency range.

The SE of the enclosure with the reco in has increased by approximately 10dB to over 10 times the SE of the enclosure without the reco inside, shown in Figure 7.8.

.

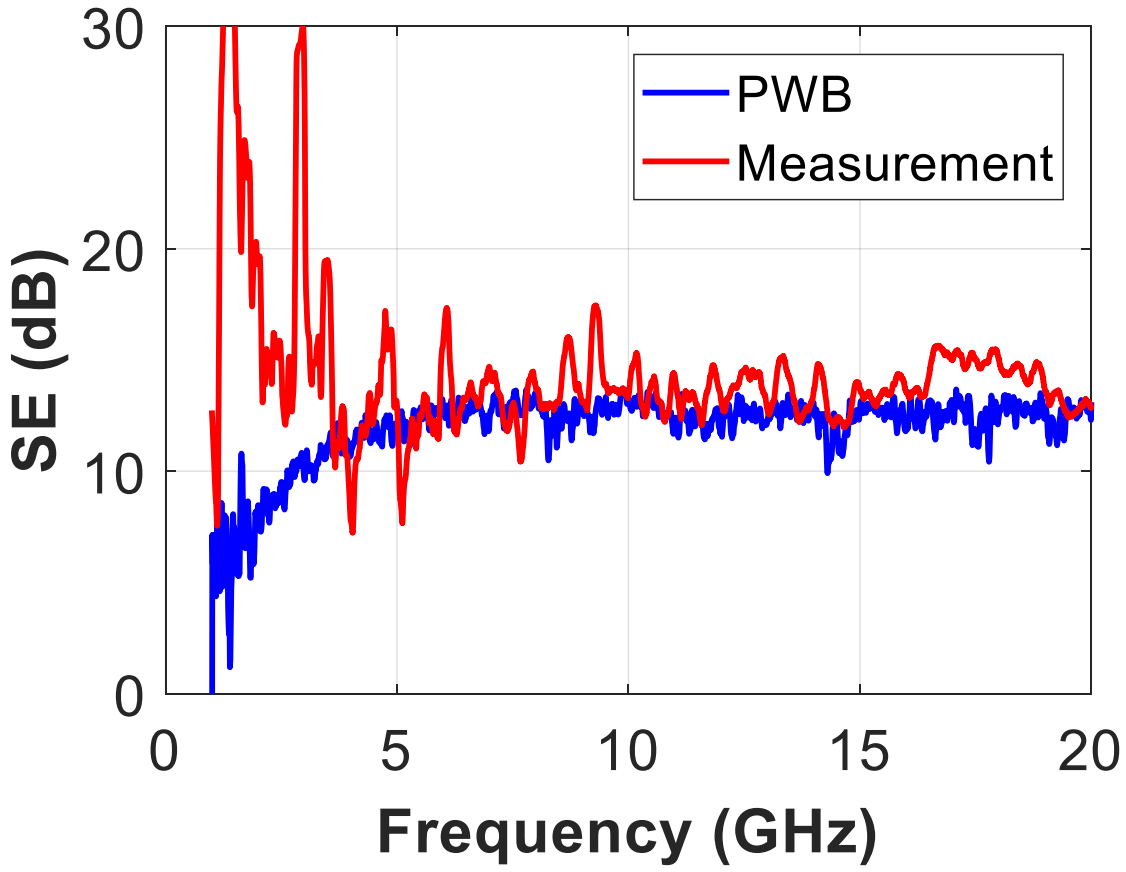

Figure 7.12: Comparison of modelled and measured SE of a single cavity enclosure with a reco inside

7.3.3. Single Cavity Enclosure with Reco Close to Enclosure Wall

The final model in the single cavity enclosure section is that of an enclosure with a reco positioned parallel to and close to the enclosure wall.

This configuration is important as it shows the need to know the separate ACSs of each side of a PCB as discussed in Chapter 5. Depending on which side of the PCB is facing the wall (either the front, component side or the back of the PCB) the SE of the enclosure will be changed.

7.2.1.7. Reco Close to Enclosure Wall Model

A diagram of the PWB model of an enclosure with a single reco positioned parallel to and close to the enclosure wall is shown in Figure 7.13. In this configuration a smaller cavity is formed between the reco and the wall it is positioned next to. This cavity will be ignored in order to simplify the model for this initial work.

The SE equation (equation (7.6)) used for the enclosure with the reco positioned centrally can be used for this model. However, the value used for the ACS of the reco will be based on the ACS of the recos measured next to the wall of the small RC which were described in Chapter 5. Equations (7.3), (7.4) and (7.5) were used to calculate the absorption of the enclosure walls and antenna and TCS of the aperture.

Three versions of this configuration will be measured and modelled:

- Double sided reco positioned 10mm from the bottom of the enclosure
- Double sided reco positioned 20mm from the bottom of the enclosure
- Single sided reco positioned 20mm from the bottom of the enclosure with the absorber facing towards the enclosure wall.

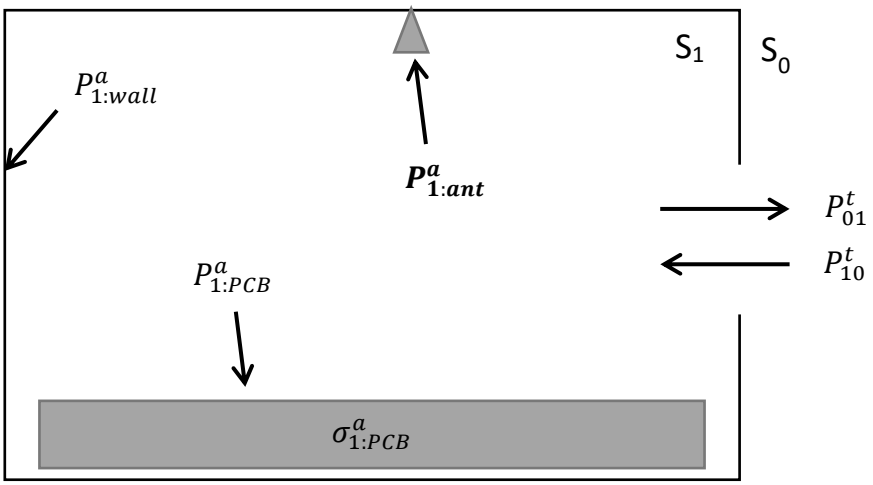

Figure 7.13: Diagram of an enclosure segmented by a PCB including methods of absorption and transmission.

Double Sided Reco

Two values of ACS are used to calculate the SE; one with the metal plate of the reco 10mm from the chamber wall and one with the metal plate of the reco 20mm from the chamber wall. These measurements were taken with the double sided reco and presented in Figure 5.3 in Chapter 5.

Single Sided Reco

In this configuration a single sided reco is positioned 20mm from the bottom of the enclosure with the absorber facing towards the enclosure. The ACS of this reco was presented in Figure 5.10 in Chapter 5.

7.2.1.8. Reco Close to Enclosure Wall Measurement

Double Sided Reco

The double sided reco placed close to the bottom of the enclosure is shown in Figure 7.14. Two measurements were made with the reco close to the bottom of the enclosure. One with the reco placed on a sheet of polystyrene of thickness 10mm. The other is with the reco placed on the bottom of the enclosure on a piece of paper to stop the absorber coming into contact with the wall. The SE of the enclosure was measured using the method described in Section 7.2.1.

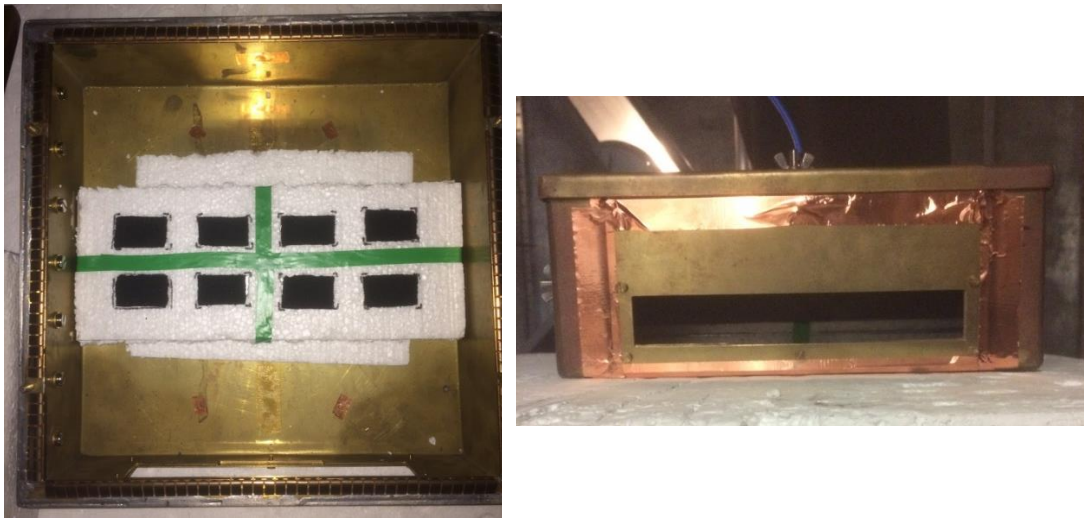

Figure 7.14: Photographs of the enclosure with the double sided reco 10mm from the bottom of the enclosure taken from the top (left photo) and from the front (right photo)

Single Sided Reco

The measurement was carried out with the single sided PCB in the 20mm position facing away from the enclosure wall and facing towards the enclosure wall.

7.2.1.9. Single Cavity with Reco Close to Enclosure Wall Results

Double Sided Reco

Figure 7.15 compares the results from the PWB and the measured results in the RC for the single cavity enclosure with a double sided reco 10mm and 20mm from the bottom enclosure wall.

The modelled results show that positioning the reco closer to the enclosure floor causes a reduction in SE. In the two results shown here the difference is greatest between 7GHz and 15GHz. In the 10mm position the ACS of the reco has been reduced more than when it is in the 20mm, this is why a slightly greater reduction in SE is seen in Figure 7.15.

The measured SE results are of a similar magnitude. Above 5GHz the SE varies between 11dB and 20dB.

Above 15GHz the SE of the PWB results and measurement results is similar; approximately between 14dB and 16dB. Below 15GHz there are significant

differences between the PWB and measurement results. This is particularly apparent between 7GHz and 15GHz where there is a difference in SE of up to 6dB.

Previous measurements (Chapter 5) have shown that the ACS of the reco is reduced the closer it is positioned to the RC wall. This causes the PWB results to show a smaller SE when the reco is positioned close to the enclosure wall. Unlike the PWB, the SE measurement results do not show a similar difference between the two positions for this double sided reco. The main difference that could be causing this is that the reco is now being measured in an enclosure rather than next to the small RC wall. This could be investigated further in future work.

Overall, the SE measurement is not as affected by the reco being close to the enclosure wall as might be expected.

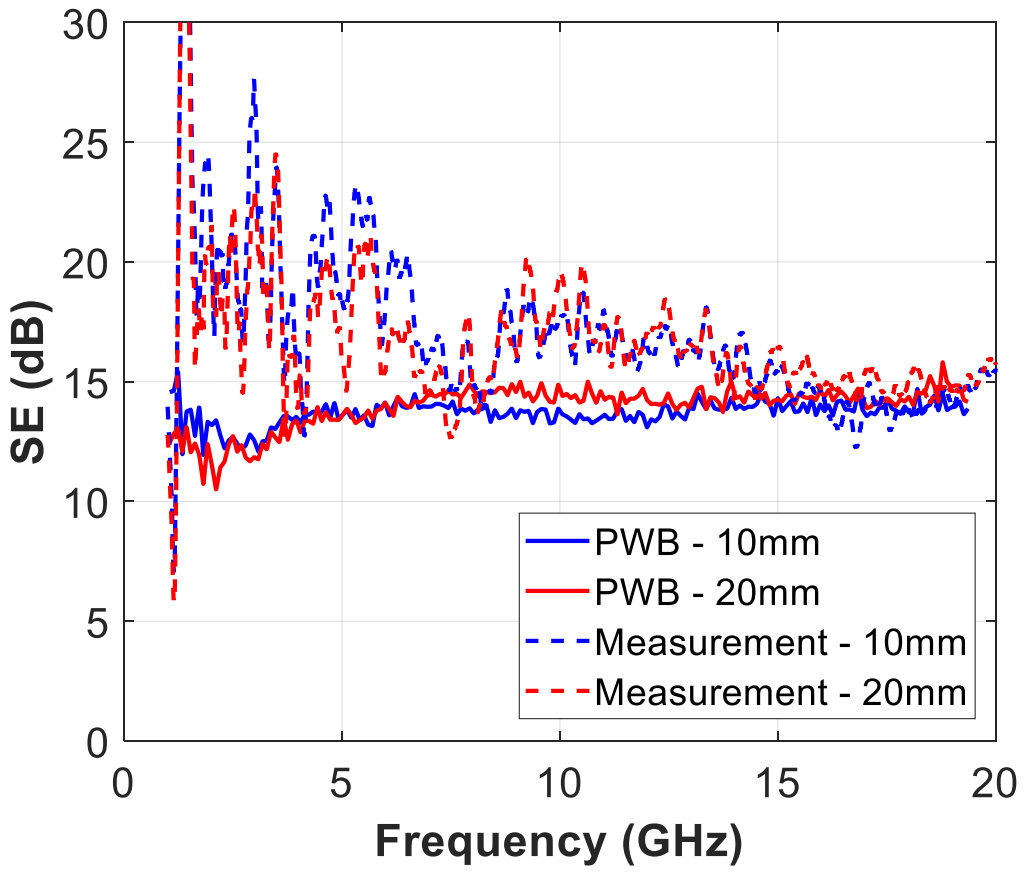

Figure 7.15: Comparison of modelled and measured SE of a single cavity enclosure with a double sided reco positioned 10mm and 20mm from the enclosure wall

Single Sided Reco

Figure 7.16 compares the results from the PWB and the measured results in the RC for the single sided reco facing the enclosure wall.

For the PWB result, positioning the single sided reco close to the enclosure floor causes a reduction in SE of between 7dB and 4dB compared to the reco positioned centrally. This is because the ACS of the reco has been reduced as has been seen in Chapter 5. The measured SE shows a similar result to the modelled SE.

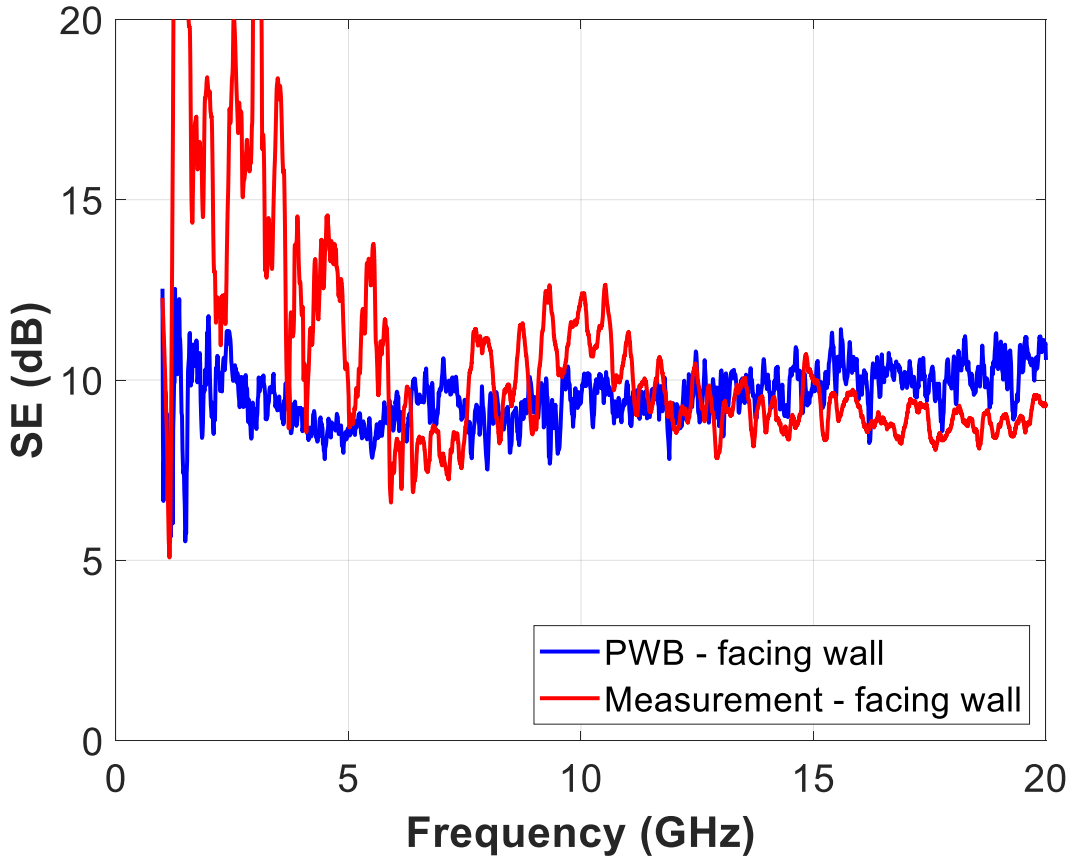

Figure 7.16: Comparison of modelled and measured SE of a single cavity enclosure with a reco positioned with the absorber facing towards the enclosure wall

7.4. Two Cavity Enclosures

In some situations, various contents divide the enclosure into multiple cavities. The next examples look at how to model an enclosure divided into two cavities and calculate the resulting SE in each cavity.

7.4.1. Simple Two Cavity Enclosure

The most basic example of a multiple cavity enclosure is an enclosure which has been split into two cavities by a metallic dividing wall.

7.2.1.10. Simple Two Cavity Enclosure Model

This two cavity enclosure can be modelled as shown in Figure 7.17 including the methods of power absorption and transmission.

The antennas are not considered in this model. Including the antennas complicates the model, as when measuring the SE the antenna is placed in one cavity but not the other. Two models would be required to consider the antennas; one with the antenna in cavity 1 and one with the antenna in cavity 2. For each model, the SE from the cavity with the antenna is used and the results from the other cavity ignored. Figure 7.10showed that the antennas are the least dominant loss mechanism; therefore, removing the antennas will have a negligible effect on the SE.

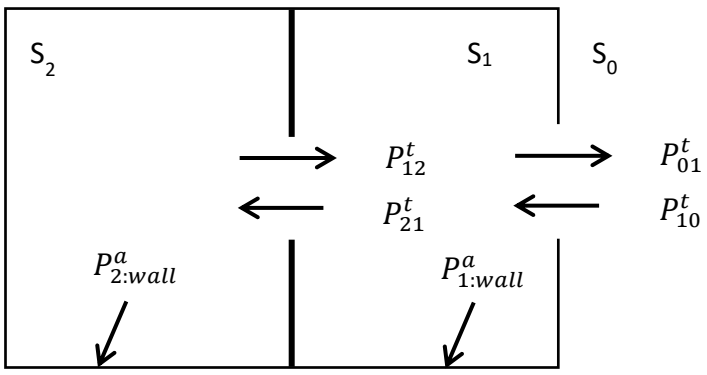

Figure 7.17: Diagram of an enclosure segmented by a cavity wall with an aperture.

The additional symbols in this model are:

- S_2 Power density in cavity 2
- $P^a_{2:wall}$ Power absorbed by cavity 2 wall
- P^t_{12} Power transmitted from cavity 2 to cavity 1 through the gaps either side of the metallic divider
- P^t_{21} Power transmitted from cavity 1 to cavity 2 through the gaps either side of the metallic divider
- Transmission through the dividing wall is not considered as the wall is metallic with no apertures in the divider itself.

The power balance equations for the two cavities are (7.7) for cavity 1 and (7.8) for cavity 2.

S1:

$$P^a_{1:wall} + P^t_{21} + P^t_{01} = P^t_{12} + P^t_{10} \quad \textbf{(7.7)}$$

S2:

$$P^a_{2:wall} + P^t_{12} = P^t_{21} \quad \textbf{(7.8)}$$

The powers transmitted through the apertures are given by the TCS multiplied by the power density in the cavity. Again, the TCSs are assumed to be the same in each direction.

Substituting the relevant equations in to the power balance equations gives (7.9) for cavity 1 and (7.10) for cavity 2.

$$\sigma^a_{1:wall}S_1 + \sigma^t_{21}S_1 + \sigma^t_{10}S_1 = \sigma^t_{12}S_2 + \sigma^t_{10}S_0 \quad \textbf{(7.9)}$$

$$\sigma^a_{2:wall}S_2 + \sigma^t_{21}S_2 = \sigma^t_{21}S_1 \quad \textbf{(7.10)}$$

Collecting the terms together gives equations (7.11) and (7.12)(7.12).

$$(\sigma^a_{1:wall} + \sigma^t_{21} + \sigma^t_{10})S_1 - (\sigma^t_{12})S_2 = \sigma^t_{10}S_0 \quad \textbf{(7.11)}$$

$$-(\sigma^t_{21})S_1 + (\sigma^a_{2:wall} + \sigma^t_{21})S_2 = 0 \quad \textbf{(7.12)}$$

(7.11) and (7.12) can be written in matrix form as:

$$\begin{bmatrix} \sigma^t_{10}S_0 \\ 0 \end{bmatrix} = \begin{bmatrix} (\sigma^a_{1:wall} + \sigma^t_{21} + \sigma^t_{10}) & -(\sigma^t_{12}) \\ -(\sigma^t_{21}) & (\sigma^a_{2:wall} + \sigma^t_{21}) \end{bmatrix} \begin{bmatrix} S_1 \\ S_2 \end{bmatrix} \quad \textbf{(7.13)}$$

Therefore the shielding effectiveness of each cavity is given by:

$$\begin{bmatrix} \frac{S_1}{S_0} \\ \frac{S_2}{S_0} \end{bmatrix} = \begin{bmatrix} (\sigma^a_{1:wall} + \sigma^t_{21} + \sigma^t_{10}) & -(\sigma^t_{12}) \\ -(\sigma^t_{21}) & (\sigma^a_{2:wall} + \sigma^t_{21}) \end{bmatrix}^{-1} \begin{bmatrix} \sigma^t_{10} \\ 0 \end{bmatrix} \quad \textbf{(7.14)}$$

The transmission cross sections of the apertures and the absorption of the enclosure walls are calculated using equations (7.3) and (7.4). The SE of each cavity is then calculated using (7.14). The following points were considered when calculating the different loss mechanisms in this configuration of the enclosure.

- $\sigma^a_{1:wall}$ and $\sigma^a_{2:wall}$ – absorption of walls in each cavity
    - The segmenting wall is 0.15m from the back of the enclosure and 0.14m from the front of the enclosure
    - Cavity 1 has a smaller surface area as it contains the aperture in the enclosure as well as the gaps either side of the divider
- σ^t_{21} – TCS of the gaps either side of the divider
    - The total TCS of the gaps is obtained by calculating the individual TCSs of each gap and then adding them together

7.2.1.11. Two Cavity Enclosure Measurement

Photographs of the two cavity enclosure set up are shown in Figure 7.18. The divider used has the gap of 8mm between the divider and wall, as described in Section 7.2.2. The divider was positioned 0.15m from the back of the enclosure and 0.14m from the front of the enclosure.

The SE of each cavity was measured using the method described in Section 7.2.1. The antenna was placed in position 2 for the SE measurement in cavity 1 and in position 6 for the SE measurement in cavity 6 (see Section 2.3.3.2 for a description of the enclosure).

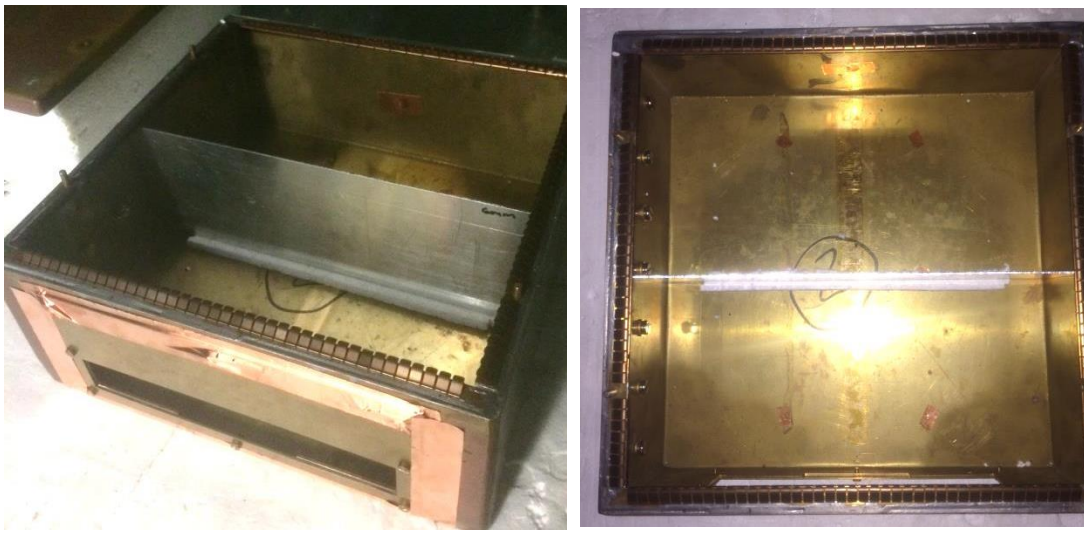

Figure 7.18: Photographs of the two cavity enclosure

7.2.1.12. Two Cavity Enclosure Results

Figure 7.19 compares the SE of each cavity calculated using the PWB and measured in a reverberation chamber.

The modelled SE of cavity 1 increases from between 1dB to 3dB over the frequency range of 1GHz to 20GHz. Cavity 2 has a higher SE which increases between 3dB and 7dB over the frequency range. At 1GHz, there is a 2dB between cavity 1 and cavity 2.

At 20GHz, there is a difference of 4dB. At this frequency, the SE of cavity 2 is over twice that of cavity 1.

From approximately 7GHz to 10GHz, the measured SE of cavity 1 increases from 2dB to 1dB. From 10GHz to 20GHz the SE decreases to between 2dB and 3dB. The SE of cavity 2 has a similar structure to the SE of cavity 1 but is approximately 1dB – 2dB higher. The maximum SE is around 14dB at just under 10GHz and is around 5dB at the end of the frequency range.

Cavity 1 has two apertures; one which links it to the external field and one that links it to cavity 2. Cavity 2 only has the aperture between itself and cavity 1. As less field is able to penetrate to cavity 2 its SE is higher. Additionally, because cavity 2 has fewer apertures it has a higher surface area. This means that more energy is absorbed in the cavity walls. However, as the apertures are the dominant loss mechanism this effect would be limited.

The SE of the measured and modelled cavities are similar from 15GHz to 20GHz. Below 15GHz the measured SE is much greater than the modelled SE. The reason for this could be due to the smaller cavities changing the frequency at which these models become useful. This needs to be investigated further.

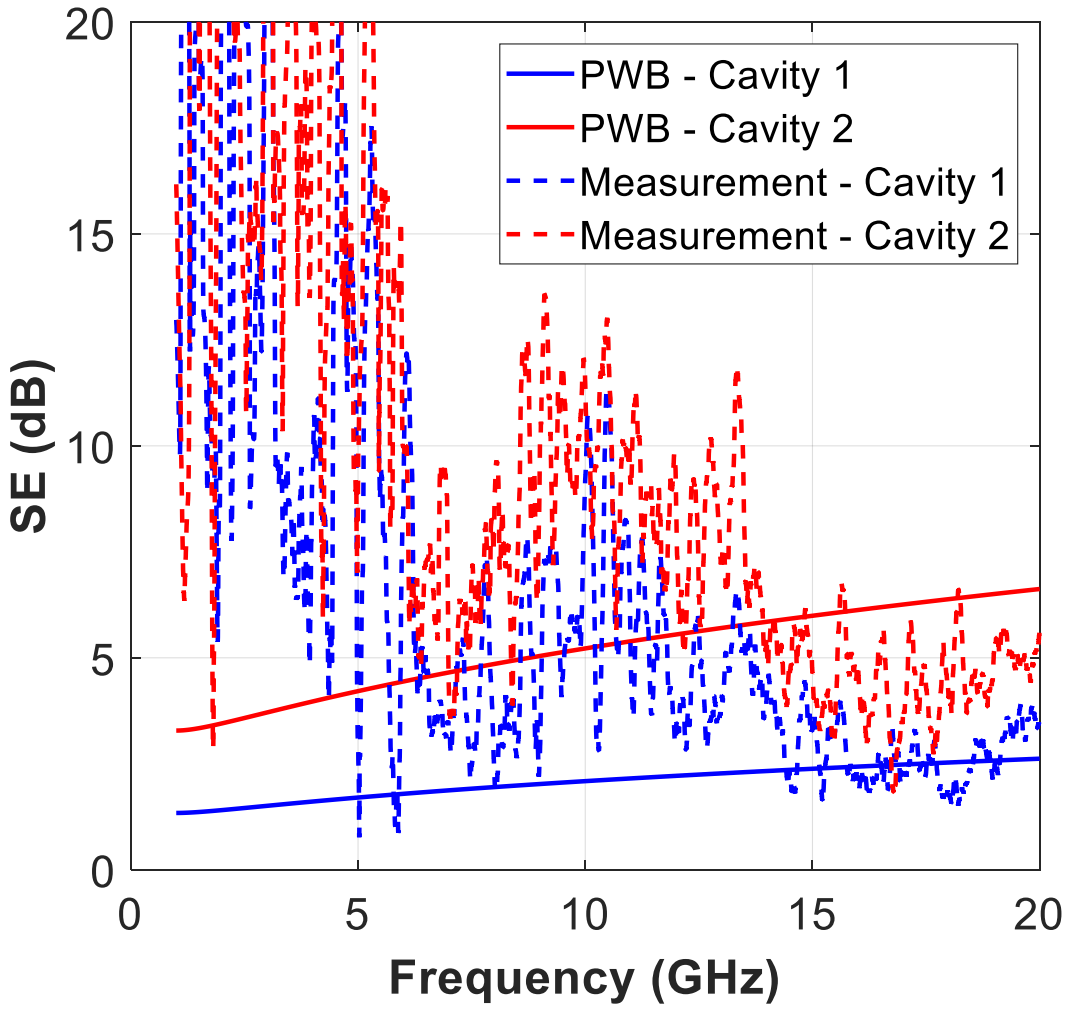

Figure 7.19: Comparison of modelled and measured SE of a two cavity enclosure with a metallic divider

7.4.2. Single Reco forming Two Cavity Enclosure

In the previous section the enclosure was divided by a metallic wall. In this section, a reco is used to divide the enclosure into two cavities. Three different configurations have been considered; a double sided reco, a single sided reco with the absorber facing into cavity 1 and a single sided reco with the absorber facing into cavity 2.

7.2.1.13. Single Reco forming Two Cavity Enclosure Model

The two cavity enclosure divided using a reco can be modelled as shown diagrammatically in Figure 7.20. Chapter 6 presented results that showed some PCBs have significant transmission through them which needs to be considered as an aperture. This is in addition to the transmission around the edges of the board.

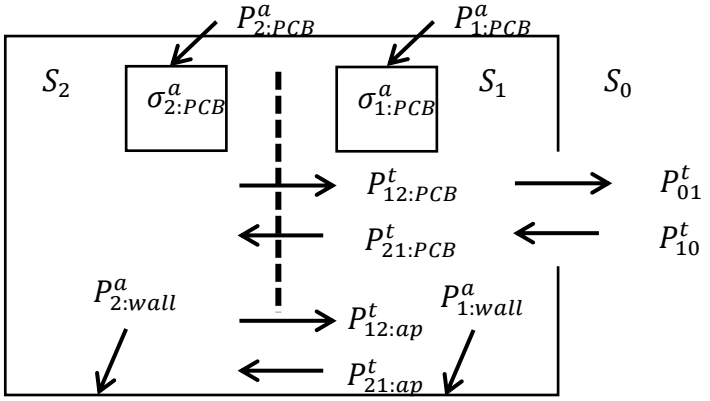

Figure 7.20: Diagram of an enclosure segmented by a PCB including methods of absorption and transmission.

The additional symbols in this model are:

- $P^a_{1:PCB}$ Power absorbed by PCB in cavity 1
- $P^a_{2:PCB}$ Power absorbed by PCB in cavity 2
- $P^t_{12:ap}$ Power transmitted from cavity 2 to 1 through the aperture around the reco
- $P^t_{21:ap}$ Power transmitted from cavity 1 to 2 through the aperture around the reco
- $P^t_{12:PCB}$ Power transmitted from cavity 2 to 1 through the reco divider
- $P^t_{21:PCB}$ Power transmitted from cavity 1 to 2 through the reco divider
- $\sigma^a_{1:PCB}$ ACS of PCB in cavity 1
- $\sigma^a_{2:PCB}$ ACS of PCB in cavity 2

The power balance equations for the two cavities are:

S1:

$$P^a_{1:wall} + P^a_{1:PCB} + P^t_{21:PCB} + P^t_{21:ap} + P^t_{01} = P^t_{12:PCB} + P^t_{12:ap} + P^t_{10} \quad \textbf{(7.15)}$$

S2:

$$P^a_{2:wall} + P^a_{2:PCB} + P^t_{12:PCB} + P^t_{12:ap} = P^t_{21:PCB} + P^t_{21:ap} \quad \textbf{(7.16)}$$

The power absorbed by the PCBs is given by (7.17) where n is the cavity and $\sigma^a_{n:PCB}$is the ACS of the PCB.

$$P^a_{n:PCB} = \sigma^a_{n:PCB} S_n \quad \textbf{(7.17)}$$

It is important to remember that the ACS of the reco in this model is the ACS for the part of the reco that is in that cavity. In the next section, the one sided measurement results of Chapter 5 are used to take this into account.

The power transmitted through the aperture around the PCB is given by the TCS multiplied by the power density in the cavity. Again, the TCS are assumed to be the same in each direction. Chapter 6 measured the power transmitted through three PCBs and calculated a TCS from these results.

Substituting these equations in to the power balance equations gives (7.18) and (7.19).

$$\sigma^a_{1:wall} S_1 + \sigma^a_{1:PCB} S_1 + \sigma^t_{21:PCB} S_1 + \sigma^t_{21:ap} S_1 + \sigma^t_{10} S_1 = \sigma^t_{12:PCB} S_2 + \sigma^t_{12:ap} S_2 + \sigma^t_{10} S_0 \quad \textbf{(7.18)}$$

$$\sigma^a_{2:wall} S_2 + \sigma^a_{2:PCB} S_2 + \sigma^t_{21:PCB} S_2 + \sigma^t_{21:ap} S_2 = \sigma^t_{21:PCB} S_1 + \sigma^t_{21:ap} S_1 \quad \textbf{(7.19)}$$

Collecting the terms together gives (7.20) and (7.21).

$$\left(\sigma^a_{1:wall} + \sigma^a_{1:PCB} + \sigma^t_{21:PCB} + \sigma^t_{21:ap} + \sigma^t_{10}\right) S_1 - \left(\sigma^t_{12:PCB} + \sigma^t_{12:ap}\right) S_2 = \sigma^t_{10} S_0 \quad \textbf{(7.20)}$$

$$\left(\sigma^t_{21:PCB} + \sigma^t_{21:ap}\right) S_1 - \left(\sigma^a_{2:wall} + \sigma^a_{2:PCB} + \sigma^t_{21:PCB} + \sigma^t_{21:ap}\right) S_2 = 0 \quad \textbf{(7.21)}$$

Equations (7.20) and (7.21) can be written in matrix form as:

$$\begin{bmatrix} \sigma_{10}^{t} S_0 \\ 0 \end{bmatrix} = \begin{bmatrix} (\sigma_{1:wall}^{a} + \sigma_{1:PCB}^{a} + \sigma_{21:PCB}^{t} + \sigma_{21:ap}^{t} + \sigma_{10}^{t}) & -(\sigma_{12:PCB}^{t} + \sigma_{12:ap}^{t}) \\ (\sigma_{21:PCB}^{t} + \sigma_{21:ap}^{t}) & -(\sigma_{2:wall}^{a} + \sigma_{2:PCB}^{a} + \sigma_{21:PCB}^{t} + \sigma_{21:ap}^{t}) \end{bmatrix} \begin{bmatrix} S_1 \\ S_2 \end{bmatrix} \quad \textbf{(7.22)}$$

Therefore the shielding effectiveness of each cavity is given by:

$$\begin{bmatrix} \frac{S_1}{S_0} \\ \frac{S_2}{S_0} \end{bmatrix} = \begin{bmatrix} (\sigma_{1:wall}^{a} + \sigma_{1:PCB}^{a} + \sigma_{21:PCB}^{t} + \sigma_{21:ap}^{t} + \sigma_{10}^{t}) & -(\sigma_{12:PCB}^{t} + \sigma_{12:ap}^{t}) \\ -(\sigma_{21:PCB}^{t} + \sigma_{21:ap}^{t}) & (\sigma_{2:wall}^{a} + \sigma_{2:PCB}^{a} + \sigma_{21:PCB}^{t} + \sigma_{21:ap}^{t}) \end{bmatrix}^{-1} \begin{bmatrix} \sigma_{10}^{t} \\ 0 \end{bmatrix} \quad \textbf{(7.23)}$$

Chapter 6 showed that not all PCBs have significant transmission and any transmission they do have may be insignificant compared to losses in the absorber or through the apertures around the PCBs. Therefore, at this stage, the transmission through the recos will be ignored in order to simplify the model. In future work the transmission could be considered.

The equation for calculating the SE is repeated below, without the transmission through the PCBs included:

$$\begin{bmatrix} \frac{S_0}{S_1} \\ \frac{S_0}{S_2} \end{bmatrix} = \begin{bmatrix} (\sigma_{1:wall}^{a} + \sigma_{1:PCB}^{a} + \sigma_{21:ap}^{t} + \sigma_{10}^{t}) & -(\sigma_{12:ap}^{t}) \\ -(\sigma_{21:ap}^{t}) & -(\sigma_{2:wall}^{a} + \sigma_{2:PCB}^{a} + \sigma_{21:ap}^{t}) \end{bmatrix}^{-1} \begin{bmatrix} \sigma_{10}^{t} \\ 0 \end{bmatrix} \quad \textbf{(7.24)}$$

The transmission cross sections of the apertures and the absorption of the enclosure walls are calculated using equations (7.3) and (7.4). The ACS of the reco used in the calculation for each configuration is discussed in the relevant sections below.

Double Sided Reco Divider

In this configuration the reco divider has absorber on both sides. There is an equal amount of absorber on each side (eight pieces) so the ACS used in each cavity is half of the total ACS of the double sided reco measured in Chapter 5 Section 5.3.2.

Single Sided Reco Divider - Absorber Facing into Cavity 1

In this configuration the reco divider has absorber on one side and no absorber on the other side. The side of the reco with the absorber faces into cavity 1. The ACS used for cavity 1 is the ACS of the single sided reco measured in Chapter 5 Section 5.3.1. As there is no absorber in cavity 2, $\sigma^{a}_{2:PCB}$ is set to zero.

Single Sided Reco Divider - Absorber Facing into Cavity 2

In this configuration the reco divider has absorber on one side and no absorber on the other side. The side of the reco with the absorber faces into cavity 2. The ACS used for cavity 2 is the ACS of the single sided reco measured in Chapter 5 Section 5.3.1. As there is no absorber in cavity 1, $\sigma^{a}_{1:PCB}$ is set to zero.

7.2.1.14. Two Cavity Enclosure with Reco Divider Measurement

Photographs of the two cavity enclosure with a reco divider are shown in Figure 7.21. The divider used has the gap of 8mm between the divider and wall. The divider was positioned 0.15m from the back of the enclosure and 0.14m from the front of the enclosure. The measurement was carried out with the double sided reco, with the single sided reco with absorber facing cavity 1 and the single sided reco with absorber facing cavity 2.

The SE of each cavity was measured using the method described in Section 7.2.1. The antenna was placed in position 2 for the SE measurement in cavity 1 and in position 6 for the SE measurement in cavity 6.

Figure 7.21: Photographs of the two cavity enclosure with a reco divider. The left photograph shows the double sided reco and the right photograph shows the single sided reco with the absorber side facing cavity 1.

7.2.1.15. Two Cavity Enclosure with Reco Divider Results

Double Sided Reco Divider

Figure 7.22 compares the SE of each cavity of the enclosure divided by the double sided reco for the PWB model and the measurement in the RC.

For the PWB, the SE of cavity 1 increases from a minimum of 6dB at 2GHz to 12dB at 5GHz. There are small variations in SE between 12dB to 13dB from 5GHz to 20GHz. The SE of cavity 2 shows a similar structure but its SE is between 29dB and 31dB from 5GHz to 20GHz. There is a difference of approximately 18dB between the two cavities.

Above 5GHz, the measured SE of cavity 1 varies between 10dB and 20dB and the SE of cavity 2 varies between 21dB to 31dB. Both measured graphs show a similar structure; the SE increases from around 6GHz to a maximum at 10GHz and then gradually decreases to 20GHz. The difference in SE between the two cavities remains the same throughout the frequency range about approximately 10dB

There is a difference between the PWB and measurement results for both cavities. For cavity 1 the PWB result is less than the measurement result. At higher frequencies, between 15GHz and 20GHz this difference is less significant. For cavity 2 the PWB result is greater than the measurement result. There is also a bigger difference than for the cavity 1 result. In this configuration the SE of both cavities is increased by the inclusion of the absorber. This also then gives a more pronounced difference in SE between the two cavities.

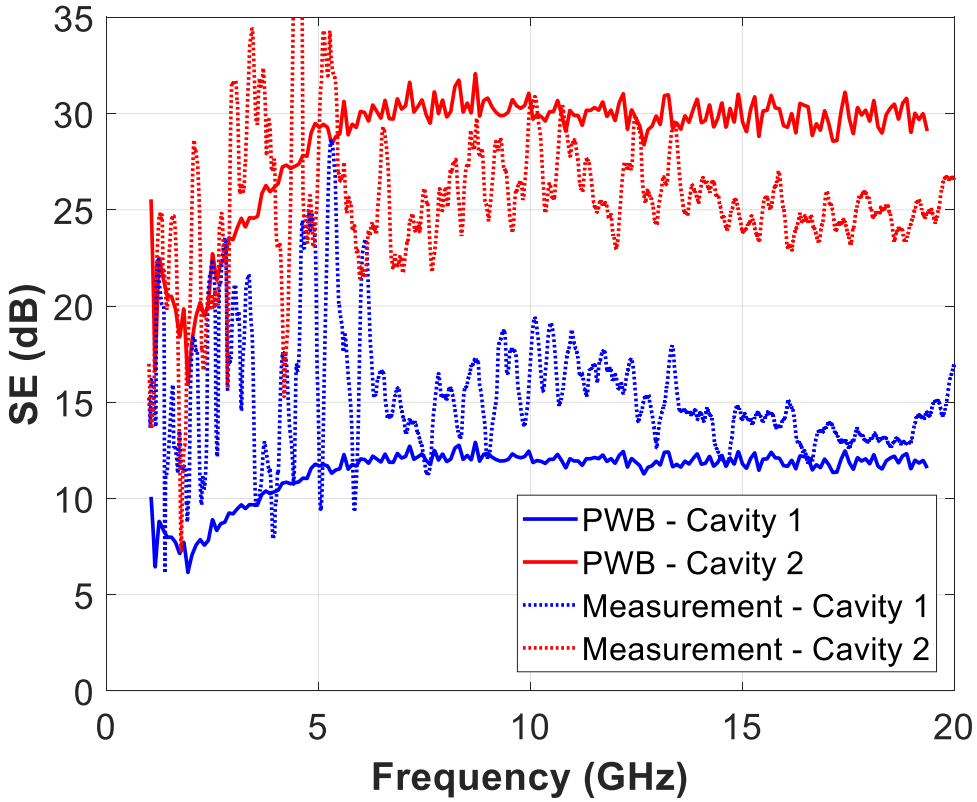

Figure 7.22: Comparison of modelled and measured SE of a two cavity enclosure with a double sided reco divider.

Single Sided Reco Divider - Absorber Facing into Cavity 1

Figure 7.22 compares the SE of each cavity of the enclosure divided by the single sided reco with the absorber facing cavity 1 calculated using the PWB and measured in an RC.

The modelled SE of cavity 1 increases from a minimum of 5dB at 2GHz to 13dB at 5GHz. There are small variations in SE between 12dB to 13dB from 5GHz to 20GHz. The SE of cavity 2 shows a similar structure but its SE is between 14dB and 17dB from 5GHz to 20GHz. There is a difference of approximately 3dB to 4dB between the two cavities.

For this configuration both cavities have a similar measured SE of between 10dB and 20dB from 5GHz to 15GHz and then settling down at approximately 12dB from 15GHz to 20GHz. Even though the absorber is only in cavity 1 the SE of both cavities has increased.

Although the results for cavity 1 show good agreement with each other the modelled result for cavity 2 is approximately 4dB higher than the measured result.

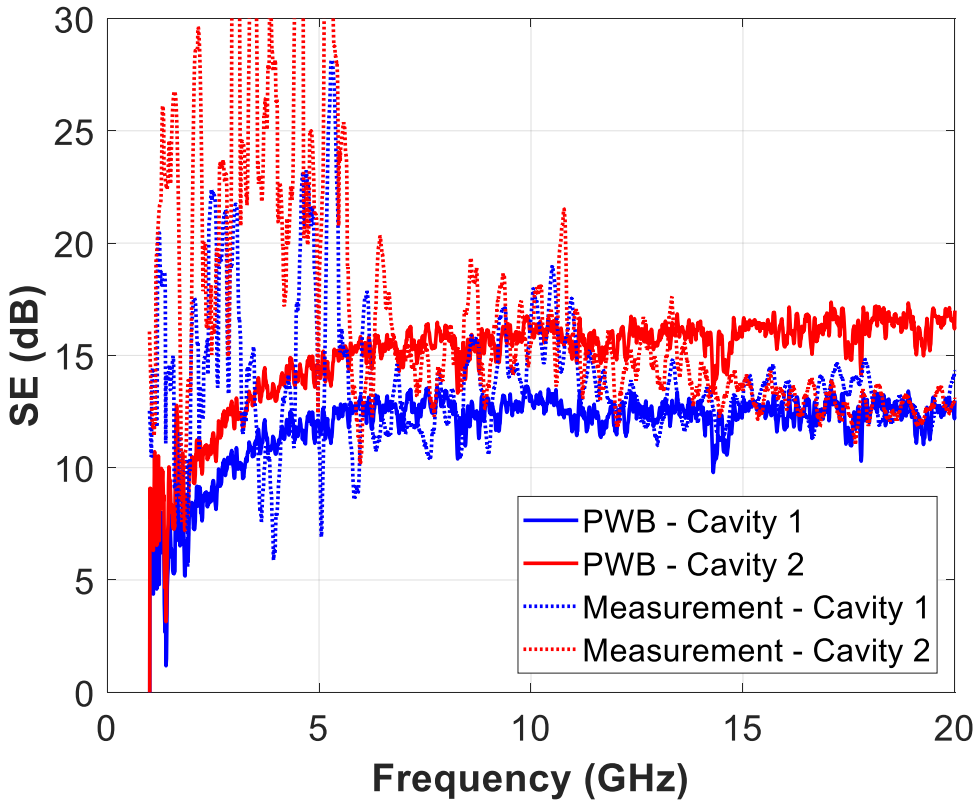

Figure 7.23: Comparison of modelled and measured SE of a two cavity enclosure with a single sided reco divider facing into cavity 1.

Single Sided Reco Divider - Absorber Facing into Cavity 2

Figure 7.24 compares the SE of each cavity of the enclosure divided by the single sided reco with the absorber facing cavity 2 calculated using the PWB and measured in an RC. The modelled SE of cavity 1 lies between 2dB and 4dB over the majority of the frequency range. The SE of cavity 1 increases from a minimum of 10dB (excluding the spike 2GHz) at 1GHz to approximately 22dB at 5GHz. There are variations in SE between 19dB to 24dB from 5GHz to 20GHz. There is a difference of approximately 20dB between the two cavities. There is much less variation in cavity 1 as there is no absorber in this cavity and it is less affected by the absorber in cavity 2.

For this configuration cavity 1 has a measured SE of between 5dB to 10dB over the majority of the frequency range. The SE of cavity 2 varies between 17dB and 23dB. The SE of cavity 1 has increased by a small amount; approximately 2dB compared to the metallic divider case. The SE of cavity 2 has increased by approximately 15dB.

The differences between the PWB and measured results are similar to the differences seen in the double reco divider configuration shown in Figure 7.22. The modelled results are lower than the measured results for cavity 1 and higher than the measured results for cavity 2.

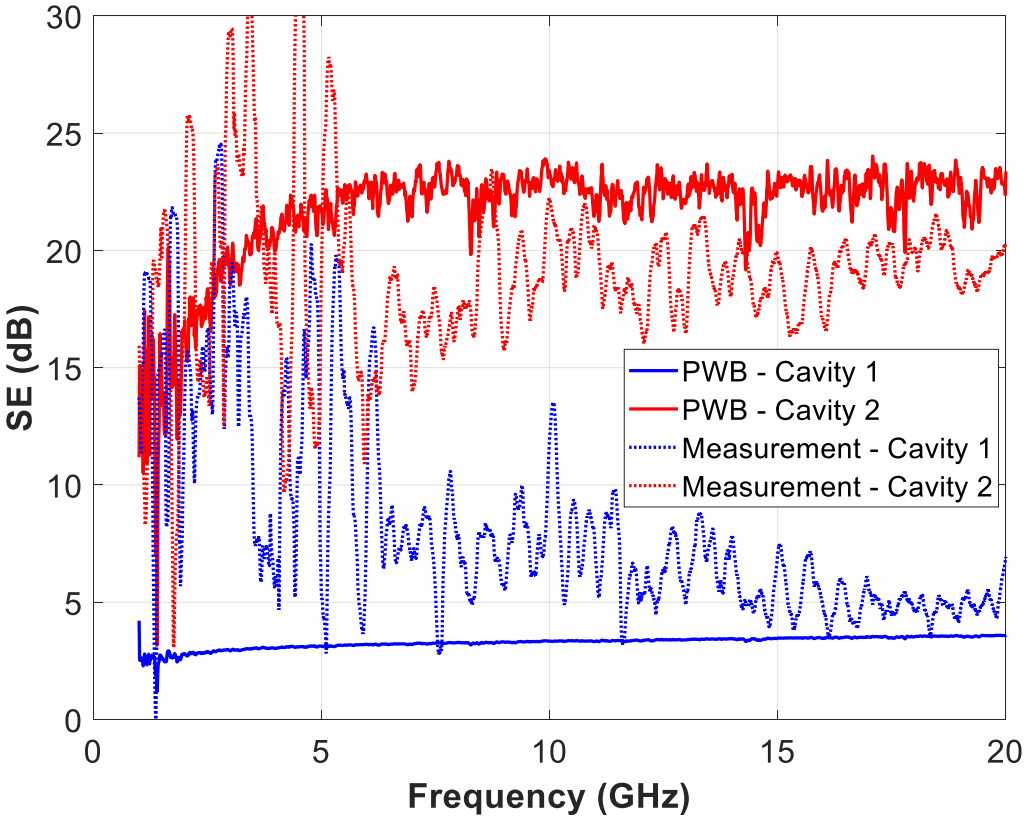

Figure 7.24: Comparison of modelled and measured SE of a two cavity enclosure with a single sided reco divider facing into cavity 2.

7.4.3. Two Cavity Enclosure formed by Stacked Recos

The next example is of an enclosure divided into two cavities by two recos in a stack.

7.2.1.16. Two Cavity Enclosure with Stacked Recos Model

The model can be drawn as shown in Figure 7.25 including the methods of power absorption and transmission. In this model the two PCBs are considered as one stacked object, as they were measured in the work presented in Chapter 3. Transmission through the divider will not be considered as the transmission through two PCBs is low enough to be considered insignificant. The main consideration in this configuration is how to take into account the ACS of two stacked PCBs.

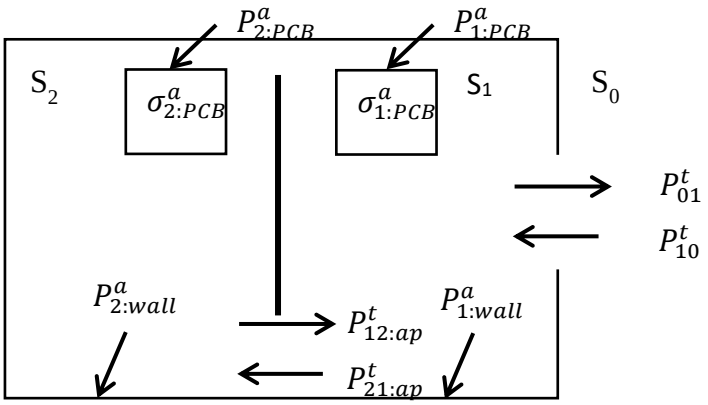

Figure 7.25: Diagram of an enclosure segmented by a PCB including methods of absorption and transmission.

The PWB matrix has been formulated by carrying out the same steps as the previous examples.

The power balance equations for the two cavities are:

S1:

$$P^a_{1:wall} + P^a_{1:PCB} + P^t_{21:ap} + P^t_{01} = P^t_{12:ap} + P^t_{10} \quad (7.25)$$

S2:

$$P^a_{2:wall} + P^a_{2:PCB} + P^t_{12:ap} = P^t_{21:ap} \quad (7.26)$$

The power absorbed by the PCBs is given by the equation where n is the cavity and $\sigma^a_{n:PCB}$is the ACS of the PCB.

$$P^a_{n:PCB} = \sigma^a_{n:PCB} S_n \tag{7.27}$$

Substituting these equations into the power balance equations gives:

$$\sigma^a_{1:wall} S_1 + \sigma^a_{1:PCB} S_1 + \sigma^t_{21:ap} S_1 + \sigma^t_{10} S_1 = \sigma^t_{12:ap} S_2 + \sigma^t_{10} S_0 \tag{7.28}$$

$$\sigma^a_{2:wall} S_2 + \sigma^a_{2:PCB} S_2 + \sigma^t_{21:ap} S_2 = \sigma^t_{21:ap} S_1 \tag{7.29}$$

Collecting the terms together gives:

$$\left(\sigma^a_{1:wall} + \sigma^a_{1:PCB} + \sigma^t_{21:ap} + \sigma^t_{10}\right) S_1 - \left(\sigma^t_{12:ap}\right) S_2 = \sigma^t_{10} S_0 \tag{7.30}$$

$$\left(\sigma^t_{21:ap}\right) S_1 - \left(\sigma^a_{2:wall} + \sigma^a_{2:PCB} + \sigma^t_{21:ap}\right) S_2 = 0 \tag{7.31}$$

This can be written in matrix form as:

$$\begin{bmatrix} \sigma^t_{10} S_0 \\ 0 \end{bmatrix} = \begin{bmatrix} \left(\sigma^a_{1:wall} + \sigma^a_{1:PCB} + \sigma^t_{21:ap} + \sigma^t_{10}\right) & -\left(\sigma^t_{12:ap}\right) \\ -\left(\sigma^t_{21:ap}\right) & \left(\sigma^a_{2:wall} + \sigma^a_{2:PCB} + \sigma^t_{21:ap}\right) \end{bmatrix} \begin{bmatrix} S_1 \\ S_2 \end{bmatrix} \tag{7.32}$$

Therefore the shielding effectiveness of each cavity is given by:

$$\begin{bmatrix} \frac{S_1}{S_0} \\ \frac{S_2}{S_0} \end{bmatrix} = \begin{bmatrix} \left(\sigma^a_{1:wall} + \sigma^a_{1:PCB} + \sigma^t_{21:ap} + \sigma^t_{10}\right) & -\left(\sigma^t_{12:ap}\right) \\ -\left(\sigma^t_{21:ap}\right) & \left(\sigma^a_{2:wall} + \sigma^a_{2:PCB} + \sigma^t_{21:ap}\right) \end{bmatrix}^{-1} \begin{bmatrix} \sigma^t_{10} \\ 0 \end{bmatrix} \tag{7.33}$$

In fact, this looks like a simpler formation than the previous example as the transmission through the recos (or PCBs) no longer needs to be considered. However, as there are now two recos stacked together the values of $\sigma^a_{1:PCB}$ and $\sigma^a_{2:PCB}$ need to be carefully thought out. The example calculation looks at how to determine these values.

Double Sided Stacked Reco Divider

In this configuration the two stacked recos have absorber on both sides. Each reco has eight pieces of absorber, four on each side. The ACS of each individual reco with four pieces of absorber on each side is half of the reco with eight pieces of absorber on each side that has been measured previously. A diagram of this configuration is shown in Figure 7.26.

In order to take into account the recos being stacked together, the absorption of the left reco is considered in cavity 2 and the absorption of the right reco is considered in cavity 1. As the recos are stacked, the area of the absorber on each reco is reduced by 75%. From the result shown in chapter 5, the absorption of each reco is therefore reduced to 75% of the total absorption of each reco. As the recos are considered as being stacked together the TCS of the aperture around the PCBs is that of the 3mm gap as this is the smallest gap.

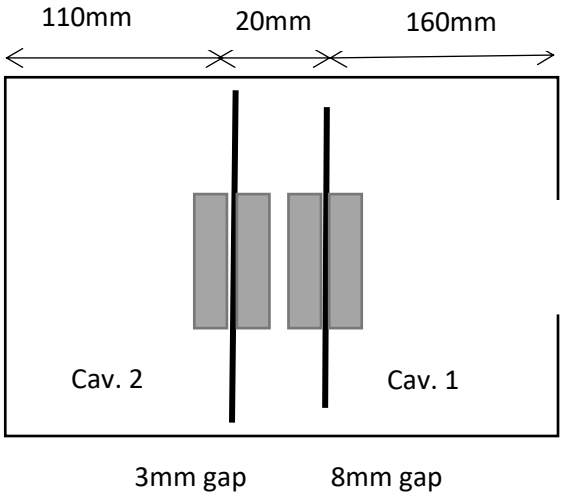

Figure 7.26: Two cavity enclosure divided by double sided stacked recos

Single Sided Stacked Reco Divider - Absorber Facing into Cavity 1

In this configuration the two stacked recos have eight pieces of absorber on one side facing into cavity 1. A diagram of this configuration is shown in Figure 7.27.

For this case, cavity 2 is considered to be empty. The metallic side of the reco forms the final side of the cavity. The absorber from both recos is located in cavity 1. The ACS of the reco on the right hand side is the ACS of a one sided reco. The ACS of the reco on the left hand side is considered to be the same as a one sided reco facing a wall, as measured in Chapter 5. This is 55% of the total ACS of a single sided reco. As the recos are considered as being stacked together the TCS of the aperture around the PCBs is that of the 3mm gap as this is the smallest gap.

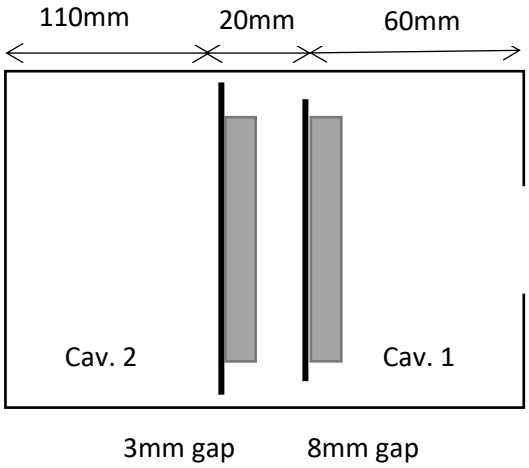

Figure 7.27: Diagram of the two cavity enclosure divided by single sided stacked recos with the absorber facing into cavity 1

Single Sided Reco Divider - Absorber Facing into Cavity 2

In this configuration the two stacked recos have eight pieces of absorber on one side facing into cavity 2. A diagram of this configuration is shown in Figure 7.28.

For this case, cavity 1 is considered to be empty and the metallic side of the reco forms the final side of the cavity. The absorber from both recos is located in cavity 2. The ACS of the reco on the left hand side is the ACS of a one sided reco. The ACS of the reco on the right hand side is considered to be the same as a one sided reco facing

a wall, as measured in Chapter 5. This is 55% of the total ACS of a single sided reco. As the recos are considered as being stacked together the TCS of the aperture around the PCBs is that of the 3mm gap as this is the smallest gap.

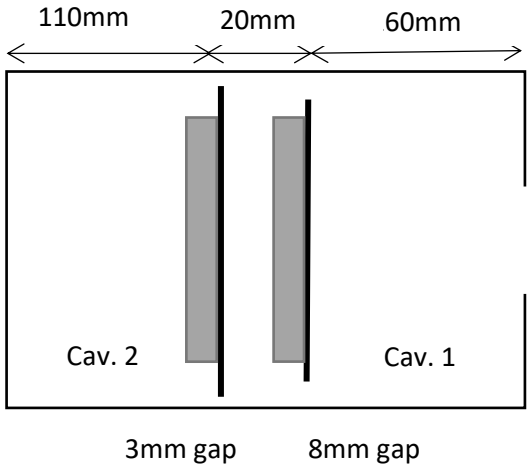

Figure 7.28: Diagram of the two cavity enclosure divided by single sided stacked recos with the absorber facing into cavity 2

7.2.1.17. Two Cavity Enclosure with Stacked Recos Measurement

Photographs of the two cavity enclosure with a stacked reco divider are shown in Figure 7.29.

The back of the enclosure is 11cm from the centre of the back reco. The front of the enclosure is 16cm from the centre of the front reco. There is 2.5cm between the centres of the recos. The front reco is the 8mm gap reco and the back reco the 3mm gap reco.

The SE of each cavity was measured using the method described in Section 7.2.1. The antenna was placed in position 2 for the SE measurement in cavity 1 and in position 6 for the SE measurement in cavity 6.

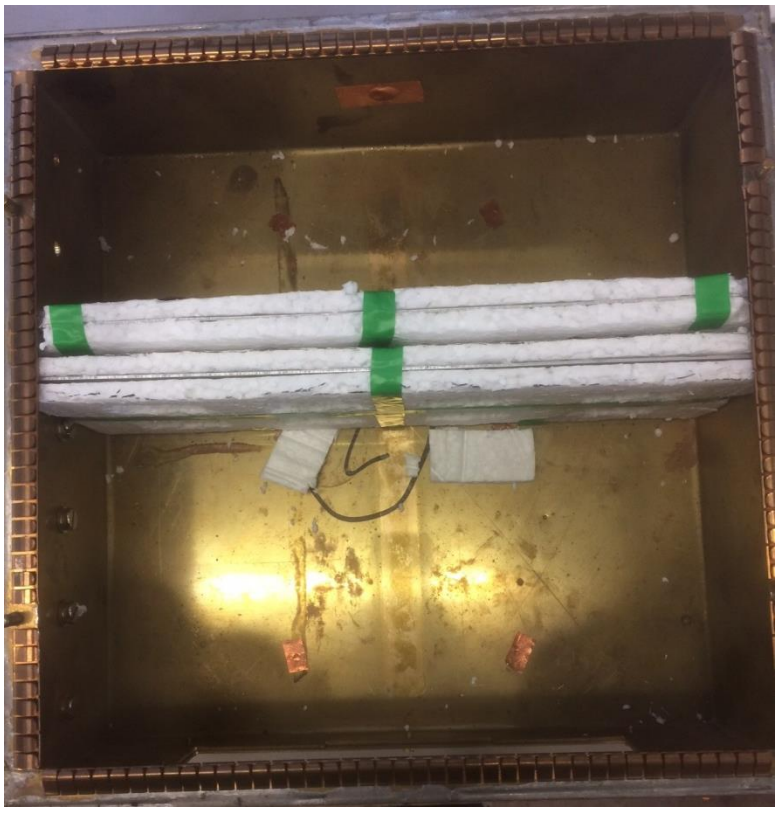

Figure 7.29: Photographs of the two cavity enclosure with a stacked reco divider. The enclosure aperture is at the bottom of the photograph and the back of the enclosure at the top of the photograph. The distance between the back of the enclosure and the centre of the back reco is 110mm and the distance between the front of the enclosure and the centre of the front reco is 160mm. There is 25mm between the centres of the recos.

7.2.1.18. Two Cavity Enclosure with Stacked PCBs Results

Double Sided Stacked Reco Divider

Figure 7.30 compares the SE of each cavity of the enclosure divided by the double sided stacked reco for the PWB model and the measurement in the RC. For the PWB, the SE of cavity 2 increases from a minimum of around 15dB at 2GHz to 28dB at 6GHz. There are small variations in SE between 27dB to 30dB from 6GHz to 20GHz. The SE of cavity 1 shows a similar structure but its SE is approximately 10dB from 6GHz to 20GHz. There is a difference of approximately 18dB between the two cavities. Above 5GHz, the measured SE of cavity 1 varies between 9dB and 15dB and the SE of cavity 2 varies between 28dB to 38dB. The difference in SE between the two cavities is approximately 20dB. The measured and PWB results for cavity 1 show very good agreement with each other. The measured result for cavity 2 is greater than the PWB result by up to 9dB. At higher frequencies, between 15GHz and 20GHz this difference is less significant.

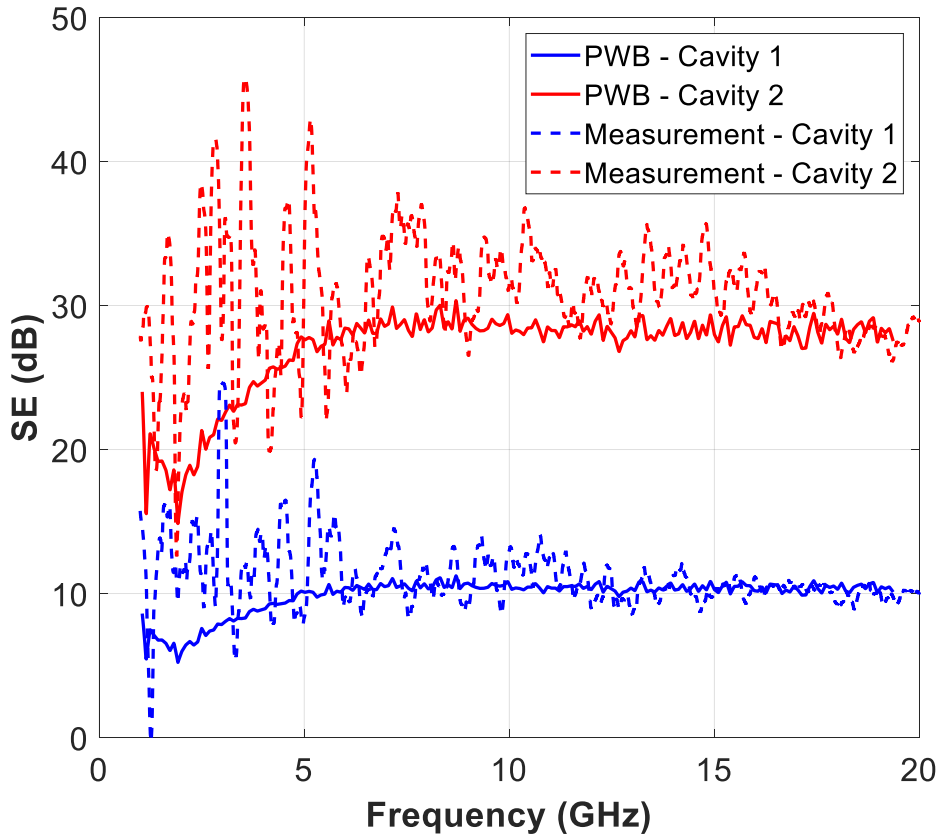

Figure 7.30: Comparison of modelled and measured SE of a two cavity enclosure with a double sided stacked reco divider

Single Sided Stacked Reco Divider - Absorber Facing into Cavity 1

Figure 7.31 compares the SE of each cavity of the enclosure divided by the single sided stacked reco, with the absorber facing into cavity 1 for the PWB model and the measurement in the RC. For the PWB, the SE of cavity 2 increases from a minimum of around 10dB at 2GHz to 18dB at 6GHz. There are small variations in SE between 16dB to 20dB from 6GHz to 20GHz. The SE of cavity 1 shows a similar structure but its SE is approximately 15dB from 6GHz to 20GHz. There is a difference of approximately 4dB – 5dB between the two cavities. Above 5GHz, the measured SE of cavity 1 varies between 10dB and 20dB and the SE of cavity 2 varies between 20dB to 30dB. The difference in SE between the two cavities is approximately 10dB. The measured and PWB results for cavity 1 are reasonably well matched. There is a difference of 2dB to 3dB over most of the frequency range. The measured SE result for cavity 2 is around 5dB to 10dB higher than the PWB result. In previous results, when a cavity has no additional absorber in the measured results is seen to be greater than the PWB result. This needs to be investigated further.

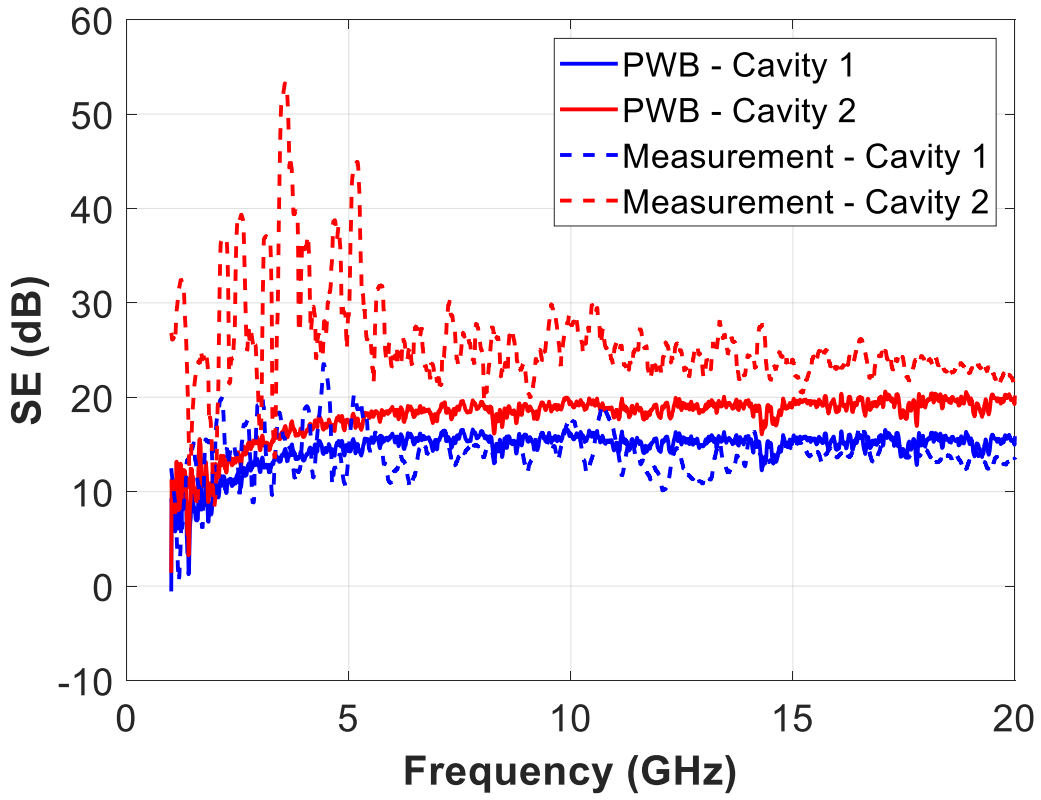

Figure 7.31: Comparison of modelled and measured SE of a two cavity enclosure with a single sided reco stacked divider facing into cavity 1.

Single Sided Stacked Reco Divider - Absorber Facing into Cavity 2

Figure 7.32 compares the SE of each cavity of the enclosure divided by the single sided stacked reco, with the absorber facing into cavity 2 for the PWB model and the measurement in the RC. For the PWB, the SE of cavity 2 increases from a minimum of around 20dB at 2GHz to 28dB at 6GHz. There are small variations in SE between 25dB to 29dB from 6GHz to 20GHz. As there is no absorber being considered in cavity 1, the SE is correspondingly low. The SE of cavity 1 increases slightly from around 2dB to 3B. There is a difference of approximately 25dB between the two cavities. Above 5GHz, the measured SE of cavity 1 varies between 3dB and 11dB and the SE of cavity 2 varies between 30dB to 40dB. The difference in SE between the two cavities varies over the frequency range. At 20GHz the difference is around 25dB, and at approximately 13GHz it is over 30dB.

The measured cavity 1 result is between 1dB to 7dB higher than the modelled result. Above 15GHz, the results are closer. The measured result for cavity 2 is significantly higher than the modelled result; there is a difference of over 10dB at some frequencies.

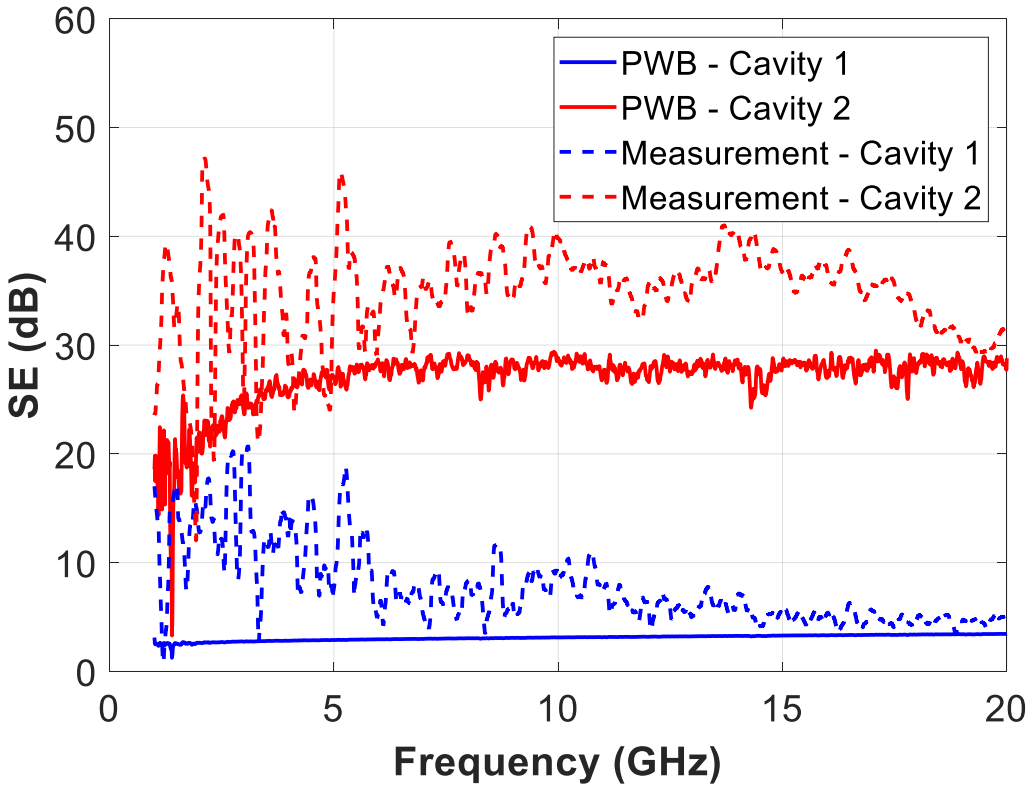

Figure 7.32: Comparison of modelled and measured SE of a two cavity enclosure with a single sided reco stacked divider facing into cavity 2.

7.5. Summary

This chapter presented PWB models of different configurations of an enclosure. The results of each model were compared with a SE measurement of the same configuration. The models used information detailed in the previous chapters of this thesis; including how ACS changes depending on position in an enclosure or whether the transmission through PCBs needs to be considered.

Results for an empty single cavity enclosure and a single cavity enclosure with a reco in two different positions were presented. Although the measured and modelled results for the empty enclosure and the enclosure with the reco positioned away from the enclosure walls showed good agreement, the results for the enclosure with the reco close to the enclosure wall were not as good.

The enclosure was divided into two cavities using a metallic divider, a single reco divider and a stacked divider formed by two recos. There were significant differences between the measured and modelled results for the two cavity enclosures. However, the modelled results could still be used to give an approximate SE of an enclosure.

This results presented in this chapter have shown that PWB modelling can be used to give an indication of the likely SE of an enclosure but more research needs to be carried out in order to develop the PWB and increase the accuracy of the modelled results. The next and final chapter of this thesis discusses the limitations of the work presented in this thesis and further work that could be carried out.

Chapter 8

Conclusions

8.1. Summary

Chapter 1 Section 1.2 states that the aim of the research presented in this thesis is to investigate the absorption cross section of PCBs and how it can be used to predict the SE of shielded enclosures populated with PCBs. This aim is split into three smaller goals:

- Obtain the ACS of a set of PCBs measured individually and in stacks. Changes in ACS due to the position of the PCB in the enclosure and changes in ACS due to other PCBs in the enclosure are investigated
- Investigate how the ACS of the PCBs vary depending on the position inside the enclosure and in relation to other PCBs and consider whether these factors are a significant influence on the SE of an enclosure
- Develop a method of predicting the SE of a shielded enclosure. An example of the SE of a realistic populated enclosure model should be compared to the SE of an actual populated enclosure.

The next sections summarise the work carried out to investigate these aims. The second part of this chapter discusses further work that could be carried out to develop and improve the research carried out so far.

8.1.1. Absorption Cross Section of Printed Circuit Boards

Chapters 3 to 5 detailed ACS measurements of PCBs in various different configurations. The PCBs were measured individually, stacked together and in different positions in the RC. An attempt was made to measure the ACS of a single side of a PCB.

The individual PCB results show how the ACS varies depending on the type and amount of components on each board as well as the size of each board. The ACS of the majority of the PCBs measured ranges from $2x10^{-3}$ m^2 to $8x10^{-3}$ m^2.

Four PCBs were measured stacked together in different configurations. The stacks consisted of two, three or four PCBs. The measured ACS of the stacked PCBs is lower than the ACS of the PCBs added together. The ACS of a stack of two PCBs is reduced

to between 75% and 85% of the total ACS of the individual PCBs. The ACS of a stack of four PCBs is reduced to 75% of the total ACS of the individual PCBs.

Measuring the PCBs in stacks shows that ACS is reduced when the PCBs are positioned close to other objects. The PCBs were measured in a number of different positions in the RC. Generally, changing the position of the PCB does not change the ACS of the PCB. However, when the front of the PCB is positioned close to and parallel to the RC wall the ACS is reduced to 55% of the total PCB ACS at some frequencies. These results are important as they apply to shielded enclosures if they are acting as a reverberant environment. This result, along with the stacked PCB measurement results, showed that further investigation was required to see the change as the PCB is moved closer to the wall and to find the ACS of a single side of a PCB.

In chapter 5, results from attempting to measure the ACS of one side of a reco are presented. Two sets of ACS measurements were carried out. The first set used a reco which was positioned at different distances from the RC wall. As the reco moved closer to the wall information about how the ACS changed was found. When the reco was positioned next to the chamber wall the results showed that the reduction in ACS is related to the reduction in the surface area of the absorber on the reco. The surface area of the absorber on a single sided reco is reduced to 55% when it is positioned next to the RC wall. The ACS of the reco in this position is also reduced by approximately 55%. The second set of measurements was of a PCB with aluminium foil covering one side. The ACS of the individually measured top and bottom of the PCB was added together and shown to be significantly higher than the ACS of the PCB measured as a whole. This could be due to a number of factors which should be investigated further (see Section 8.2.1.1 below).

8.1.2. Transmission through Printed Circuit Boards

The transmission through three PCBs was investigated using the AEG absorber box. No information was available on the transmission through PCBs but it is necessary to know the transmission when formulating a power balance model. The measurements divided the PCBs into two groups, two PCBs with a low TCS and one PCB with a higher TCS. The transmission of the low transmission PCBs was measured

as a minimum of -60dB. However, this was the noise floor of the measurement. The high transmission PCB has a measured transmission of between -20dB and -50dB.

8.1.3. Shielding Effectiveness of Enclosures with Contents

The final chapter of this thesis presents several models of an enclosure with and without contents in. The purpose of these models is to show that power balance modelling can be used to predict the SE of an enclosure with contents in. To create the model, the research into PCB ACS and the transmission through PCBs detailed in the previous chapters was used. The PWB models are compared to SE measurements of a shielded enclosure made in a reverberation chamber.

The measured and modelled results for the empty enclosure and the enclosure with the reco positioned away from the enclosure show good agreement. However, the results from the enclosure with the reco close to the enclosure wall need more investigation.

Differences between the measured and modelled results for the two cavity enclosures were observed. The modelled result gives a rough approximation of the SE of the enclosure, compared to the measured results. Section 8.2 discusses how the PWB models can be developed to improve the results.

8.1.4. Overall Conclusions

The hypothesis in Chapter 1 Section 1.2 of this thesis states that:

The shielding effectiveness of a simple enclosure populated by PCBs can be predicted using the PCB's absorption cross section and transmission cross section.

Overall, the work in this thesis shows that PWB models can be used to predict the SE of an enclosure with contents in. However, for more accurate results and for the models to become useful further work needs to be carried out. This is discussed in Section 8.2.

Including the contents of an enclosure can significantly change the shielding effectiveness of the enclosure. For shielding effectiveness, the enclosure and its

contents should be considered as a single system rather than as separate equipment. When designing equipment and systems, an accurate SE is important to know. Not having an accurate idea of the SE of a system may lead to increased weight and cost and also increase the time of the design process if the shielding is underestimated. If overestimated, the enclosure may not provide enough protection from EM sources leading to damage or malfunction of the equipment.

8.2. Further Work

This section discusses improvements that could be made to the work detailed in this thesis and what can be carried out to develop this work. Wider areas of interest are also discussed.

8.2.1. Improvements and Developments to Current Work

8.2.1.1. Absorption Cross Section of Printed Circuit Boards

Two different methods of calculating the ACS of PCBs were used during the course of this work. The second method, using inverse Fourier transforms [53], is a more precise method but was developed part way through this work and so was only applied to a small number of measurements. A small set of PCBs taken from two similar pieces of communication equipment were measured throughout this work. By measuring PCBs with a greater range of sizes, shapes, components and technology more information on PCB ACS can be gathered and then used in the PWB models. In future the inverse Fourier transform technique method should be used for ACS measurements. At the lower frequencies measured in the work presented here, the results were unusable. By measuring PCBs in a larger chamber with a lower LUF the ACS at lower frequencies may be found. However, there is a limit to how small the PCBs can be.

The method of finding the ACS of one side of a PCB, or reco, should be improved. The foil measurements showed a difference between the total ACS of the PCB and the sum of the two sides. Finding out why this is the case would improve the results. This could be done by exploring the transmission through the PCB and by looking at the reflection from the PCB and the foil covering it.

8.2.1.2. Transmission through Printed Circuit Boards

Only three PCBs were measured for this work and it would be very beneficial to measure a greater range of PCBs to find out how transmission through the boards varies PCB to PCB. In order to do this it would be useful to improve the measurement method and equipment, as currently it can only be carried out on larger PCBs. The transmission of the PCBs was also limited to a smaller frequency range (500MHz to 8GHz) and being able to measure the transmission up to 20GHz would improve the results for use in the power balance models.

8.2.1.3. Shielding Effectiveness of Enclosures with Contents

The previous two sections discuss improving the knowledge of the absorption and transmission of PCBs. Using this improved knowledge in the models will improve the results of the models. The measurements and models use recos as the contents. Using PCBs may be more representative of real enclosures and allow any differences between using recos and PCBs to be shown.

There are differences between the measured and modelled results, particularly for the two cavity enclosures. It would be useful to investigate what happens in the small cavities which are formed between a reco placed next to the enclosure wall or between recos stacked together. One method of doing this could be to divide an enclosure into three cavities using two recos and then decreasing the distance between the recos. This information may also help to find the ACS of one side of a PCB and show how the ACS of a stack of PCBs should be considered in different cavities. When the more basic configurations have been refined, more complex configurations can be calculated.

It may worth looking into including the transmission through single PCBs in the model to see what effect this has on SE. If measurements of a greater number of PCBs show a higher transmission, then this may need to be considered.

8.2.2. Future Work

The focus of the research in this thesis is the ACS of PCBs. In real equipment, PCBs will not be the only contents found inside enclosures. Other items, such as fans or

cabling, will also need to be considered when using PWB models to predict SE. Cables may be of particular interest as they could act as antennas inside the enclosure. The ACSs measured have been of the whole, or one side of, the PCBs. Measuring the ACS of different types of components individually would be very useful information to have. This may allow an estimate of the ACS of a PCB to be made by considering the types of components on it.

The measurements carried out have been of unpowered PCBs. An initial ACS measurement of a powered FPGA development board showed no difference between the ACS of a powered and unpowered PCB. Further work in the AEG confirmed this initial result [58].

Knowing the reflection coefficients of a PCB may aid the understanding of what happens when a PCB is close to a wall or another PCB. An attempt to calculate these values was made using the data obtained from the absorber box measurements. However, it proved too difficult to separate the effect of the absorber box itself from the PCB information.

In addition to calculating the SE of an enclosure using RC measurements and PWB modelling, full wave modelling such as using Finite Difference Time Domain (FDTD) techniques could be used. Results from full wave modelling could be used to validate the PWB and measured results. Techniques such as FDTD would be useful to find the field at different points in small cavities, such as between an object and the enclosure wall, as making a real measurement would be difficult due to the space constraint. It could also be useful for investigating the reflection coefficients of PCBs. Additionally, models of enclosures and their contents could be used as an alternative to measuring the system as equipment such as RCs may not be available for engineers to use.

Finally, the SE of an enclosure with contents in, compared to an empty enclosure, is different because the PCBs are absorbing the energy inside the enclosure. It is important to know where the energy is being absorbed in the PCB. If it is being absorbed into the PCB substrate this is less concerning than if the energy is coupling

onto the PCB tracks or into the components themselves. Finding out what is happening to the energy could have important implications for PCB susceptibility.

Nomenclature

Symbols

Symbol	Meaning
<>	Average
σ_a	ACS
λ	Wavelength
π	pi
%	Percentage
S	Power density
P	Power
η	Efficiency
c_0	Speed of light in a vacuum
f	frequency
V	Volume
θ	angle
N	Number of independent samples
S_{xx}	S-parameter
K	K-factor
Q	Q-factor
ω	Angular frequency
U	Stored energy
P_d	Average power dissipated
S	Surface area
δ	Skin depth
σ	Conductivity
μ	Permeability
E	Electric field
H	Magnetic field
k	Wavenumber
G	Mean net transfer function

L	Chamber loading function
γ	Shadowing factor
W	Window function
τ	Time constant
T	Transmission

Acronyms and Abbreviations

Acronym/Abbreviation	In Full…
ACS	Absorption Cross Section
AEG	Applied Electromagnetics Group
BW	Bandwidth
c_0	Speed of light in a vacuum
CEM	Computational Electromagnetics
dB	Decibels
E	Electric Field
EM	Electromagnetic
EMC	Electromagnetic Compatibility
EUT	Equipment Under Test
f	Frequency
FDTD	Finite Difference Time Domain
G	Giga
GHz	Gigahertz
G_{no}	Mean net transfer function without PCB
G_r	Relative mean net transfer function given by G_{no}/G_{wo}
G_{wo}	Mean net transfer function with PCB
H	Magnetic Field
Hz	Hertz
ICT	Information Communication Technology
IEEE	Institute of Electrical and Electronic Engineers
LUF	Lowest Usable Frequency
m	metre

M	Mega
MHz	Megahertz
mm	Millimetre
n/a	Not applicable
OUT	Object Under Test
PCB	Printed Circuit Board
PDP	Power Density Profile
PWB	Power Balance Model
Q Factor	Quality Factor
RAM	Radio Frequency Absorbing Material
RC	Reverberation Chamber
Reco	Representative Contents
RHS	Right Hand Side
s	second
SE	Shielding Effectiveness
SMA	Sub Miniature version A
S-parameter	Scattering Parameter
TCS	Transmission Cross Section
tx	Transmission
UoY	University of York
USOM	Unknown, Short, Open, Matched
V	Volume
VNA	Vector Network Analyser

References

[1] Standard Method for Measuring the Effectiveness of Electromagnetic Shielding Enclosures, IEEE-STD 299, Institute of Electrical and Electronics Engineers, Piscataway, NJ, USA, Feb. 2007.

[2] Measurement of Electromagnetic Interference Characteristics, MIL-STD-462, 1999

[3] Standard Method for Measuring the Shielding Effectiveness of Enclosures and Boxes Having All Dimensions Between 0.1 m and 2 m, IEEE-STD 299.1, Institute of Electrical and Electronics Engineers, Piscataway, NJ, USA, Oct. 2013.

[4] Carlberg, U., Kildal, P.-S., Wolfgang, A., Sotoudeh, O. and Orlenius, C., “Calculated and measured absorption cross sections of lossy objects in reverberation chamber,” IEEE Transactions on Electromagnetic Compatibility, vol. 46, no. 2, pp. 146-154, May 2004

[5] D. A. Hill, M. T. Ma, A. R. Ondrejka, B. F. Riddle, M. L. Crawford and R. T. Johnk, "Aperture excitation of electrically large, lossy cavities," IEEE Transactions on Electromagnetic Compatibility, vol. 36, no. 3, pp. 169-178, Aug 1994.

[6] I. Junqua, J.-P. Parmantier, and F. Issac, “A network formulation of the power balance method for high-frequency coupling,” Electromagnetics, vol. 25, nos. 7/8, pp. 603--622, 2005.

[7] Hill, D.A., Electromagnetic Theory of Reverberation Chambers, NIST Technical Note 1506, Dec. 1998.

[8] Crawford, M.L. and Koepke, G.H., Design, Evaluation, and Use of a Reverberation Chamber for Performing Electromagnetic Susceptibility / Vulnerability Measurements, NBS Technical Note 1092, 1986.

[9] D. A. Hill, "Boundary fields in reverberation chambers," in *IEEE Transactions on Electromagnetic Compatibility*, vol. 47, no. 2, pp. 281-290, May 2005.

[10] BS EN 61000-4-21:2011, Electromagnetic Compatibility (EMC) Part 4-21: Testing and Measurement Techniques – Reverberation Chamber Test Methods, 2011

[11] Ministry of Defence Defence Standard 59-411 Parts 1-5 Electromagnetic Compatibility Issue 2, 2011

[12] MIL-STD-461G, Department of Defense Interface Standard Requirements for the Control of Electromagnetic Interference Characteristics of Subsystems and Equipment, 2015

[13] DO-160G, Environmental Conditions and Test Procedures for Airborne Equipment, 2010

[14] V. Rajamani, C. F. Bunting and J. C. West, "Stirred-Mode Operation of Reverberation Chambers for EMC Testing," in *IEEE Transactions on Instrumentation and Measurement*, vol. 61, no. 10, pp. 2759-2764, Oct. 2012.

[15] Herke, D.L. and Barber, G.D.M., The use of mode stirred chambers in EM evaluation testing, 10th International Conference on Electromagnetic Compatibility, (Conf. Publ. No. 445), 1997

[16] Fall, A.K. and Besnier, P. and Lemoine, C. and Zhadobov, M. and Sauleau, R., Determining the lowest usable frequency of a frequency-stirred reverberation chamber using modal density, International Symposium on Electromagnetic Compatibility (EMC Europe), 2014

[17] D. A. Hill, "Electronic mode stirring for reverberation chambers," in *IEEE Transactions on Electromagnetic Compatibility*, vol. 36, no. 4, pp. 294-299, Nov 1994.

[18] Holloway C.L., Hill, D.A., Ladbury, J., Koepke, G. and Garzia, R., “Shielding Effectiveness Measurements of Materials Using Nested Reverberation Chamber”, Trans Electromag. Compat., vol. 45, no. 2, May 2003

[19] Marvin, A.C. and Yuhui He, A study of enclosure shielding effectiveness measurement using frequency stirring in a mode-stirred chamber, IEEE International Symposium on Electromagnetic Compatibility, 2008

[20] C. L. Holloway, D. A. Hill, J. M. Ladbury, P. F. Wilson, G. Koepke and J. Coder, "On the Use of Reverberation Chambers to Simulate a Rician Radio Environment for the Testing of Wireless Devices," in *IEEE Transactions on Antennas and Propagation*, vol. 54, no. 11, pp. 3167-3177, Nov. 2006.

[21] C. Lemoine, E. Amador and P. Besnier, "On the K -Factor Estimation for Rician Channel Simulated in Reverberation Chamber," in *IEEE Transactions on Antennas and Propagation*, vol. 59, no. 3, pp. 1003-1012, March 2011.

[22] IEEE Standard 299.1, IEEE Standard Method for Measuring the Shielding Effectiveness of Enclosures and Boxes Having All Dimensions Between 0.1m and 2m, 2013

[23] Cerri, G., Primiani, V.M., Pennesi, S., and Russo, P., “Source Stirring Mode for Reverberation Chambers”, Trans Electromag. Compat., vol. 47, no. 4, Nov 2005

[24] A. C. Marvin *et al*., "A wide-band hybrid antenna for use in reverberation chambers," *2013 IEEE International Symposium on Electromagnetic Compatibility*, Denver, CO, 2013, pp. 222-226

[25] S. A. Schelkunoff. The Impedance Concept and Its Application to Problems of Reflection, Shielding and Power Absorption. *Bell System Technical Journal*, 17:17–31, 1938.

[26] H. Kaden, *Wirbelstrome und Schirmung in der Nachrichtentechnik*. Springer-Verlag Berlin, 1959.

[27] R. Armstrong, A. Marvin and J. Dawson, "An experimental investigation of the use of Q-factor to determine the shielding effectiveness of electrically large equipment enclosures with apertures," *10th International Symposium on Electromagnetic Compatibility*, York, 2011, pp. 148-152

[28] A. Marvin and Yong Cui, "Anechoic and reverberation chamber shielding measurement at frequencies above 1 GHz," *2006 IEEE International Symposium on Electromagnetic Compatibility, 2006. EMC 2006.*, Portland, OR, USA, 2006, pp. 410-415

[29] M. P. Robinson *et al*., "Shielding effectiveness of a rectangular enclosure with a rectangular aperture," in *Electronics Letters*, vol. 32, no. 17, pp. 1559-1560, 15 Aug. 1996

[30] M. P. Robinson *et al*., "Analytical formulation for the shielding effectiveness of enclosures with apertures," in *IEEE Transactions on Electromagnetic Compatibility*, vol. 40, no. 3, pp. 240-248, Aug. 1998

[31] B. Nie and P. Du, "An Efficient and Reliable Circuit Model for the Shielding Effectiveness Prediction of an Enclosure With an Aperture," in *IEEE Transactions on Electromagnetic Compatibility*, vol. 57, no. 3, pp. 357-364, June 2015.

[32] T. Konefal, J. F. Dawson, A. C. Marvin, M. P. Robinson and S. J. Porter, "A fast multiple mode intermediate level circuit model for the prediction of shielding

effectiveness of a rectangular box containing a rectangular aperture," in *IEEE Transactions on Electromagnetic Compatibility*, vol. 47, no. 4, pp. 678-691, Nov. 2005

[33] J. R. Solin, "Formula for the Field Excited in a Rectangular Cavity With a Small Aperture," in *IEEE Transactions on Electromagnetic Compatibility*, vol. 53, no. 1, pp. 82-90, Feb. 2011.

[34] J. R. Solin, "Formula for the Field Excited in a Rectangular Cavity With an Electrically Large Aperture," in *IEEE Transactions on Electromagnetic Compatibility*, vol. 54, no. 1, pp. 188-192, Feb. 2012

[35] J. R. Solin, "Formula for the Field Excited in a Rectangular Cavity With an Aperture and Lossy Walls," in *IEEE Transactions on Electromagnetic Compatibility*, vol. 57, no. 2, pp. 203-209, April 2015

[36] A. C. Marvin, J. F. Dawson, S. Ward, L. Dawson, J. Clegg and A. Weissenfeld, "A proposed new definition and measurement of the shielding effect of equipment enclosures," in *IEEE Transactions on Electromagnetic Compatibility*, vol. 46, no. 3, pp. 459-468, Aug. 2004

[37] A. Marvin and Yong Cui, "Towards evaluating the shielding of enclosures with contents at frequencies above 1 GHz," *2005 International Symposium on Electromagnetic Compatibility, 2005. EMC 2005.*, Chicago, IL, 2005, pp. 200-205 Vol. 1

[38] L. Klinkenbusch, "On the shielding effectiveness of enclosures," in *IEEE Transactions on Electromagnetic Compatibility*, vol. 47, no. 3, pp. 589-601, Aug. 2005.

[39] Su-han Kim and Jae-hyun Lee, "Analysis for shielding effectiveness of an enclosure with a dielectric-backed aperture and a PCB," *2008 Electrical Design of Advanced Packaging and Systems Symposium*, Seoul, 2008, pp. 61-64

[40] D. W. P. Thomas *et al*., "Model of the electromagnetic fields inside a cuboidal enclosure populated with conducting planes or printed circuit boards," in *IEEE Transactions on Electromagnetic Compatibility*, vol. 43, no. 2, pp. 161-169, May 2001

[41] Azaro, A., Semianalytical Approach for the Evaluation of Radiated Immunity on a Printed Circuit Board in Metallic Enclosures, *Microwave and Optical Technology Letters,* 27(3), 2000

[42] Melia, G., *Electromagnetic Absorption by the Human Body from 1GHz to 15GHz*, PhD thesis, University of York, 2013

[43] I. D. Flintoft, S. J. Bale, S. L. Parker, A. C. Marvin, J. F. Dawson and M. P. Robinson, "On the Measurable Range of Absorption Cross Section in a Reverberation Chamber," in *IEEE Transactions on Electromagnetic Compatibility*, vol. 58, no. 1, pp. 22-29

[44] F. A. Benson, "Waveguide Attenuation and its Correlation with Surface Roughness," in *Proceedings of the IEE - Part III: Radio and Communication Engineering*, vol. 100, no. 64, pp. 85-90, March 1953.

[45] Marvin, A.C. and Yong Cui, Shielding Measurements of Equipment Enclosures in the Radiating Near Field, *IEEE Transactions on Electromagnetic Compatibility*, 49(4):860-867, 2007

[46] I. Junqua, J-P. Parmantier, S. Bertuol, “Fundamentals of the PWB Approach,”, HIRF Synthetic Environment Research Program Report, September 2010

[47] Emerson & Cuming Microwave Products, “Eccosorb LS,” LS absorber datasheet [online], Nov. 2007. Available: http://www.eccosorb.com/Collateral/Documents/English-US/LS.pdf

[48] I. D. Flintoft, S. L. Parker, S. J. Bale, A. C. Marvin, J. F. Dawson and M. P. Robinson, "Measured Average Absorption Cross-Sections of Printed Circuit Boards from 2 to 20 GHz," in *IEEE Transactions on Electromagnetic Compatibility*, vol. 58, no. 2, pp. 553-560, April 2016

[49] J.D. Kraus, Electromagnetics, 4th edition. McGraw-Hill, 1991, p. 638.

[50] C. A. Balanis, Antenna Theory Analysis and Design, 2nd edition. USA: John Wiley & Sons, 1997

[51] I. D. Flintoft *et al*., "Representative Contents Design for Shielding Enclosure Qualification From 2 to 20 GHz," in *IEEE Transactions on Electromagnetic Compatibility*, vol. 60, no. 1, pp. 173-181, Feb. 2018.

[52] A. C. Marvin, J. F. Dawson, S. Ward, L. Dawson, J. Clegg and A. Weissenfeld, "A proposed new definition and measurement of the shielding effect of equipment

enclosures," in *IEEE Transactions on Electromagnetic Compatibility*, vol. 46, no. 3, pp. 459-468, Aug. 2004.

[53] X. Zhang, M. P. Robinson, I. D. Flintoft and J. F. Dawson, "Efficient Determination of Reverberation Chamber Time Constant," in *IEEE Transactions on Electromagnetic Compatibility*, vol. 60, no. 5, pp. 1296-1303, Oct. 2018

[54] X. Zhang, M. P. Robinson, I. D. Flintoft and J. F. Dawson, "Inverse Fourier transform technique of measuring averaged absorption cross section in the reverberation chamber and Monte Carlo study of its uncertainty," *2016 International Symposium on Electromagnetic Compatibility - EMC EUROPE*, Wroclaw, 2016, pp. 263-267

[55] ETS Lindgren. (2019). *3115 Double-Ridged Guide Antenna* [Online]. Available: http://www.ets-lindgren.com/products/antennas/double-ridged-guide/4002/400203

[56] Catrysse, J.; Pissoort, D. & Vanhee, F., "Shielding effectiveness of planar materials: (semi) - Standardized measurements from LF to µW", *Workshop on Aerospace EMC (Aerospace EMC)* , 1-5 , May, 2016

[57] Marvin, A. C.; Dawson, L.; Flintoft, I. D. & Dawson, J. F., "A Method for the Measurement of Shielding Effectiveness of Planar Samples Requiring No Sample Edge Preparation or Contact", IEEE Transactions on Electromagnetic Compatibility , vol. 51, no. 2 , 255-262 , May, 2009

[58] Kane Yee, "Numerical solution of initial boundary value problems involving maxwell's equations in isotropic media," in *IEEE Transactions on Antennas and Propagation*, vol. 14, no. 3, pp. 302-307, May 1966

[59] W. J. R. Hoefer, "The Transmission-Line Matrix Method - Theory and Applications," in *IEEE Transactions on Microwave Theory and Techniques*, vol. 33, no. 10, pp. 882-893, Oct. 1985.

[60] J. Yan, J. Dawson and A. Marvin, "Effect of power state on absorption cross section of personal computer components: Applications to enclosure shielding," *2017 International Symposium on Electromagnetic Compatibility - EMC EUROPE*, Angers, 2017, pp. 1-5